

# Synthesis of a novel layered double hydroxide derived from dolomite and its functionalized fabrication for removal of borate

邱, 心泓

<https://doi.org/10.15017/1470567>

---

出版情報：九州大学, 2014, 博士（工学）, 課程博士  
バージョン：  
権利関係：全文ファイル公表済



# **Synthesis of a novel layered double hydroxide derived from dolomite and its functionalized fabrication for removal of borate**



Xinhong Qiu

September, 2014

# Contents

<b>Chapter 1 Introduction.....</b>	<b>1</b>
<b>1.1 Boron: its distribution in nature and its important roles .....</b>	<b>1</b>
<b>1.2 Chemistry of boron in aqueous solutions.....</b>	<b>3</b>
<b>1.3 Toxicity of boron and drinking water standards .....</b>	<b>5</b>
<b>1.4 Technologies for boron removal .....</b>	<b>7</b>
1.4.1 Coagulation-precipitation .....	7
1.4.2 Membrane methods .....	8
1.4.3 Sorption processes .....	9
<b>1.5 Layered double hydroxides (LDHs) .....</b>	<b>13</b>
1.5.1 Basic structure of LDHs .....	13
1.5.2 Representative synthetic method of LDHs .....	14
1.5.3 Cations in the metallic host layers of LDHs.....	16
1.5.4 Molar ratio of $M^{2+} / M^{3+}$ in LDHs .....	17
1.5.5 Anions in LDHs.....	17
1.5.6 Specific properties of LDHs .....	19
<b>1.6 Sorption applications of layered double hydroxide .....</b>	<b>20</b>
<b>1.7 Shortcoming of traditions LDHs without modification.....</b>	<b>23</b>
<b>1.8 Objective and outline of this thesis .....</b>	<b>23</b>
<b>Chapter 2 Sorption of borate by a layered double hydroxides prepared using dolomite as a magnesium source .....</b>	<b>37</b>
<b>2.1 Introduction .....</b>	<b>37</b>
<b>2.2 Materials and methods .....</b>	<b>38</b>
2.2.1 Chemicals .....	38
2.2.2 Preparation of $CO_3$ -DLDH .....	39
2.2.3 Characterization.....	40
2.2.4 Sorption batch tests.....	41

<b>2.3 Results and Discussion.....</b>	<b>42</b>
2.3.1 Characterization.....	42
2.3.2 Effect of calcination temperature on the sorption of borate .....	46
2.3.3 Effect of pH on the sorption of borate .....	55
2.3.4 Effect of competing anions on sorption of borate .....	57
<b>2.4. Conclusion.....</b>	<b>59</b>
<b>Chapter 3 One-step synthesis of layered double hydroxide-intercalated gluconate for removal of borate.....</b>	<b>62</b>
<b>3.1 Introduction .....</b>	<b>62</b>
<b>3.2 Experimental method.....</b>	<b>63</b>
3.2.1 Chemicals .....	63
3.2.2 Preparation of hydrotalcite with gluconate radical intercalation.....	63
3.2.3 Characterization.....	64
3.2.4 Sorption experiments .....	65
<b>3.3. Results and discussion.....</b>	<b>66</b>
3.3.1 Characterization.....	66
3.3.2 Removal of borate using different LDHs .....	75
3.3.3 Sorption mechanism .....	77
3.3.4 Effect of co-existing anions on borate sorption.....	83
3.3.5 Comparison of G-LDHs with boron-specific resin .....	85
3.3.6 Temperature effect on the sorption of borate by G-LDH-1.5.....	87
3.3.7 Effect of pH on the sorption of borate by G-LDH-1.5 .....	88
<b>3.4. Conclusion.....</b>	<b>89</b>
<b>Chapter 4 Sorption of borate onto layered double hydroxides assembled on filter paper through in situ hydrothermal crystallization.....</b>	<b>93</b>
<b>4.1. Introduction .....</b>	<b>93</b>
<b>4.2 Experimental method.....</b>	<b>94</b>
4.2.1 Chemicals .....	94
4.2.2 Synthesis of materials .....	94
4.2.2.1 Preparation of filter paper modified by LDHs with carbonate interlayer.....	94
4.2.2.2 Preparation of filter paper modified by LDHs intercalated with chloride.....	94

4.2.2.3 Preparation of filter paper modified by LDHs intercalated with gluconate ..	95
4.2.3 Characterization.....	96
4.2.4 Sorption experiments.....	97
4.2.4.1 Time effect on sorption of boron by different materials .....	97
4.2.4.2 Sorption densities of different materials.....	97
4.2.4.3 Effect of competing anions.....	97
<b>4.3 Results and discussion.....</b>	<b>98</b>
4.3.1 Characterizations .....	98
4.3.2 Boron removal by F-LDH .....	107
4.3.2 Sorption of borate in the presence of coexisting anions .....	112
<b>4.4 Conclusion.....</b>	<b>114</b>
<b>Chapter 5 Conclusions.....</b>	<b>117</b>
<b>Acknowledgement .....</b>	<b>121</b>

## Chapter 1 Introduction

### 1.1 Boron: its distribution in nature and its important roles

Boron is a ubiquitous element in rocks, soil and water, and is an essential element for life on earth [1, 2]. There are more than 200 minerals containing boron, and some of them are important sources of boron (**Table.1.1**).

Table 1.1 Naturally occurring boron-containing minerals

Mineral	Chemical composition	Content rate of Boron (%)
Boracite	$\text{Mg}_6\text{B}_{14}\text{O}_{26}\text{Cl}_2$	19.30
Colemanite	$\text{Ca}_2\text{B}_6\text{O}_{11} \cdot 5\text{H}_2\text{O}$	15.78
Hydroboracite	$\text{CaMgB}_6\text{O}_{11} \cdot 6\text{H}_2\text{O}$	15.69
Kernite	$\text{Na}_2\text{B}_4\text{O}_7 \cdot 4\text{H}_2\text{O}$	14.90
Priceite	$\text{Ca}_4\text{B}_{10}\text{O}_{19} \cdot 7\text{H}_2\text{O}$	15.48
Proberite	$\text{NaCaB}_5\text{O}_9 \cdot 5\text{H}_2\text{O}$	15.39
Sassolite	$\text{H}_3\text{BO}_3$	17.48
Szaibelyite	$\text{MgBO}_2 \cdot \text{OH}$	12.85
Tincal (borax)	$\text{Na}_2\text{B}_4\text{O}_7 \cdot 10\text{H}_2\text{O}$	11.34
Tincalconite	$\text{Na}_2\text{B}_4\text{O}_7 \cdot 5\text{H}_3\text{O}$	15.16
Ulexite	$\text{NaCaB}_5\text{O}_9 \cdot 8\text{H}_2\text{O}$	13.34

The average content of boron in the earth's crust is 10 mg/L [3]. In soils, its average concentration is in the range of 10–20 mg/L. The content of boron in rocks typically ranges from 5 mg/L in basalts to 100 mg/L in sedimentary shale. Seawater contains an average of 4.6 mg/L boron, with variation in concentration from 0.5 to 9.6

mg/L. The concentration of boron in fresh water is generally from <0.01 mg/L to 1.5 mg/L, and increases significantly in areas where soils are boron enriched [2, 4].

Many researchers have reported that boron is an essential or at least a beneficial element for human beings and animals [5-8]. As Brown et al. [9] mentioned, boron is essential for plant cell wall structure and function, likely through its role as a stabilizer of the cell wall pectic network and subsequent regulation of cell wall pore size. Reports also indicated that boron is an important nutrient for healthy bones and joints [10] and suggested that boron has beneficial effects related to bone metabolism [11]. In addition, boron compounds are used in many important industrial areas because of their special nature [12, 13]. The yield from the main boron-exporting countries has risen from year to year (**Table 1.2**). Boric acid and sodium borates are considered to be crucial raw compounds in modern industries and are extensively used in glass manufacturing, semiconductor products, and pharmaceutical preparations, among other applications.

Table 1.2 Annual production of borates

Country	tonnes				
	2005	2006	2007	2008	2009
Russia	400 000	400 000	400 000	400 000	410 000
Turkey	2 087 000	2 373 345	1 997 163	2 139 224	1 682 000
Argentina	632 792	533 535	669 578	789 954	500 433
Chile	460 683	459 645	535 071	590 999	613 135
Peru	32 611	—	233 991	349 891	187 221
China	280 000	290 000	290 000	280 000	290 000
Kazakhstan	30 000	30 000	30 000	30 000	30 000

## 1.2 Chemistry of boron in aqueous solutions

In aqueous environments, as previously reported, dissolved boron is present as several species, depending on the concentration of boron and the aqueous pH [14]. At low boron concentrations ( $< 25$  mmol/L), dissolved boron is mainly found as monomeric boron species,  $\text{H}_3\text{BO}_3$  and  $\text{B}(\text{OH})_4^-$ . At  $\text{pH} < 7$ , boric acid is predominant, whereas at high pH ( $> 11$ ), tetrahydroxyborate dominates, as indicated in Fig. 1. However, when the boron concentration is higher than 25 mmol/L, triborate ( $\text{B}_3\text{O}_4(\text{OH})_3^-$ ) and tetraborate ( $\text{B}_4\text{O}_5(\text{OH})_4^{2-}$ ) ions can be formed, depending on pH (**Fig. 1.1**). Considering that the concentration of boron is below 25 mmol/L in seawater and fresh water, only monomers,  $\text{H}_3\text{BO}_3$  and  $\text{B}(\text{OH})_4^-$ , are present in natural water. For these two species, the most important of their properties in relation to boron removal from water is that the  $\text{H}_3\text{BO}_3$  is electrically neutral, while  $\text{B}(\text{OH})_4^-$  has a distinct electric charge. Because of this aspect of boron chemistry, boron is an element able to enter the food chain, as well as biomass, from both natural sources and human activities. Excess concentration in drinking water results in a threat to human health, whereas excess concentrations in rivers can result in destruction of forests.



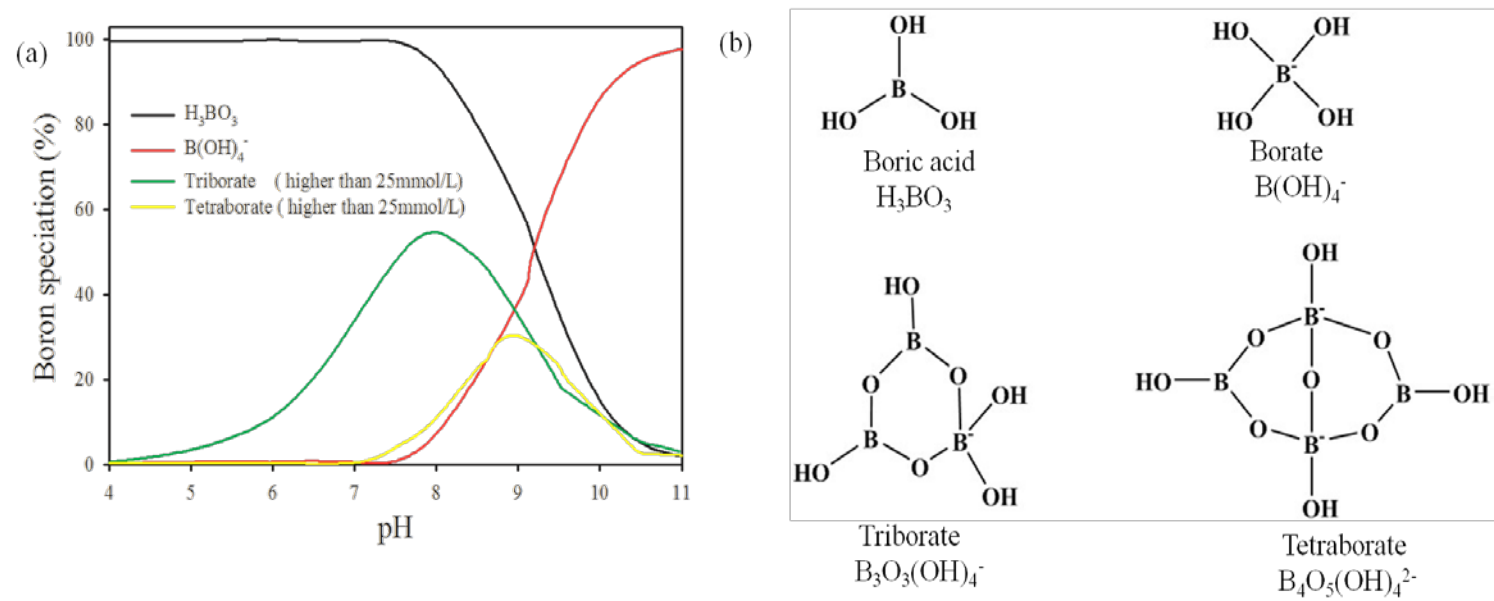


Fig. 1.1 (a) Molar fractions of boron species vs. pH in solutions with different borate concentrations; (b) Structures of some boron species in aqueous solution [15-17].

### **1.3 Toxicity of boron and drinking water standards**

Although boron is an essential element for numerous living organisms, as mentioned above, excess intake of boron causes adverse effects on the growth of animals and plants [18]. Many toxic effects have been reported, including yellow tips of leaves, defoliation, spots on fruits, decay and falling of unripe fruit, in plants irrigated with water containing excessive amounts of boron [2, 19-22]. The known toxicity mechanism of boron in plants has been summarized, and Reid et al. proposed [23] that there are three main candidate sites: (1) disruption of cell wall development; (2) metabolic disruption by binding to the ribose moieties of ATP, NADH or NADPH; and (3) disruption of cell division and development by binding to ribose, either as the free sugar or within RNA. Although humans are becoming more and more aware of the toxic effects of boron in plants, boron toxicity is still a worldwide problem that significantly limits crop yields in agricultural areas of Australia, North Africa, and West Asia [24]. The range of boron concentration between deficiency and excess is narrow, although boron toxicity is more difficult to manage than boron deficiency, which can be avoided by proper fertilization [25].

In contrast with the understanding of the adverse effects of boron in plants, much remains unknown about the toxicity of boron in animals and humans. Boron can affect the function or composition of several body systems, including the brain, skeleton and immune system. Chronic exposure to boron may cause cutaneous disorders [26], retarded growth and have an adverse impact on the male reproductive system in rats and mice [27, 28]. In humans, the signs of acute toxicity include nausea, vomiting, diarrhea, dermatitis and lethargy [29]. However, Nielsen [30] suggested that

boron has low toxicity and toxicity signs in animals generally occur only after dietary B exceeds 100 µg/g.

Since the toxicity has not been fully studied and boron was not considered a toxic substance, there was no regulation of boron in the WHO International Standards for drinking water until 1993 [2]. In 1993, the WHO added a permissible boron level of 0.3 mg/L in drinking water as laboratory studies gradually elucidated the harmful effects of boron on animals. However, this value was increased to 0.5 mg/L, because there is no effective method to remove the boron from solution to meet the requirement. In 2011, the WHO recommended and changed the maximum permissible concentration of boron to 2.4 mg/L in their guidelines [31]. **Table 1.3** summarizes the boron standards for drinking water in several regions. As can be seen from the table, most countries do not follow the WHO standards because of the different conditions in different countries, so the maximum permissible concentration of boron in drinking water has been revised in different countries.

Table 1.3 Guidelines from different regions for B in drinking water

Boron in drinking water standards by regions.	Maximum boron concentration (mg/L)	References
WHO	2.4	[31]
Japan	1	[32]
China	0.5	[33]
Saudi Arabia	0.5	[34]
USA	---	[35]
European Union	1	[36]
New Zealand	1.4	[37]
Australia	4	[38]
Canada	5	[39]

## **1.4 Technologies for boron removal**

Wastewaters and residues discharged from industrial production generally contain boron, which affects the environment and squanders boron resources. The elimination of boric pollutants from water and the improved use of boron resources could have significant implications. Unfortunately, there is no simple and economical method for boron removal from natural and wastewaters [40]. The major source of the difficulty is that a large proportion of the boron generally exists as uncharged boric acid. In addition, boric acid changes its structure and nature with changing environmental conditions and concentration. Although this is a difficult problem, numerous methods for removing boron from aqueous solution have been explored by different researchers internationally; the approaches include precipitation [41, 42], membrane methods [43, 44], and sorption processes [45, 46].

### **1.4.1 Coagulation-precipitation**

The coagulation-precipitation process is one method for removal of borate. Using lime for borate removal has been systematically tested by Farmer and Kydd [47]. They suggested that coagulation-precipitation is affected by pH, reaction time, temperature and borate concentration in the solution. When the molar ratio of B/Ca is adjusted to 2.65, the concentration of boric acid solution could be reduced from 6200 mg/L to 450 mg/L at 25°C [48]. In 2005, Remy et al. [49] developed an optimized precipitation process for boron removal and found that the residual boron concentration in solution was reduced from 700 to less than 50 mg/L under the optimal conditions (50 g/L of powdery lime, at 90°C, for 2 h).

Not only lime, but also metal salts such as the salts of calcium, magnesium, aluminum, zinc, manganese, iron(II), and iron(III) have been investigated for

coagulation-precipitation of borate [40]. Experimental results showed that boron can be effectively removed from the solution by iron salts, with the residual concentration of boron in the solution being lower than 10 mg/L [50]. Since traditional coagulation-precipitation methods are not effective and not feasible for this purpose, new technology such as electrocoagulation was also investigated for boron removal. In 2005, Yilmaz et al.[51] studied the feasibility of the removal of boron from aqueous solution by electrocoagulation, and found that a large proportion of the boron could be removed within 2 h.

However, coagulation-precipitation not only requires a large amount of alkaline reagents (to adjust pH) and metal salts as precursors, but also results in an increased amount of sludge for disposal, this then causes another environmental problem.

#### **1.4.2 Membrane methods**

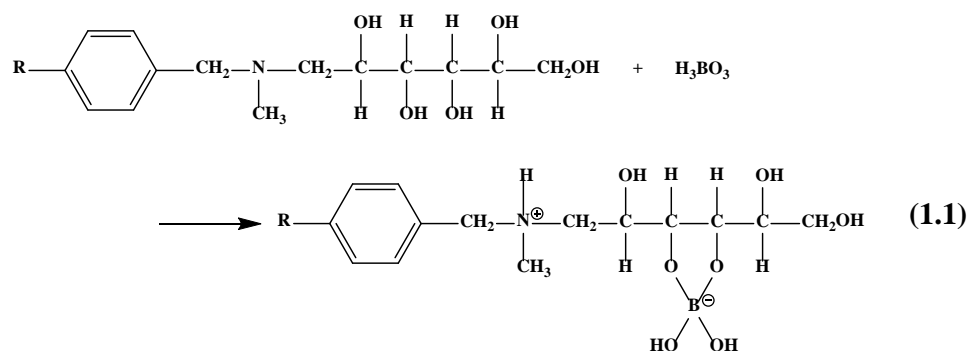
Membrane technology has been widely adopted in wastewater and drinking water treatment. Many contaminants have been successfully removed by this technology [52-54]. However, boron compounds can be found in various forms dependent on the water origin and chemistry, and membrane technology fails to remove boron to meet the drinking water guidelines, so some further process is needed [55]. Therefore, new technologies and materials (especially reverse osmosis, RO) have developed quickly to solve this problem.

The pH value for membrane processes has been adjusted to 10-11 to enhance the amount of negatively charged  $B(OH)_4^-$  in solution by many researchers. The results showed that increasing the pH above the  $pK_a$  (9.23) of boric acid can increase the rejection by 50–98% during membrane reverse osmosis [55-57]. This is because the uncharged boric acid easily permeates through the RO membrane [58, 59]. However,

the higher pH conditions may result in the precipitation of  $\text{Mg}(\text{OH})_2$  and  $\text{Ca}(\text{OH})_2$  on the surface of the RO membranes, reducing the permeability [60]. To settle this problem, multistage RO membrane processes were designed and applied for boron removal. One such system comprised a first stage RO operating without pH change, and a second stage RO operating with alkalization [2, 61]. In addition, other technologies have been used to support the RO process, including electrodialysis [62] and ion-exchange resins [63].

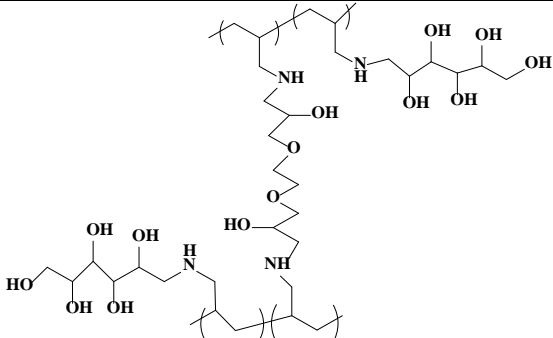
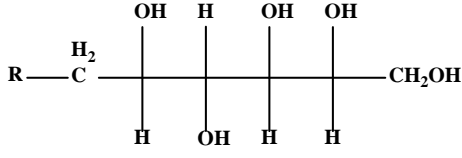
### **1.4.3 Sorption processes**

Sorption processes are useful and have the advantages of being cheaper and producing less bulky wastes, compared to other methods [64]. Therefore, as core technologies for the sorption of boron, adsorbents have been widely studied [65, 66]. Some of the most promising adsorbents for boron removal are hydroxyl-containing boron-selective adsorbents, such as boron-specific resin. Most boron-specific resins (since 1959) have been synthesized by linking N-methyl-D-glucamine (NMDG) to a copolymer of styrene and divinylbenzene. The principle, and the reason why boron compounds can be efficiently and selectively removed by NMDG resins, is that the *o*-hydroxyl groups in NMDG form complexes with borate. Because of this good performance, different NMDG resins have been commercially synthesized by different companies and launched into the market, including Amberlite IRA743 (Rohm & Haas Corporation) and Dianion CRB05 (Mitsubishi Chemicals). The theoretical capacity of commercial Amberlite IRA 743 resin was around 0.91 mmol/g [67] and Harada et al. found that the sorption ability of CRB 05 was closed to 1.3 mmol/g [68].

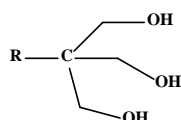


Although NMDG was very successful in boron removal, many researchers are still conducting studies to find new types of boron-specific resin. **Table 1.4** summarizes different kinds of boron-specific resins including their structures and sorption capacities. It can be noted that polyhydroxyl groups are found in these resins, similar to the groups in NDMG. In addition, another significant feature of boron-specific resins is that they can be reused by soaking in acid solution.

Table 1.4 Structures of different adsorbents and their boron sorption capacities

Researchers	Functional group	Sorption capacity (meq/L)
Harada et al.	 <p><b>Polyallylamine-beads-glucose</b></p>	2.31[68]
Tao Qi et al.	 <p><b>N-methyl-D-glucamine</b></p>	1.38 [69]

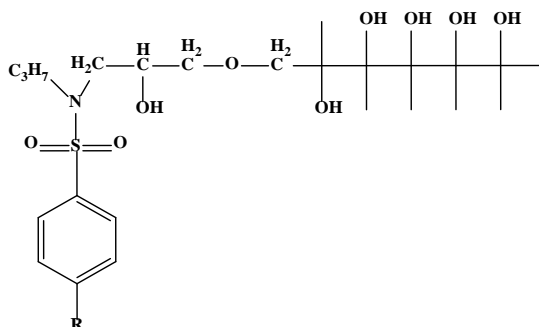
Tao Qi et al.



0.72 [69]

**2-amino-2-hydroxymethyl-1,3-propanediol**

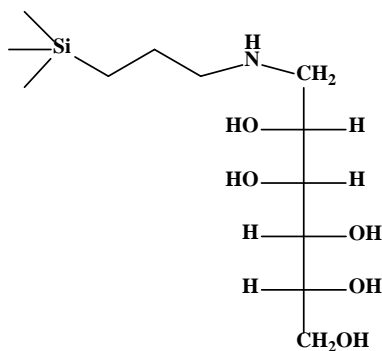
Bicak et al.



1.2[70]

**Sorbitol-Modified poly(N-glycidyl styrene sulfonamide)**

Gertrudis et al.



1.85[71]

**mannose**

However, the prices of CRB 02 and Amberlite IRA743 resins are about 397 \$/kg and 325 \$/kg; this expense limits their application. Therefore, other adsorbents with lower cost, such as activated carbon [72], metal oxides [73] and layered double hydroxides [66] have been considered and developed. For drinking water treatment, activated carbon adsorption is an effective and low-cost technological method. However, activated carbon does not have high boron adsorption capacity. In 1996 Rajaković and Ristić prepared a series of activated carbons, impregnated with calcium and barium chlorides, and citric and tartaric acids and used these materials for borate



removal [74]. The results showed that the sorption ability of borate by unmodified activated carbon was 0.14 mmol/g and the maximum sorption ability was obtained using carbons modified by tartaric acids; however, this value was only 0.33 mmol/g. This is far below the values seen for other sorbents such as metal oxides, especially magnesium oxide (MgO).

García-Soto et al. [75] found that the adsorption efficiency of borate on different metallic oxides increased as the basicity of the metallic oxides increased. According to Rodionov and Okay [76, 77], the adsorption of borate onto different metallic oxides was in the order of  $\text{ZrO}_2 > \text{La}_2\text{O}_3 > \text{SiO}_2 > \text{TiO}_2 > \text{Fe}_2\text{O}_3 > \text{Al}_2\text{O}_3$ . García-Soto et al. showed that the sorption density of borate by MgO was 50.14 mmol/g. The reaction mechanism of  $\text{H}_3\text{BO}_3/\text{B}(\text{OH})_4^-$  with MgO in the aqueous phase was investigated by Sasaki et al.[4]. In their study, the molecular form of  $\text{H}_3\text{BO}_3$  was more reactive with MgO, and acted as a trigger during reaction with MgO surface, releasing  $\text{Mg}^{2+}$  to produce an unstable complex leading to precipitation of  $\text{Mg}(\text{OH})_2$ , which is a sink for immobilization of  $\text{H}_3\text{BO}_3/\text{B}(\text{OH})_4^-$ . In addition, wastes that contain metallic oxides were also used for borate removal. Red mud was used for adsorptive removal of boron from aqueous solution by Cengeloglu et al. in 2007 [78]. They found that adsorption equilibrium was attained within 20 min and that the amount of boron adsorbed on neutralized red mud was 0.89 mmol/g at pH 7. Clay minerals are also effective natural adsorbents, and some clay minerals after simple treatment, such as calcination, showed good borate sorption performance. One publication from Sasaki et al. showed that the sorption density of borate was up to 1.5 mmol/g for calcined dolomite; greater adsorption was seen for dolomite calcined at 700°C than at 800-900°C. For a given calcination temperature, calcining under flowing Ar gas rather than static air also increased the boron adsorption [79].

While some improvements have been made in new adsorbents for boron removal, they are still not particularly effective because of the variability of borate in different waters, and the low selectivity of the adsorbents. However, these common adsorbents are much less expensive than NMG resin [80]. Therefore, if these common adsorbents can be modified to add hydroxyl-groups and develop a cheaper, more efficient and more selective sorbent, it could be interesting and useful for boron removal. In the present work, low cost, layered double hydroxides (LDHs) will be used as a base material, and try to modify them to obtain cheap, easy to synthesize materials which are capable of adsorbing boron. The unusual structure of LDHs makes them promising materials to achieve this goal.

## 1.5 Layered double hydroxides (LDHs)

### 1.5.1 Basic structure of LDHs

Layered double hydroxides (LDHs), are also described as hydrotalcite-like compounds, by reference to the naturally occurring hydrotalcite mineral. They are a family of anionic-exchangeable clays with a large variety of compositions and physicochemical properties [81] and are used in a wide variety of applications. Such compounds comprise a regular assembly of interlayer anions and positively charged metallic-hydroxide layers; their structure is similar to that of brucite ( $\text{Mg}(\text{OH})_2$ ), in which the main layers are formed by  $\text{MO}_6$  octahedra that share edges [82]; the classical structure of LDHs is shown in **Fig 1.2**. The chemical compositions of LDHs have the general expression:  $[\text{M}(\text{II})_{1-x}\text{M}(\text{III})_x(\text{OH})_2]^{x+} (\text{A}^{n-})_{x/n} \cdot m\text{H}_2\text{O}$ , in which M(II) and M(III) are the divalent and trivalent metallic cations, located in the main layer;  $\text{A}^{n-}$  is the interlayer anion; m is the number of interlayer water molecules [83, 84], and x is the molar ratio of  $\text{M}^{3+}/(\text{M}^{2+}+\text{M}^{3+})$  [85, 86].

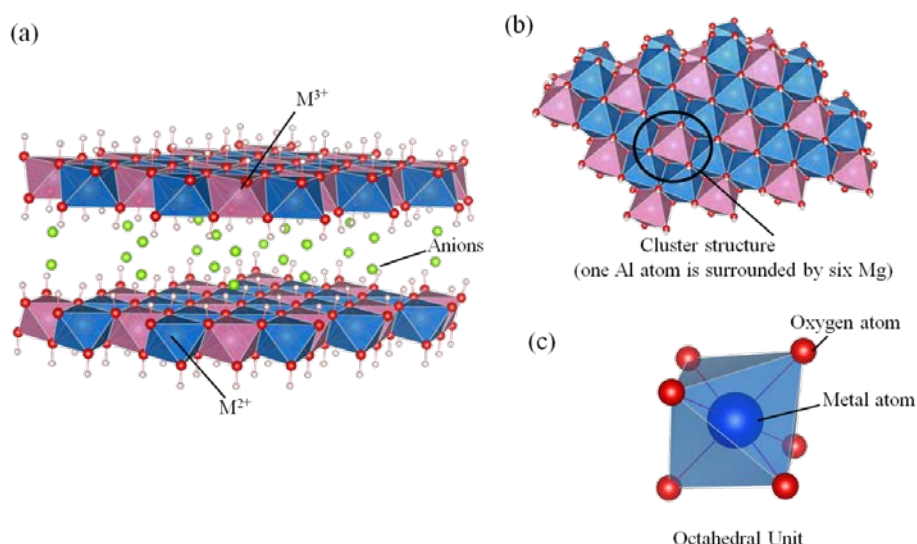


Fig. 1.2 Schematic representations of the LDH structure. (a) Oblique view; (b) Top view; (c) Octahedral unit.

### 1.5.2 Representative synthetic method of LDHs

Although the existence of hydrotalcites in the natural environment is rather limited, these materials can be easily synthesized and modified under laboratory conditions [87]. Syntheses for LDHs have progressed tremendously since they were first synthesized artificially through coprecipitation by Feitknecht et al. in 1942 [88]. At present, there are many methods that have been developed and commonly used for preparation of LDHs.

The simplest and most commonly used method is co-precipitation. Briefly, aqueous solutions of  $M^{2+}$  and  $M^{3+}$  containing the targeted anions to be incorporated into the LDHs are used as precursors [89]. To ensure simultaneous precipitation of two or more cations, the pH value of this precursor solution is usually adjusted to be alkaline and then maintained at the desired pH for co-precipitation of metals in solution. After that, a thermal aging process is often used to increase yields and crystallization of LDHs. A traditional aging process involves keeping the aqueous suspension in a

heated reactor at temperatures between 25 and 100°C for several hours or several days [89-91]. Another new and effective method is microwave treatment [92] and it was reported that microwave heating is a suitable method to rapidly prepare well-crystallized LDHs without impurities (e.g.  $\text{Mg}(\text{OH})_2$  and  $\text{Al}(\text{OH})_3$ ) [93].

Generally speaking, poorly crystalline precipitates are obtained through co-precipitation. To get well crystallized and hexagonally shaped LDHs, Costantino et al. [94] firstly invented and optimized synthetic conditions of LDHs by the urea method, where the molar ratio of urea/(M(II) + M(III)) is adjusted to 3.3. Then clear solutions were heated to 60–100°C for around 36 h. As a result, Mg-Al-LDH, Zn-Al-LDH and Ni-Al-LDH were successfully prepared, and the products displayed uniform sizes and platelet-like primary particles with well-defined hexagonal shapes [94-96] (**Fig. 1.3**). Meanwhile, the urea method can also be used for in situ hydrothermal crystallization for preparation of layered double hydroxide films on the surface of glass [97] or eggshell membranes [98].

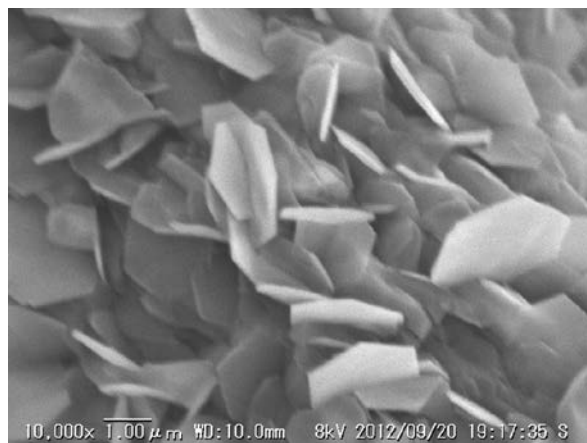


Fig. 1.3 SEM image of Mg-Al-LDH prepared by urea method in author's lab. A horizontal bar indicates 1.00  $\mu\text{m}$ .

However, the interlayer in the LDHs prepared by this method contains carbonate anions, and these LDHs cannot be easily intercalated by ion-exchange or other methods without changing their shapes and structures [99]. The metal sources for LDH synthesis by hydrothermal methods can be metallic oxides, as well as metallic salts. In 2005, Zhi et al. prepared Mg-Al-LDH from bimetallic oxides of Mg and Al upon hydrothermal treatment, and the formation mechanism has been extensively investigated [100]. Meanwhile, hydrothermal methods are also applied for preparation of LDHs with organic guest layers if the organic species have low affinity with the metallic layers of LDHs [101,102].

### 1.5.3 Cations in the metallic host layers of LDHs

Previous reports have mentioned that  $\text{M}^{2+}$  and  $\text{M}^{3+}$  cations, which have a similar ionic radius to that of Mg, can be accommodated in the brucite-like sheets and form LDHs [103,104]. So far, various divalent cations (e.g. Mg, Fe, Co, Cu, Ni and Zn) and trivalent cations (e.g. Al, Fe, Cr and Mn) have been successfully incorporated into host layers of LDHs [17, 103]. As synthesis technologies develop, more and more

new types of LDHs with containing three different metals (i.e. ternary LDHs) can be prepared, and even quaternary LDHs have been reported [105, 106]. In addition, the range of metallic atoms that can be doped into the LDH matrix may be larger than the general rules mentioned above. A novel LDH including  $\text{Li}^+$  and  $\text{Al}^{3+}$  in the host layers  $([\text{LiAl}_2(\text{OH})_6]^+(\text{A}^{n-})_{x/n} \cdot m\text{H}_2\text{O})$  has been synthesized [107, 108].

#### 1.5.4 Molar ratio of $\text{M}^{2+}/\text{M}^{3+}$ in metallic layers of LDHs

The chemical compositions of the host layers of LDHs could be adjusted during the synthetic process by simply changing the molar ratio of the raw materials. Thus, the chemical properties and charge density of the host layers can also be changed. Nonetheless, those adjustments should be within a reasonable range. Reports have proposed that single phase LDHs can be formed with stoichiometries ( $x$ ) between 0.20 and 0.33 [17]. In this range, the content of trivalent cation increases with increasing  $x$ , and this results in increasing positive charge in the host layer. In one of most commonly used LDHs, the molar ratio of  $\text{Mg}^{2+}/\text{Al}^{3+}$  in Mg-Al LDH is generally in the range of 2.0–4.0. Because the atomic size of Al is smaller than that of Mg, the cell parameters  $a$  and  $c$  which are related to the distance between neighboring atoms and the interlayer distance are decreased when the molar ratio of  $\text{Mg}^{2+}/\text{Al}^{3+}$  is decreased. This leads to a decrease in electrostatic attraction of the host layers when fewer divalent Mg ions are substituted with trivalent Al in the LDHs.

#### 1.5.5 Anions as intercalators in LDHs

Once some of the  $\text{M}^{2+}$  cations in the brucite-like sheets are substituted by  $\text{M}^{3+}$ , anions are attracted into the interlayer of LDHs to balance the charge. The type of anions in the layers can be adjusted during the synthetic process or changed by ion-exchange from the already-generated products as required. Typical anions such as  $\text{NO}_3^-$ ,  $\text{Cl}^-$ ,  $\text{SO}_4^{2-}$ ,  $\text{OH}^-$  and  $\text{CO}_3^{2-}$  have been intercalated into LDHs. Around 20 years

ago, systematic studies on the properties of LDHs were carried by Miyata [109-111], who found that the attractive force between poly-valent anions and the host layer was far greater than that between monovalent anions and the host layer. The affinities between the host layer and anions were in the sequence  $\text{CO}_3^{2-} > \text{SO}_4^{2-} > \text{OH}^- > \text{F}^- > \text{Cl}^- > \text{Br}^- > \text{NO}_3^- > \text{I}^-$ . In addition, with changes in the total amount of  $\text{OH}^-$  and the types of anions in the interlayer of LDHs, the interlayer distance is varied. Different interlayer distances for common anions were summarized by Miyata (and reproduced in **Table 1.5**) [110]. In general, the size of anions and their valence state influence the interlayer distance, with the size having a particularly strong effect. For example, Bruna et al. intercalated dodecylsulfate into the structure of Mg-Al-LDH. The interlayer distance was expanded to 25.9 Å, as a result of the molecular size of dodecylsulfate (**Fig. 1.4**) [112].

Table 1.5 Basal spacings ( $d$ ) of LDHs intercalated with different anions by Miyata [110]

Anions	$\text{OH}^-$	$\text{F}^-$	$\text{Cl}^-$	$\text{Br}^-$	$\text{NO}_3^-$	$\text{I}^-$	$\text{CO}_3^{2-}$	$\text{SO}_4^{2-}$
Basal spacing (Å)	7.55	7.66	7.86	7.95	8.79	8.16	7.65	8.58

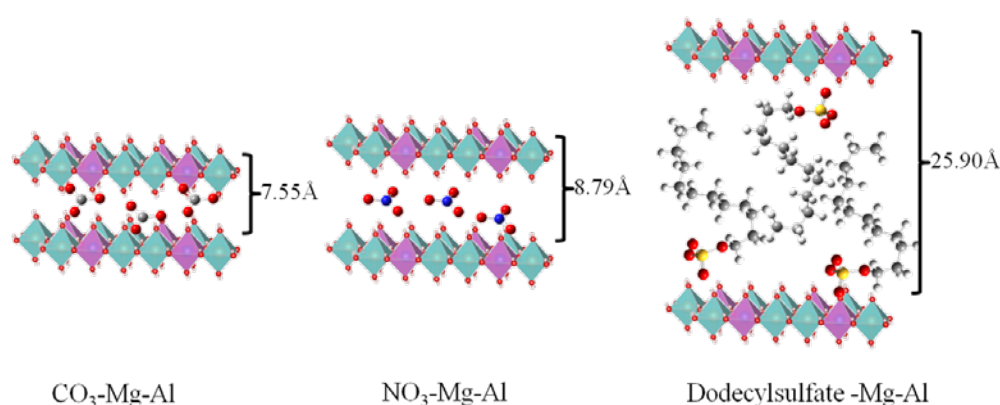


Fig. 1.4 Schematic illustration of Mg-Al type LDHs with different anions, resulting in different interlayer spacings.

### 1.5.6 Specific properties of LDHs

Because of their unusual structures, hydrotalcite and hydrotalcite-like compounds have the following peculiar properties:

#### (1) Adjustability of the chemical constituents in the metal hydroxide layers

The  $M^{2+}$  and  $M^{3+}$  in the metal hydroxide host layer of LDHs can be replaced with other metallic ions of the same chemical valence and similar ionic radius, thus forming new layered compounds with different properties.

#### (2) Adjustability of anions in the interlayer

The anions in LDHs can be replaced by other inorganic and organic anions, so that LDHs have a supermolecular intercalated structure with multiple applications and tailored performance. By adjusting the proportions of divalent and trivalent metal ions, one can adjust the electric charge density in the host layers, thus changing the number of negative ions in the guest layers to design the required material [89, 103].

#### (3) Thermal stability

LDHs can be decomposed when heated. The thermal decomposition leads to desorption of interlayer water molecules, depriving the anion in the guest layer of water, dehydrating the hydroxyls in the host layer, and generating new crystals. Taking carbonate intercalated LDHs as an example, when heated to lower than 200°C in the air atmosphere, the LDHs only lose the interlayer water, and the remaining structure is unaffected; when heated to 250-450°C, the interlayer water continues to evaporate, the hydroxyl dehydrates slightly and the carbonates in the interlayer decompose; when heated to higher than 450°C, almost all interlayer water evaporates,



and most carbonates become CO<sub>2</sub>, accompanied by the formation of bimetallic oxide [113, 114].

#### (4) Memory effect

After calcination at a certain temperature, LDHs turn into bimetallic oxides. The bimetallic oxides can then be transformed back into the orderly layered structure of LDHs by immersion in a solution containing specific anions [115, 116]. In general, if LDHs are calcined at temperatures under 500°C, the crystal structure can be restored. Taking Mg-Al-LDH as an example, after being baked at less than 500°C, the Mg-Al-LDH can be restored by soaking the calcined product in water. This unique property is important for absorption. When the calcination temperature is over 1000°C, a product with spinel structure is formed, which cannot be restored fully [117].

## 1.6 Applications of layered double hydroxide to sorbents

For the past few years, LDHs have drawn much attention because of their adjustable chemical composition and excellent performance. Their unusual crystal structure, in which the metallic layer in the LDHs is positively charged and contains layers of exchangeable anions, allows these hydrotalcite-like compounds to be applied in environmental remediation as anion absorbents (**Fig. 1.5**). Many studies about the sorption of toxic contaminants, including phosphate [118], arsenic [119], selenite [120], fluorine [121], chromate [122] and borate [123] have been reported.

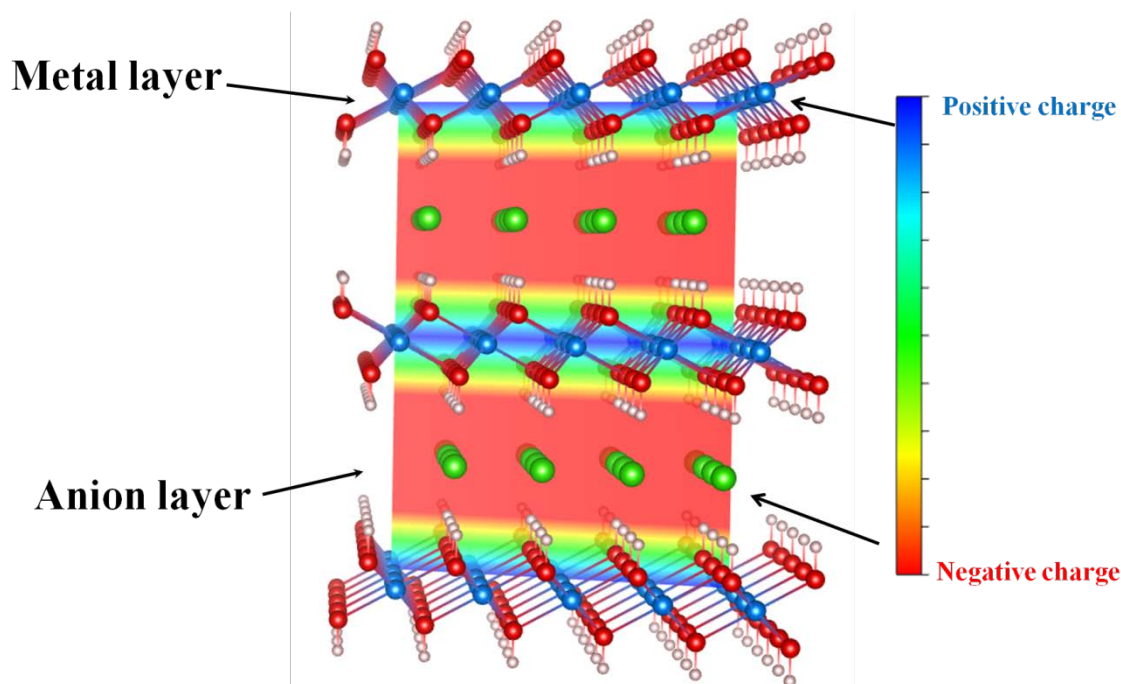


Fig. 1.5 Electronic density distribution in LDHs by DFT calculation (software for calculation: Abinit [124]; visualization software:VESTA [125], resolution: 2Å).

Adsorption of Cr(VI) by various uncalcined and calcined layered double hydroxides, including Mg-Al, Ni-Al and Zn-Cr types was investigated by Goswamee et al. [126]. The adsorption rate and density of  $\text{Cr}_2\text{O}_7^{2-}$  through ion-exchange by uncalcined LDHs was slower and smaller than that of calcined samples, in which adsorption occurs through rehydration. In addition, calcined Mg-Al-LDH showed higher adsorption capacity than either Ni-Al-LDH or Zn-Cr-LDH. Similar results were also found by Das et al., who studied adsorption of phosphate by various calcined layered double hydroxides (LDHs) such as Mg-Al, Zn-Al, Ni-Al, Co-Al, Mg-Fe, Zn-Fe, Ni-Fe and Co-Fe [118].

In addition, the removal capacity of calcined LDHs is generally higher than that of LDHs without calcination. Cheng et al. examined phosphate adsorption by Zn-Al LDHs, both uncalcined and calcined at different temperatures [127]. In their study,

samples calcined samples at 300°C showed higher phosphate uptake than uncalcined Zn-Al LDHs. Adsorption of phosphate onto LDHs calcined at different temperatures could be attributed to a combination of different mechanisms, such as anion exchange and co-precipitation during the regeneration of LDHs. Yang et al. investigated the removal of traces of arsenic and selenium from solution by calcined and uncalcined Mg-Al-LDH [128], and showed that the calcined LDHs could adsorb more arsenic and selenium than the uncalcined LDHs. This was because calcination increased the surface area, and also probably because the interlayer of the calcined LDHs contains fewer carbonate anions than that of the uncalcined LDHs.

In relation to boron removal, Ferreira et al. prepared LDHs with different kinds of metallic ions (Mg-Al-LDH and Mg-Fe-LDH) and evaluated their boron-removal efficiency [46]. In 2005, they found that the sorption of borate by Mg-Al-LDH was 14.0 mg/g; this was higher than that of Mg-Fe-LDH (3.6 mg/g) since removal of borate by Mg-Fe LDHs only occurs by surface adsorption. In 2010, Kentjono et al. [66] applied this method for treating real optoelectronic wastewater containing high concentrations of boron and iodine. The maximum boron uptake capacity was around 37.90 mg/g and LDHs showed better performance for removal of boron than other. This result is consisting to previously reported methods [66, 123] and demonstrated that LDHs were very effective for boron removal and showed their potential for application as a pretreatment process to reduce the boron concentration in wastewater before biological treatment.

Moreover, hydrotalcite-like materials with the organic anions in their interlayers have gradually becomes a focus of a significant amount of research. After the negative organic ions are introduced, the hydrotalcite interlayer can become a functional composite with different performance, thus greatly extending the range of

applications of hydrotalcite in the area of absorption. After the organic metallic complex anions are introduced into the hydrotalcite interlayer, some heavy-metal positive ions can form more stable compounds with the complex anions and finally be removed by the hydrotalcite-like matter. Rojas et al. [129] adopted ion-exchange to introduce  $[\text{Zn}(\text{EDTA})]^{2-}$  into the Zn-Al hydrotalcite interlayer and used the resulting composite to remove copper ions from solution. The hydrotalcite quickly absorbed the copper ions; adsorption equilibrium was reached within 30 min, with the concentration of Cu falling to less than 0.05 mmol/L. Kameda et al. used citric acid, tartaric acid and malic acid as interlayer anions in hydrotalcite. Their organic-LDHs had special sequestration performance, capturing  $\text{Cu}^{2+}$  and  $\text{Cd}^{2+}$  from water [130]. By substituting the inorganic anions in the interlayer with specific organic anions, one can obtain a special interlayer hydrotalcite with tailored functional performance. These materials can be a cost-effective way of removing particular ions from solution, and are thus worth developing and testing.

## **1.7 Shortcoming of traditions LDHs without modification**

(1) LDHs are more prone to absorb negative ions with high negative valences. In practical applications, the water body often contains various interfering anions, thus resulting in a decrease of the absorption efficiency of the target anions on the LDHs.

(2) LDH particles are powder-like, and too small to be efficiently applied to practical water treatment.

## **1.8 Objective and outline of this thesis**

Along with economic development and the exploitation of boron resources in the world, mass production and use of electronic products and pharmaceuticals have

brought boron into our living environment. Although there are many aspects of the effects of boron on the human body that are unclear at present, it is essential to develop effective ways of removing boron from wastewater and drinking water.

Layered double hydroxides (LDHs) are a type of adsorbent that has many advantages over traditional remediation technologies. Adding an organic interlayer to an LDH can improve its performance and extend the range of potential applications of LDHs – such materials have become very attractive in environmental research. There are many reports on synthesis and characterization of LDHs with organic anions and their application to pollutant removal. Although the use of LDHs for boron removal has been reported, LDHs still have some shortcomings for practical applications.

Therefore, this study firstly explored the feasibility of preparing LDHs by using natural minerals (dolomite) as Mg resource. Then, gluconate was chosen as the interlayer anion in the LDHs because it can rapidly react with boric acid, and thus is expected to improve the selectivity of LDHs for borate removal, as well as enhance the stability of the resultant complexes. Finally, the LDHs were immobilized onto filter paper, to make them easier to use in practical water-treatment systems. The effects of solution conditions including concentration, pH, and temperature on the removal of borate were studied and various characterization methods used to analyze the sorption mechanism of borate onto different LDHs. In addition, to simulate practical situations, different interfering anions were injected into borate solutions and their effects on borate removal by LDHs examined to test the selectivity of the products.

**The major aspects of the research in this thesis are:**

(1) Taking natural dolomite as the raw material source of magnesium for the synthesis of LDH, and using co-precipitation with aluminum nitrate, Mg-Al type LDHs were prepared. Afterwards, the material were characterized and their ability to adsorb boron was studied under different conditions. The details of the sorption process were examined through XRD and  $^{11}\text{B}$ -NMR.

(2) Through a microwave-assisted hydrothermal treatment, cheap and eco-friendly gluconate was intercalated into LDHs in a one-step synthesis. The use of these materials to remove borate was examined under a variety of conditions. The selectivity of boron removal in the presence of other competing or interfering anions was also studied. Through NMR and XRD analysis, the mechanism of borate removal by this new type of LDHs was discussed.

(3) An in-situ synthetic method was used to grow LDHs with different interlayer anions onto cellulose filter paper. Then gluconate was inserted into the interlayer of the LDHs by interlayer ion-exchange. Finally, these materials were used for borate removal, and their selectivity was also examined.

## References:

- [1] S. Nishihama, Y. Sumiyoshi, T. Ookubo, K. Yoshizuka, Adsorption of boron using glucamine-based chelate adsorbents, *Desalination*, 310 (2013) 81-86.
- [2] J. Wolska, M. Bryjak, Methods for boron removal from aqueous solutions-A review, *Desalination*, 310 (2013) 18-24.
- [3] M. Badruk, N. Kabay, M. Demircioglu, H. Mordogan, U. Ipekoglu, Removal of boron from wastewater of geothermal power plant by selective ion-exchange resins. I. Batch sorption – elution studies, *Sep. Sci. Technol.*, 34 (1999) 2553-2569.
- [4] K. Sasaki, X.H. Qiu, S. Moriyama, C. Tokoro, K. Ideta, J. Miyawaki, Characteristic sorption of  $\text{H}_3\text{BO}_3/\text{B}(\text{OH})_4^-$  on magnesium oxide, *Mater. Trans.*, 54 (2013) 1809-1817.

- [5] J.G. Penland, The importance of boron nutrition for brain and psychological function, *Biol. Trace Elem. Res.*, 66 (1998) 299-317.
- [6] F.H. Nielsen, B.J. Stoecker, J.G. Penland, Boron as a dietary factor for bone microarchitecture and central nervous system function, Springer, 2007, pp.277-290.
- [7] P. Wójcik, R. Dris, R. Niskanen, S.M. Jain, The importance of boron in apple production., *Crop management and postharvest handling of horticultural crops. Vol 3: Crop fertilization, nutrition and growth*, (2003) 77-92.
- [8] M. Tariq, C. Mott, The significance of boron in plant nutrition and environment-A review, *J.Agron.*, 6 (2007) 1-10.
- [9] P.H. Brown, N. Bellaloui, M.A. Wimmer, E.S. Bassil, J. Ruiz, H. Hu, H. Pfeffer, F. Dannel, V. Römheld, Boron in plant biology, *Plant Biol.*, 4 (2002) 205-223.
- [10] R.E. Newnham, Essentiality of boron for healthy bones and joints, *Environ. Health Persp.*, 102 (1994) 83-85.
- [11] Y. Bai, C.D. Hunt, Dietary boron enhances efficacy of cholecalciferol in broiler chicks, *J. Trace. Elem. Exp. Med.*, 9 (1996) 117-132.
- [12] T. Itakura, R. Sasai, H. Itoh, Precipitation recovery of boron from wastewater by hydrothermal mineralization, *Water Res.*, 39 (2005) 2543-2548.
- [13] M. Özdemir, İ. Kıpçak, Recovery of boron from borax sludge of boron industry, *Miner. Eng.*, 23 (2010) 685-690.
- [14] P.P. Power, W.G. Woods, The chemistry of boron and its speciation in plants, *Plant Soil*, 193 (1997) 1-13.
- [15] M.Marston, A boron selective resin for seawater desalination, *Proceedings of European Desalination Society Conference on Desalination and the Environment*, Santa Margherita Ligure, Italy, 2005.
- [16] D.E. Garrett, Borates. Handbook of deposits, properties, processing and Use, 1998.
- [17] F.L. Theiss, G.A. Ayoko, R.L. Frost, Removal of boron species by layered double hydroxides: A review, *J. Colloid Interf. Sci.*, 402 (2013) 114-121.
- [18] H. Tsai, S. Lo, J. Kuo, Using pretreated waste oyster and clam shells and microwave hydrothermal treatment to recover boron from concentrated wastewater, *Bioresource Technol.*, 102 (2011) 7802-7806.

- [19] N. Nadav, Boron removal from seawater reverse osmosis permeate utilizing selective ion exchange resin, *Desalination*, 124 (1999) 131-135.
- [20] L. Melnyk, V. Goncharuk, I. Butnyk, E. Tsapiuk, Boron removal from natural and wastewaters using combined sorption/membrane process, *Desalination*, 185 (2005) 147-157.
- [21] R.O. Nable, G.S. Bañuelos, J.G. Paull, Boron toxicity, *Plant Soil*, 193 (1997) 181-198.
- [22] K.W. McLeod, T.G. Ciravolo, Boron tolerance and potential boron removal by bottomland tree seedlings, *Wetlands*, 18 (1998) 431-436.
- [23] R.J. Reid, J.E. Hayes, A. Post, J.C.R. Stangoulis, R.D. Graham, A critical analysis of the causes of boron toxicity in plants, *Plant, Cell, Environ.*, 27 (2004) 1405-1414.
- [24] J. C. Cristóbal, J. Rexach, A. González Fontes, Boron in plants: deficiency and toxicity, *Journal of Integr. Plant Biol.*, 50 (2008) 1247-1255.
- [25] J. Takano, K. Miwa, T. Fujiwara, Boron transport mechanisms: collaboration of channels and transporters, *Trends Plant Sci.*, 13 (2008) 451-457.
- [26] N. Hilal, G.J. Kim, C. Somerfield, Boron removal from saline water: A comprehensive review, *Desalination*, 273 (2011) 23-35.
- [27] I.P. Lee, R.J. Sherins, R.L. Dixon, Evidence for induction of germinal aplasia in male rats by environmental exposure to boron, *Toxicol. Appl. Pharm.*, 45 (1978) 577-590.
- [28] W.W. Ku, R.E. Chapin, R.F. Moseman, R.E. Brink, K.D. Pierce, K.Y. Adams, Tissue disposition of boron in male Fischer rats, *Toxicol. Appl. Pharm.*, 111 (1991) 145-151.
- [29] C.H. Linden, A.H. Hall, K.W. Kulig, B.H. Rumack, Acute ingestions of boric acid, *Clinical Toxicology*, 24 (1986) 269-279.
- [30] F.H. Nielsen, Boron in human and animal nutrition, *Plant Soil*, 193 (1997) 199-208.
- [31] World Health Organization, *Guidelines for Drinking-water Quality*, 2011.
- [32] Norwegian Institute of Public Health, *Seawater Desalination Facility on Okinawa* in, 2006.
- [33] China's ministry of environmental protection, *GB 5749-2006*, 2006.
- [34] Saudi Arabian Standards Organization, *Bottled drinking water*, in, Saudi Arabian Standards Organization, 2000.



- [35] US Environmental Protection Agency, Edition of the drinking water standards and health advisories, in, Washington, DC, 2006.
- [36] European Economic Area, The quality of water intended for human consumption, in, Council Directive, 98/83/EC, 1998.
- [37] New Zealand Ministry of Health, Drinking-water Standards for New Zealand 2005, 2005.
- [38] National Health and Medical Research Council, Draft-Australian drinking water guidelines, in, National Health and Medical Research Council, 2009.
- [39] Committee on Drinking Water, Guidelines for canadian drinking water quality summary table in, 2008.
- [40] Y. Xu, J. Jiang, Technologies for boron removal, *Ind. Eng. Chem. Res.*, 47 (2007) 16-24.
- [41] A.E. Yilmaz, R. Boncukcuoğlu, M.M. Kocakerim, A quantitative comparison between electrocoagulation and chemical coagulation for boron removal from boron-containing solution, *J. Hazard. Mater.*, 149 (2007) 475-481.
- [42] N. Bektaş, S. Öncel, H.Y. Akbulut, A. Dimoglo, Removal of boron by electrocoagulation, *Environ. Chem. Lett.*, 2 (2004) 51-54.
- [43] M. R. Pastor, A. Ferrándiz Ruiz, M.F. Chillón, D. P. Rico, Influence of pH in the elimination of boron by means of reverse osmosis, *Desalination*, 140 (2001) 145-152.
- [44] H. Hyung, J. Kim, A mechanistic study on boron rejection by sea water reverse osmosis membranes, *J. Membrane Sci.*, 286 (2006) 269-278.
- [45] R. Kunin, A.F. Preuss, Characterization of a boron-specific ion exchange resin, *Ind. Eng. Chem. Res.*, 3 (1964) 304-306.
- [46] O.P. Ferreira, S.G. de Moraes, N. Durán, L. Cornejo, O.L. Alves, Evaluation of boron removal from water by hydrotalcite-like compounds, *Chemosphere*, 62 (2006) 80-88.
- [47] J.B. Farmer, J.A. Kydd, Removal of boron from solution with inorganic precipitants, Part III: Lime, Technical Report TR-78-14, Borax Technical, Ltd, London, 1978.
- [48] J.A. Kydd, Removal of boron from solution with inorganic precipitants, Part XII, restricted quantities of Lime; Technical Report TR-80-25, Borax Technical, Ltd., London, 1980.

- [49] P. Remy, H. Muhr, E. Plasari, I. Ouerdiane, Removal of boron from wastewater by precipitation of a sparingly soluble salt, *Environ. Prog.*, 24 (2005) 105-110.
- [50] J.B. Farmer, J.A. Kydd, Removal of boron from solution with inorganic precipitants, Technical Report TR-80-6, London, 1980.
- [51] A.E. Yilmaz, R. Boncukcuoğlu, M.M. Kocakerim, B. Keskinler, The investigation of parameters affecting boron removal by electrocoagulation method, *J. Hazard. Mater.*, 125 (2005) 160-165.
- [52] P.I. Ndiaye, P. Moulin, L. Dominguez, J.C. Millet, F. Charbit, Removal of fluoride from electronic industrial effluent by RO membrane separation, *Desalination*, 173 (2005) 25-32.
- [53] H.A. Qdais, H. Moussa, Removal of heavy metals from wastewater by membrane processes: a comparative study, *Desalination*, 164 (2004) 105-110.
- [54] P. Xu, M. Capito, T.Y. Cath, Selective removal of arsenic and monovalent ions from brackish water reverse osmosis concentrate, *J. Hazard. Mater.*, 260 (2013) 885-891.
- [55] B. Teychene, G. Collet, H. Gallard, J. Croue, A comparative study of boron and arsenic (III) rejection from brackish water by reverse osmosis membranes, *Desalination*, 310 (2013) 109-114.
- [56] D. Prats, M.F. Chillón-Arias, M. Rodríguez-Pastor, Analysis of the influence of pH and pressure on the elimination of boron in reverse osmosis, *Desalination*, 128 (2000) 269-273.
- [57] M. Taniguchi, Y. Fusaoka, T. Nishikawa, M. Kurihara, Boron removal in RO seawater desalination, *Desalination*, 167 (2004) 419-426.
- [58] J. Redondo, M. Busch, J. De Witte, Boron removal from seawater using FILMTEC™ high rejection SWRO membranes, *Desalination*, 156 (2003) 229-238.
- [59] H. Koseoglu, N. Kabay, M. Yüksel, M. Kitis, The removal of boron from model solutions and seawater using reverse osmosis membranes, *Desalination*, 223 (2008) 126-133.
- [60] D. Hasson, H. Shemer, I. Brook, I. Zaslavski, R. Semiat, C. Bartels, M. Wilf, Scaling propensity of seawater in RO boron removal processes, *J. Membrane Sci.*, 384 (2011) 198-204.

- [61] P. Glueckstern, M. Priel, Optimization of boron removal in old and new SWRO systems, *Desalination*, 156 (2003) 219-228.
- [62] M.F. Chillón Arias, L. Valero I Bru, D. Prats Rico, P. Varó Galvañ, Approximate cost of the elimination of boron in desalinated water by reverse osmosis and ion exchange resins, *Desalination*, 273 (2011) 421-427.
- [63] M.F. Chillón Arias, L. Valero I Bru, D. Prats Rico, P. Varó Galvañ, Approximate cost of the elimination of boron in desalinated water by reverse osmosis and ion exchange resins, *Desalination*, 273 (2011) 421-427.
- [64] P. Koilraj, K. Srinivasan, High Sorptive Removal of Borate from Aqueous Solution Using Calcined ZnAl Layered Double Hydroxides, *Ind. Eng. Chem. Res.*, 50 (2011) 6943-6951.
- [65] Y. Cengeloglu, A. Tor, G. Arslan, M. Ersoz, S. Gezgin, Removal of boron from aqueous solution by using neutralized red mud, *J. Hazard. Mater.*, 142 (2007) 412-417.
- [66] L. Kentjono, J.C. Liu, W.C. Chang, C. Irawan, Removal of boron and iodine from optoelectronic wastewater using Mg – Al (NO<sub>3</sub>) layered double hydroxide, *Desalination*, 262 (2010) 280-283.
- [67] L. Wang, T. Qi, Z. Gao, Y. Zhang, J. Chu, Synthesis of N-methylglucamine modified macroporous poly(GMA-co-TRIM) and its performance as a boron sorbent, *React. Funct. Polym.*, 67 (2007) 202-209.
- [68] A. Harada, T. Takagi, S. Kataoka, T. Yamamoto, A. Endo, Boron adsorption mechanism on polyvinyl alcohol, *Adsorption*, 17 (2011) 171-178.
- [69] T. Qi, A. Sonoda, Y. Makita, H. Kanoh, K. Ooi, T. Hirotsu, Synthesis and borate uptake of two novel chelating resins, *Ind. Eng. Chem. Res.*, 41 (2002) 133-138.
- [70] N. Bicak, B.F. Senkal, Sorbitol-modified poly (N-glycidyl styrene sulfonamide) for removal of boron, *J. Appl. Polym. Sci.*, 68 (1998) 2113-2119.
- [71] G. Rodríguez-López, M.D. Marcos, R. Martínez-Máñez, F. Sancenón, J. Soto, L.A. Villaescusa, D. Beltrán, P. Amorós, Efficient boron removal by using mesoporous matrices grafted with saccharides, *Chem. Commun.*, (2004) 2198-2199.
- [72] L.V. Rajakovi, M.D. Risti, Sorption of boric acid and borax by activated carbon impregnated with various compounds, *Carbon*, 34 (1996) 769-774.

- [73] M. Konstantinou, G. Kassetas, I. Pashalidis, Boron adsorption on alumina ( $\text{Al}_2\text{O}_3$ ) and magnesia ( $\text{MgO}$ ) in aqueous solutions: a comparative study, *International Journal of Envir.*, 6 (2006) 466-479.
- [74] L.V. Rajaković, M.D. Ristić, Sorption of boric acid and borax by activated carbon impregnated with various compounds, *Carbon*, 34 (1996) 769-774.
- [75] M.M. de la Fuente García-Soto, E. Muñoz Camacho, Boron removal by means of adsorption processes with magnesium oxide—Modelization and mechanism, *Desalination*, 249 (2009) 626-634.
- [76] A.I. Rodionov, O.M. Voitova, N.Y. Romanov, The current state of the problem of the elimination of boron from waste waters, *Russ. Chem. Rev.*, 60 (1991) 1271.
- [77] O. Okay, H. Güçlü, E. Soner, T. Balkaş, Boron pollution in the Simav River, Turkey and various methods of boron removal, *Water Res.*, 19 (1985) 857-862.
- [78] Y. Cengeloglu, A. Tor, G. Arslan, M. Ersoz, S. Gezgin, Removal of boron from aqueous solution by using neutralized red mud, *J. Hazard. Mater.*, 142 (2007) 412-417.
- [79] K. Sasaki, X.H. Qiu, Y. Hosomomi, S. Moriyama, Tsuyoshi, Hirajima, Effect of natural dolomite calcination temperature on sorption of borate onto calcined products, *Micropor Mesopor Mat.*, 171 (2013) 1-8.
- [80] H. Liu, B. Qing, X. Ye, Q. Li, K. Lee, Z. Wu, Boron adsorption by composite magnetic particles, *Chem. Eng. J.*, 151 (2009) 235-240.
- [81] S. Cadars, G. Layrac, C. Gerardin, M. Deschamps, J.R. Yates, D. Tichit, D. Massiot, Identification and quantification of defects in the cation ordering in Mg/Al layered double hydroxides, *Chem. Mater.*, 23 (2011) 2821-2831.
- [82] M. Del Arco, S. Gutiérrez, C. Martín, V. Rives, J. Rocha, Synthesis and characterization of layered double hydroxides (LDH) intercalated with non-steroidal anti-inflammatory drugs (NSAID), *J. Solid State Chem.*, 177 (2004) 3954-3962.
- [83] F. Bruna, R. Celis, M. Real, J. Cornejo, Organo/LDH nanocomposite as an adsorbent of polycyclic aromatic hydrocarbons in water and soil-water systems, *J. Hazard. Mater.*, (2012).
- [84] X. Guo, F. Zhang, D.G. Evans, X. Duan, Layered double hydroxide films: synthesis, properties and applications, *Chem. Commun.*, 46 (2010) 5197-5210.

- [85] F. Cavani, F. Trifirò, A. Vaccari, Hydrotalcite-type anionic clays: Preparation, properties and applications., *Catal. Today*, 11 (1991) 173-301.
- [86] A.I. Khan, D.O. Hare, Intercalation chemistry of layered double hydroxides: recent developments and applications, *J. Mater. Chem.*, 12 (2002) 3191-3198.
- [87] D. Wan, H. Liu, R. Liu, J. Qu, S. Li, J. Zhang, Adsorption of nitrate and nitrite from aqueous solution onto calcined (Mg–Al) hydrotalcite of different Mg/Al ratio, *Chem. Eng. J.*, 195–196 (2012) 241-247.
- [88] W. Feitknecht, Über die Bildung von Doppelhydroxyden zwischen zwei- und dreiwertigen Metallen, *Helv. Chim. Acta*, 25 (1942) 555-569.
- [89] X. Duan, D.G. Evans, Layered double hydroxides, Springer, 2006.
- [90] F. Cavani, F. Trifirò, A. Vaccari, Hydrotalcite-type anionic clays: Preparation, properties and applications., *Catal. Today*, 11 (1991) 173-301.
- [91] J.S. Valente, F. Tzompantzi, J. Prince, J.G. Cortez, R. Gomez, Adsorption and photocatalytic degradation of phenol and 2, 4 dichlorophenoxyacetic acid by Mg – Zn – Al layered double hydroxides, *Appl. Catal. B: Environ.*, 90 (2009) 330-338.
- [92] Z. Yang, K. Choi, N. Jiang, S. Park, Microwave synthesis of hydrotalcite by urea hydrolysis, *B.Kor. Chem Soc.*, 28 (2007) 2029.
- [93] S. Möhmel, I. Kurzawski, D. Uecker, D. Müller, W. Gessner, The influence of a hydrothermal treatment using microwave heating on the crystallinity of layered double hydroxides, *Cryst. Res. Technol.*, 37 (2002) 359-369.
- [94] U. Costantino, F. Marmottini, M. Nocchetti, R. Vivani, New Synthetic routes to hydrotalcite-like compounds–characterisation and properties of the obtained materials, *Eur. J. Inorg. Chem.*, 1998 (1998) 1439-1446.
- [95] M.M. Rao, B.R. Reddy, M. Jayalakshmi, V.S. Jaya, B. Sridhar, Hydrothermal synthesis of Mg–Al hydrotalcites by urea hydrolysis, *Mater. Res. Bull.*, 40 (2005) 347-359.
- [96] M. Ogawa, H. Kaiho, Homogeneous precipitation of uniform hydrotalcite particles, *Langmuir*, 18 (2002) 4240-4242.
- [97] X. Guo, F. Zhang, S. Xu, D.G. Evans, X. Duan, Preparation of layered double hydroxide films with different orientations on the opposite sides of a glass substrate by in situ hydrothermal crystallization, *Chem. Commun.*, 44 (2009) 6836-6838.

- [98] X. Guo, F. Zhang, Q. Peng, S. Xu, X. Lei, D.G. Evans, X. Duan, Layered double hydroxide/eggshell membrane: An inorganic biocomposite membrane as an efficient adsorbent for Cr(VI) removal, *Chem. Eng. J.*, 166 (2011) 81-87.
- [99] N. Iyi, T. Matsumoto, Y. Kaneko, K. Kitamura, Deintercalation of carbonate ions from a hydrotalcite-like compound: Enhanced decarbonation using acid-salt mixed solution, *Chem. Mater.*, 16 (2004) 2926-2932.
- [100] Z.P. Xu, G.Q.M. Lu, Hydrothermal synthesis of layered double hydroxides (LDHs) from mixed MgO and Al<sub>2</sub>O<sub>3</sub>: LDH formation mechanism, *Chem. Mater.*, 17 (2005) 1055-1062.
- [101] D. Wang, F.R. Costa, A. Vyalikh, A. Leuteritz, U. Scheler, D. Jehnichen, U. Wagenknecht, L. Haussler, G. Heinrich, One-step synthesis of organic LDH and its comparison with regeneration and anion exchange method, *Chem. Mater.*, 21 (2009) 4490-4497.
- [102] R. Zhang, H. Huang, W. Yang, X. Xiao, Y. Hu, Preparation and characterization of bio-nanocomposites based on poly (3-hydroxybutyrate-co-4-hydroxybutyrate) and CoAl layered double hydroxide using melt intercalation, *Compos Part A: Appl Sci Manufac*, 43 (2012) 547-552.
- [103] K. Goh, T. Lim, Z. Dong, Application of layered double hydroxides for removal of oxyanions: A review, *Water Res.*, 42 (2008) 1343-1368.
- [104] H. Yan, J. Lu, M. Wei, J. Ma, H. Li, J. He, D.G. Evans, X. Duan, Theoretical study of the hexahydrated metal cations for the understanding of their template effects in the construction of layered double hydroxides, *J. Mol. Struc-Theochem*, 866 (2008) 34-45.
- [105] S. Velu, K. Suzuki, T. Osaki, Selective production of hydrogen by partial oxidation of methanol over catalysts derived from CuZnAl-layered double hydroxides, *Catal. Lett.*, 62 (1999) 159-167.
- [106] Y. Chen, F. Li, S. Zhou, J. Wei, Y. Dai, Y. Chen, Structure and photoluminescence of Mg-Al-Eu ternary hydrotalcite-like layered double hydroxides, *J. Solid State Chem.*, 183 (2010) 2222-2226.
- [107] A.M. Fogg, J.S. Dunn, S. Shyu, D.R. Cary, D. O'Hare, Selective ion-exchange intercalation of isomeric dicarboxylate anions into the layered double hydroxide [LiAl<sub>2</sub>(OH)<sub>6</sub>]Cl·H<sub>2</sub>O, *Chem. Mater.*, 10 (1998) 351-355.

- [108] X. Hou, A.G. Kalinichev, R.J. Kirkpatrick, Interlayer structure and dynamics of Cl-LiAl<sub>2</sub>-layered double hydroxide: <sup>35</sup>Cl-NMR observations and molecular dynamics modeling, *Chem. Mater.*, 14 (2002) 2078-2085.
- [109] S. Miyata, T. Kumura, Synthesis of new hydrotalcite-like compounds and their physico-chemical properties, *Chem. Lett.*, (1973) 843-848.
- [110] S. Miyata, Anion-exchange properties of hydrotalcite-like compounds, *Clay. Clay Miner.*, 31 (1983) 305-311.
- [111] S. Miyata, The Syntheses of Hydrotalcite-Like Compounds and Their Structures and Physico-Chemical Properties I: The Systems Mg<sup>2+</sup>-Al<sup>3+</sup>-NO<sup>3-</sup>, Mg<sup>2+</sup>-Al<sup>3+</sup>-Cl<sup>-</sup>, Mg<sup>2+</sup>-Al<sup>3+</sup>-ClO<sub>4</sub><sup>-</sup>, Ni<sup>2+</sup>-Al<sup>3+</sup>-Cl<sup>-</sup> and Zn<sup>2+</sup>-Al<sup>3+</sup>-Cl<sup>-</sup>, *Clay. Clay Miner.*, 23 (1975) 369-375.
- [112] F. Bruna, R. Celis, M. Real, J. Cornejo, Organo/LDH nanocomposite as an adsorbent of polycyclic aromatic hydrocarbons in water and soil-water systems, *J. Hazard. Mater.*, 225-226 (2012) 74-80.
- [113] M.K. R.Reddy, Z.P. Xu, G.Q.M. Lu, J.C. D. Da Costa, Layered double hydroxides for CO<sub>2</sub> capture: Structure evolution and regeneration, *Ind. Eng. Chem. Res.*, 45 (2006) 7504-7509.
- [114] Y. Kim, W. Yang, P.K.T. Liu, M. Sahimi, T.T. Tsotsis, Thermal evolution of the structure of a Mg-Al-CO<sub>3</sub> layered double hydroxide: Sorption reversibility aspects, *Ind. Eng. Chem. Res.*, 43 (2004) 4559-4570.
- [115] J. Rocha, M. Del Arco, V. Rives, M. A. Ulibarri, Reconstruction of layered double hydroxides from calcined precursors: a powder XRD and <sup>27</sup>Al MAS NMR study, *J. Mater. Chem.*, 9 (1999) 2499-2503.
- [116] T. Hibino, A. Tsunashima, Characterization of repeatedly reconstructed Mg-Al hydrotalcite-like compounds: gradual segregation of aluminum from the structure, *Chem. Mater.*, 10 (1998) 4055-4061.
- [117] F. Millange, R.I. Walton, D. O'Hare, Time-resolved X-ray diffraction study of the liquid-phase reconstruction of Mg-Al-carbonate hydrotalcite-like compounds, *J. Mater. Chem.*, 10 (2000) 1713-1720.
- [118] J. Das, B.S. Patra, N. Baliarsingh, K.M. Parida, Adsorption of phosphate by layered double hydroxides in aqueous solutions, *Appl. Clay Sci.*, 32 (2006) 252-260.

- [119] K. Goh, T. Lim, Z. Dong, Enhanced arsenic removal by hydrothermally treated nanocrystalline mg/al layered double hydroxide with nitrate intercalation, *Environ. Sci. Technol.*, 43 (2009) 2537-2543.
- [120] Y. You, G.F. Vance, H. Zhao, Selenium adsorption on Mg-Al and Zn-Al layered double hydroxides, *Appl. Clay Sci.*, 20 (2001) 13-25.
- [121] L. Lv, J. He, M. Wei, D.G. Evans, Z. Zhou, Treatment of high fluoride concentration water by MgAl-CO<sub>3</sub> layered double hydroxides: Kinetic and equilibrium studies, *Water Res.*, 41 (2007) 1534-1542.
- [122] S.W. Rhee, M.J. Kang, H. Kim, C.H. Moon, Removal of aquatic chromate ion involving rehydration reaction of calcined layered double hydroxide (Mg-Al-CO<sub>3</sub>), *Environ. Technol.*, 18 (1997) 231-236.
- [123] A.N. Ay, B. Zümreoglu-Karan, A. Temel, Boron removal by hydrotalcite-like, carbonate-free Mg - Al - NO<sub>3</sub>-LDH and a rationale on the mechanism, *Micropor. Mesopor. Mat.*, 98 (2007) 1-5.
- [124] M. Fuchs, M. Scheffler, Ab initio pseudopotentials for electronic structure calculations of poly-atomic systems using density-functional theory, *Comput. Phys. Commun.*, 119 (1999) 67-98.
- [125] K. Momma, F. Izumi, VESTA 3 for three-dimensional visualization of crystal, volumetric and morphology data, *J. Appl. Crystallogr.*, 44 (2011) 1272-1276.
- [126] R.L. Goswamee, P. Sengupta, K.G. Bhattacharyya, D.K. Dutta, Adsorption of Cr (VI) in layered double hydroxides, *Appl. Clay Sci.*, 13 (1998) 21-34.
- [127] X. Cheng, X. Huang, X. Wang, D. Sun, Influence of calcination on the adsorptive removal of phosphate by Zn - Al layered double hydroxides from excess sludge liquor, *J. Hazard. Mater.*, 177 (2010) 516-523.
- [128] L. Yang, Z. Shahrivari, P.K. Liu, M. Sahimi, T.T. Tsotsis, Removal of trace levels of arsenic and selenium from aqueous solutions by calcined and uncalcined layered double hydroxides (LDH), *Ind. Eng. Chem. Res.*, 44 (2005) 6804-6815.
- [129] R. Rojas, M.R. Perez, E.M. Erro, P.I. Ortiz, M.A. Ulibarri, C.E. Giacomelli, EDTA modified LDHs as Cu<sup>2+</sup> scavengers: Removal kinetics and sorbent stability, *J. Colloid Interf. Sci.*, 331 (2009) 425-431.



- [130] T. Kameda, H. Takeuchi, T. Yoshioka, Uptake of heavy metal ions from aqueous solution using Mg – Al layered double hydroxides intercalated with citrate, malate, and tartrate, *Sep. Purif. Technol.*, 62 (2008) 330-336.

## **Chapter 2 Sorption of borate by a layered double hydroxides prepared using dolomite as a magnesium source**

### **2.1 Introduction**

Co-precipitation is the most commonly used method because of its simplicity and productivity [1]. In co-precipitation, divalent and trivalent metallic ions and/or metallic oxides are usually used as precursors. Xu and Lu [2] used MgO as a precursor and added different sodium salts to form LDHs containing different anions as intercalators in aqueous solutions. The MgO used in this method is mainly derived from calcined products of natural minerals such as hydromagnesite ( $\text{Mg}_2(\text{CO}_3)(\text{OH})_2$ ) and magnesite ( $\text{MgCO}_3$ ). These magnesium resources are mainly distributed in China, Russia, and South Korea, and are less available in other countries [3]. Compared with hydromagnesite and magnesite, dolomite ( $\text{CaMg}(\text{CO}_3)_2$ ) is more widely distributed worldwide, and is less expensive (2,000 to 3,000 Japanese yen/ton) [4]. By calcination of dolomite, a certain amount of MgO can be provided for the synthesis of LDHs [6]. Through this way, the preparation cost of LDHs for environmental remediation can be decreased. In addition, it was considered that the LDHs is transformed into bimetallic oxides (with a similar structure to that of MgO) after calcination [5], and that these bimetallic oxides can transform back into LDHs during the borate removal. Therefore, in the present work, layered double hydroxides was prepared using dolomite as a magnesium source ( $\text{CO}_3$ -DLDH), and the optimal calcination temperature of  $\text{CO}_3$ -DLDH was investigated by comparing the borate sorption ability. In addition, the mechanism of sorption of boron by  $\text{CO}_3$ -DLDH calcined at the optimal temperature

was examined using FTIR spectra and  $^{11}\text{B}$ -NMR of the solid residues after sorption of borate. Furthermore, the effects of pH, initial dosage of  $\text{CO}_3\text{-DLDH}$ , and competitive anions on the removal of boron at the optimal temperature were also investigated.

## 2.2 Materials and methods

### 2.2.1 Chemicals

Aluminum hydroxide ( $\text{Al}(\text{OH})_3$ , special grade, Wako Industrial Chemicals, Osaka, Japan), boric acid ( $\text{H}_3\text{BO}_3$ , special grade, Wako Industrial Chemicals), and sodium bicarbonate ( $\text{Na}_2\text{CO}_3$ , special grade, Wako Industrial Chemicals) were used as received without purification. Natural dolomite was obtained from Ogano Mines by Yoshizawa Lime Co., Ltd. (Tochigi, Japan). The elemental composition of the raw dolomite was determined using inductively coupled plasma atomic emission spectroscopy (ICP-AES, Seiko Instruments, Chiba, Japan) in triplicate after acid decomposition with 1 M HCl. The results are summarized in **Table 2.1**. The molar ratio of Ca/Mg was around 1.58, suggesting that the specimen includes not only dolomite but also other calcium compounds [17].

Table 2.1 Chemical composition in the raw dolomite and after calcination

	Raw material (mg/g)	After calcination 900 °C (mg/g)
Ca	267.49±1.99	438.22±4.62
Mg	102.72±0.031	179.72±0.97
Na	0.21±0.0043	1.41±0.14
K	0.27±0.0042	0.62±0.0049
Si	1.17±0.091	3.25±0.31
B	0.10±0.016	0.08±0.0070
Al	0.35±0.0034	0.98±0.14
Fe	0.30±0.00	0.64±0.15
Sr	0.16±0.0021	0.11±0.022
others	627.23	374.83

### 2.2.2 Preparation of CO<sub>3</sub>-DLDH

CO<sub>3</sub>-DLDH was synthesized by co-precipitation. Natural dolomite and Al(OH)<sub>3</sub> were weighed to give a Mg/Al molar ratio of 2.0, physically mixed, and ground in a mortar. The ground powders were then heated in a muffle furnace, TME 2200 (Eyela, Tokyo, Japan) up to 900 °C at a rate of 10 °C/min, maintained at 900 °C for 3 h, and left to cool down to room temperature. Subsequently, the product was dispersed in 100 mL of 0.25 M Na<sub>2</sub>CO<sub>3</sub> under stirring for 3 h; the solution pH was adjusted to 10.0 ± 0.2 by adding 1 M HNO<sub>3</sub> solution. The precipitates were collected by filtration, thoroughly washed with deionized water, and freeze dried overnight. The formation of LDHs was confirmed by XRD; the product will be referred to as CO<sub>3</sub>-DLDH in this paper.

CO<sub>3</sub>-DLDH was calcined at temperatures between 300 and 700 °C to optimize the calcining temperature for maximum boron sorption capacity. Calcinations were performed in a furnace. Samples calcined at 300, 500 and 700 °C were designated CO<sub>3</sub>-DLDH-300, CO<sub>3</sub>-DLDH-500 and CO<sub>3</sub>-DLDH-700, respectively.

### 2.2.3 Characterization

The crystalline phases within the various CO<sub>3</sub>-DLDH samples were determined using an X-ray diffractometer (Ultima IV, Rigaku, Akishima, Japan) with Cu K $\alpha$  radiation. The accelerating voltage and applied current were 40 kV and 40 mA, respectively, with a scanning speed of 2°/min and a scanning step of 0.02°. BET specific surface area measurements were performed through multi-point nitrogen adsorption using an AUTOSORB-1 surface analyzer (Yuasa, Osaka, Japan). Thermogravimetric analysis (TG-DTA, 2000SA, Bruker, Japan) was performed from room temperature to 800 °C at a heating rate of 10 °C/min. FTIR spectra were recorded on a FTIR 670 Plus (JASCO, Hachioji, Japan). The morphologies of the products calcined at different temperatures were observed using a field emission scanning electron microscopy (FE-SEM) SU8000 (Hitachi, Japan) at 1 kV accelerating voltage.

Solid-state <sup>11</sup>B-NMR spectra of the solid residues after sorption of borate were collected using a single pulse method on a JEOL ECA 800 (Akishima, Japan) spectrometer equipped with a 4 mm high-speed magic angle spinning probe, and controlled by Delta NMR software version 4.3 (JEOL). At a field strength of 18.8 T, the resonant frequency for <sup>11</sup>B was 256.6 MHz. Typical acquisition parameters were as follows: 15 kHz spinning speed, 2.5  $\mu$ s pulse length, 10 s recycle delay, and 63 to 341 scans depending on boron content.

#### 2.2.4 Sorption batch tests

Sorption of borate onto products calcined at different temperatures was carried out. 0 to 30 mM  $\text{H}_3\text{BO}_3$  solutions were prepared by adjusting the initial pH from 4.0 to 11.0 using 1 M NaOH and 1 M  $\text{HNO}_3$ . For sorption experiments, 0.100 g of a calcined product was added to 40 mL of borate solution. The mixture was shaken at 100 rpm with 8 cm stroke length in a shaking incubator (TB-16R, Takasaki Kagaku, Kawaguchi, Japan) at room temperature. After equilibrium was reached, the supernatants were filtered (0.20  $\mu\text{m}$   $\phi$ ) and total concentrations of B, Mg, and Al were determined by ICP-AES. Solid residues after sorption were collected and examined by XRD, FTIR, and  $^{11}\text{B}$ -NMR analyses using the same methods as described for the characterization of sorbents before sorption.

To explore the effects of competitive anions on the sorption of boron by  $\text{CO}_3$ -DLDH-700, 0.100 g sorbent was added into 40 mL of 5.5 mM boron solution containing 50 mM competing anion (either  $\text{CO}_3^{2-}$ ,  $\text{SO}_4^{2-}$  or  $\text{Cl}^-$ ) and the mixtures were shaken for 72 h. After this time, the supernatant was removed out and filtered through 0.2  $\mu\text{m}$  membrane before determination of B content by ICP-AES.

0.100g of  $\text{CO}_3$ -DLDH-700 was added into 40ml with 5 mM borate solution. Sorption experiment was carried under the condition of 200 rpm and 25  $^\circ\text{C}$ . After 96 hours, sample was taken out, and then solids and liquid have been separated by vacuum filtration. The concentration of borate has been measured by ICP-AES. Solid residues after washing were set into a muffle furnace and calcinated at 700  $^\circ\text{C}$ , then was reused for the next borate sorption cycles.

## 2.3 Results and Discussion

### 2.3.1 Characterization

The XRD patterns of CO<sub>3</sub>-DLDH calcined at different temperatures are shown in **Fig. 2.1**. In the XRD pattern of CO<sub>3</sub>-DLDH before calcination (**Fig. 2.1(a)**), the basal characteristic diffraction peaks at  $2\theta$  values of 11.1° (003), 22.3° (006), and 34.6° (009) were indicative of the formation of Mg-Al-LDH hydrotalcite (JCPDS 048-0601), with an interlayer spacing of 7.93 Å [6,7]. Aside from hydrotalcite in **Fig. 2.1(a)**, the other peaks were assigned to calcium carbonate (CaCO<sub>3</sub>, JCPDS 78-3262). The hydrotalcite and CaCO<sub>3</sub> contents in the non-calcined CO<sub>3</sub>-DLDH were quantitatively determined as 32 wt% and 68 wt% by analysis of XRD patterns using “Maud” software [8].

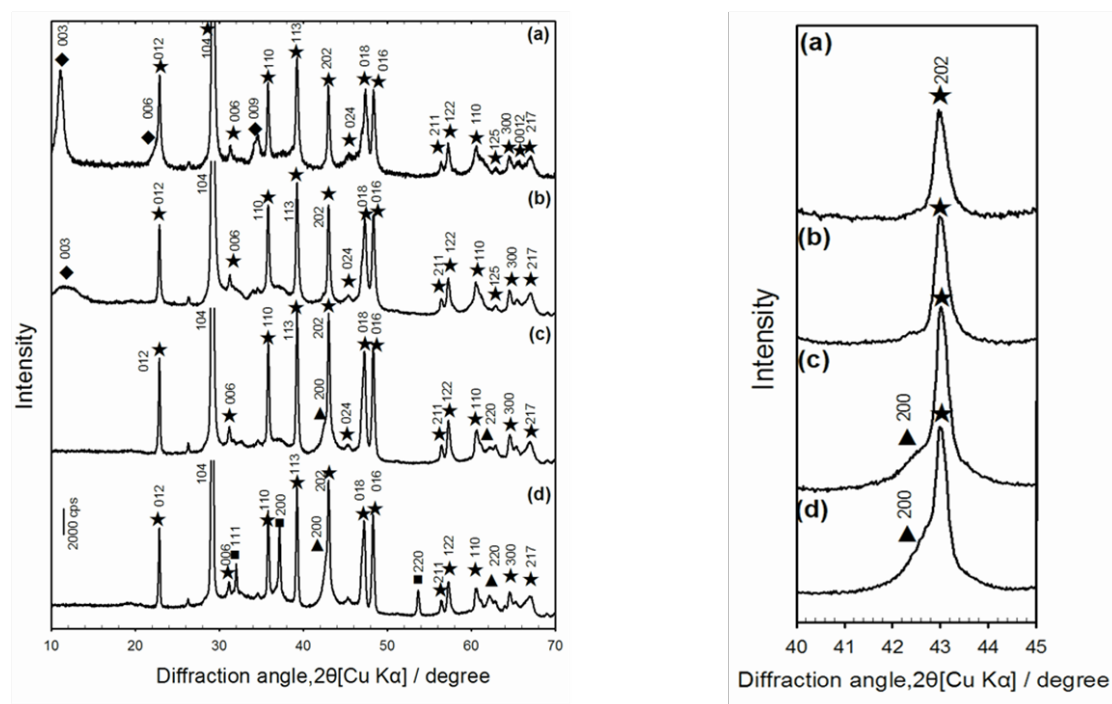


Fig. 2.1 XRD patterns of (a) CO<sub>3</sub>-DLDH, (b) CO<sub>3</sub>-DLDH-300, (c) CO<sub>3</sub>-DLDH-500 and (d) CO<sub>3</sub>-DLDH-700. The range of diffraction angle is from 10 ° to 70° in  $2\theta$  in left and expanded from 40° to 45° in the right side. Symbols: ▲, MgO (JCPDS 45-946); ■, CaO (JCPDS 70-5499); ★, CaCO<sub>3</sub> (JCPDS 78-3262); ◆, Mg-Al-LDH (JCPDS 048-0601).

The crystalline LDHs phase was progressively transformed into Mg-Al bimetallic oxide with increasing calcination temperature, as previously reported [9]. When the calcination temperature increased to 300 °C, the characteristic XRD reflections from LDHs, such as (003), (006) and (009), became broadened because of the loss of interlayer water (**Fig. 2.1(b)**). After calcining at 500 °C, the LDHs reflection had completely disappeared as the interlayer anionic species, mainly carbonate, were lost and the host layer structure was transformed from a bimetallic hydroxide into amorphous bimetallic oxides, in which  $\text{Al}^{3+}$  ions are partially substituted for  $\text{Mg}^{2+}$  in “MgO” (**Fig. 2.1(c)**) [5]. Though the diffraction peak from the (200) plane in MgO (JCPDS 45-946) overlaps that of the (202) plane in  $\text{CaCO}_3$ , the broadness of peak at  $2\theta = 42.7^\circ$  suggests that the formation of MgO started as calcination temperature increased (**Fig. 2.1**). This is supported by the appearance of a diffraction peak at  $62.2^\circ$ , which corresponds to the (220) diffraction peak of MgO. Furthermore, in the XRD pattern for the product calcined at 700 °C (**Fig. 2.1(d)**), additional peaks assigned to CaO were observed at  $2\theta = 37.3$  and  $53.7^\circ$  (JCPDS 70-5499); this CaO arises from partial decarbonation of  $\text{CaCO}_3$ . According to Millange et al. [5], the calcination products of LDHs have a MgO-like structure, where Al ions are dissolved in the lattice and sit on the Mg sites to form a solid solution. Therefore, when LDHs was calcined at a lower temperature, it is unlikely that diffraction peaks from  $\text{Al}_2\text{O}_3$  will appear in the XRD pattern.

The XRD patterns in **Fig. 2.1** indicate that the layered structure of the LDHs had started to collapse after calcination at 300 °C, and was completely transformed into bimetallic oxides at 700 °C. These XRD results are consistent with the three-step decomposition of  $\text{CO}_3\text{-DLDH}$  [10], as is also shown in the TG/DTA (**Fig. 2.2**). The first stage, from room temperature until 189 °C, and corresponding to 3.7% weight



loss, was caused by the evaporation of adsorbed water and interlayer water from CO<sub>3</sub>-DLDH. The second stage, which occurred from 189 to 578 °C and involved a weight loss of 11.0%, was caused by the simultaneous elimination of intercalated CO<sub>3</sub><sup>2-</sup> and strongly bound water and dehydration of the brucite-like octahedral layers. The third stage starts at 580 °C and corresponds to 15.9% weight loss, and is attributed to partial decarbonation of CaCO<sub>3</sub> with small particle sizes [11].

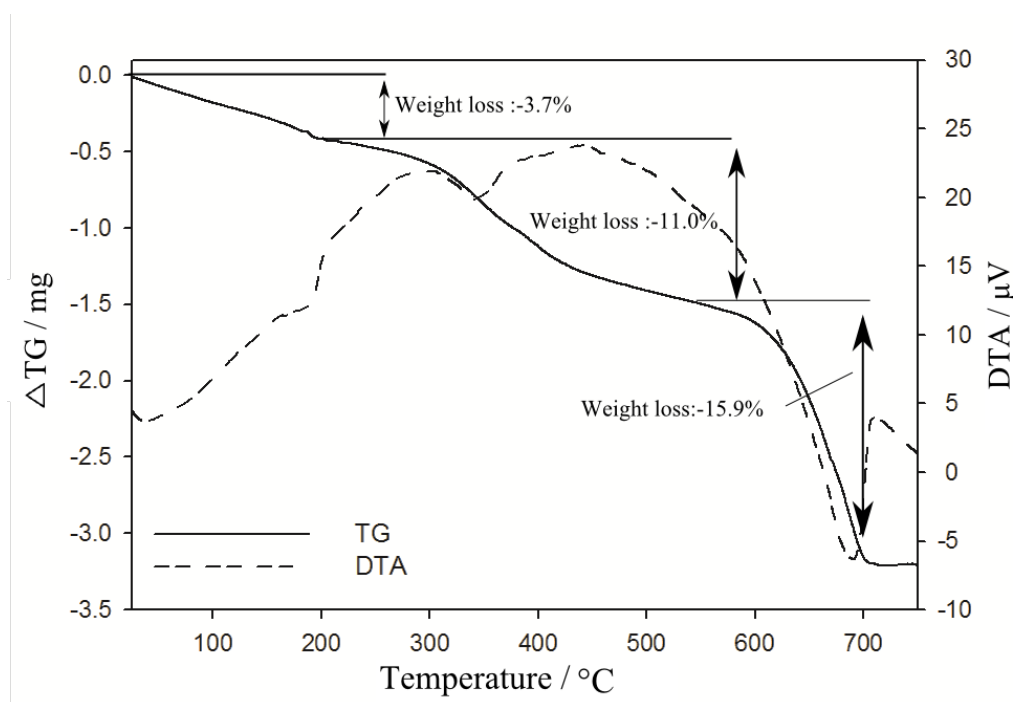


Fig. 2.2 TG/DTA analysis of CO<sub>3</sub>-DLDH from room temperature to 800 °C.

Specific surface areas of CO<sub>3</sub>-DLDH calcined at different temperatures are summarized in **Table 2.2**. The specific surface area did not consistently increase with increasing calcination temperature. The uncalcined sample mainly contained LDHs and CaCO<sub>3</sub>, and had the largest BET surface area of 57.5 m<sup>2</sup>/g. The BET surface areas of CO<sub>3</sub>-DLDH-300 and CO<sub>3</sub>-DLDH-500 decreased to 51.48 and 44.54 m<sup>2</sup>/g, respectively. CO<sub>3</sub>-DLDH-300 and CO<sub>3</sub>-DLDH-500 were considered to be dehydrated. CO<sub>3</sub>-DLDH-500 was also believed to have lost most of its CO<sub>3</sub><sup>2-</sup> to release some

sorption sites, and form an amorphous mixed oxide phase. However, higher calcination temperatures may cause the agglomeration and sintering of LDH particles. Thus, the surface area decreased as the calcination temperature increased. The specific surface area of CO<sub>3</sub>-DLDH-700 increased again, approaching a similar value to that of the uncalcined sample. This phenomenon may be ascribed to partial decarbonation of CaCO<sub>3</sub>.

Table 2.2 BET specific surface area of different materials

Sample	Specific surface area (m <sup>2</sup> /g)
Dolomite before calcination	5.3
Dolomite-calcined at 900 °C	6.9
CO <sub>3</sub> -DLDH	57.5
CO <sub>3</sub> -DLDH-300	51.5
CO <sub>3</sub> -DLDH-500	44.5
CO <sub>3</sub> -DLDH-700	57.0

SEM images of the starting material, uncalcined CO<sub>3</sub>-DLDH and CO<sub>3</sub>-DLDH calcined at 300, 500, and 700 °C are shown in Fig. 3. The starting material, a mixture of calcined dolomite and Al<sub>2</sub>O<sub>3</sub>, showed irregular shapes of aggregated particles (**Fig. 2.3(a)**). After synthesis of LDHs through co-precipitation, flaky particles with 400 nm width appeared (**Fig. 2.3(b)**). After calcining at 300 °C, the layered structure of CO<sub>3</sub>-DLDH-300 did not change, although the LDH in the product lost some interlayer water molecules, resulting in the disappearance of XRD peaks assigned to LDHs. The flaky appearance could still be clearly seen, but the particles were aggregated because of sintering (**Fig. 2.3(c)**). Aggregation was also observed and became more serious in CO<sub>3</sub>-DLDH-500 (**Fig. 2.3(d)**), significantly decreasing the specific surface area of the material. When the calcination temperature increased to 700 °C, the hydroxide components were completely transformed into metallic oxides, but their morphology

was still different to that of the starting materials and kept the flaky appearance (**Fig. 2.3(e)**).

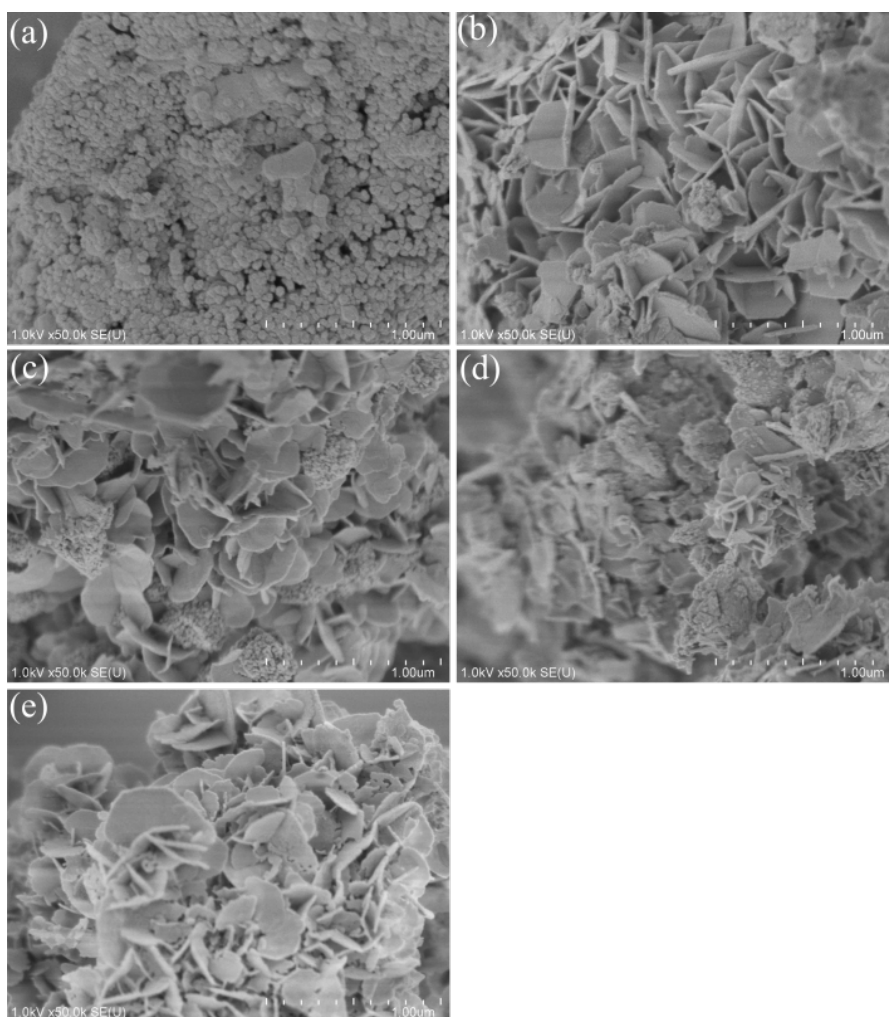


Fig. 2.3 FE-SEM images of (a) Dolomite +  $\text{Al}_2\text{O}_3$ , (b)  $\text{CO}_3$ -DLDH, (c)  $\text{CO}_3$ -DLDH-300, (d)  $\text{CO}_3$ -DLDH-500 and (e)  $\text{CO}_3$ -DLDH-700. Horizontal bars indicate 1  $\mu\text{m}$ .

### 2.3.2 Effect of calcination temperature on the sorption of borate

**Fig. 2.4** shows typical time courses of B, Mg, Al concentrations and pH during batch sorption tests with uncalcined and calcined  $\text{CO}_3$ -DLDH. And **Fig. 2.5** shows that the sorption isotherms of borate by calcined  $\text{CO}_3$ -DLDH, uncalcined  $\text{CO}_3$ -DLDH, calcinated dolomite and dolomite without calcination.

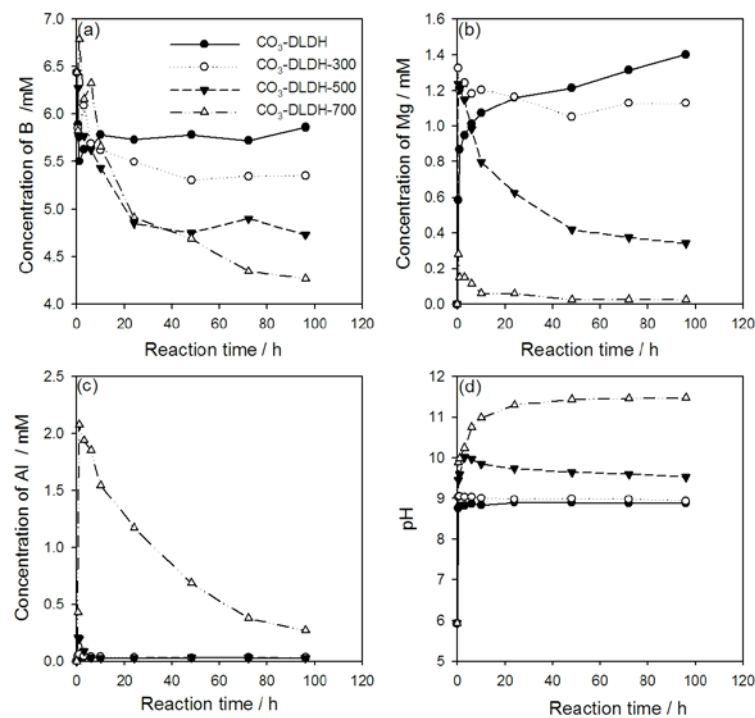


Fig. 2.4 Changes of (a) B, (b) Mg, (c) Al concentrations and (d) pH during sorption of 6.5 mM B on  $\text{CO}_3\text{-DLDH}$ ,  $\text{CO}_3\text{-DLDH-300}$ ,  $\text{CO}_3\text{-DLDH-500}$  and  $\text{CO}_3\text{-DLDH-700}$ .

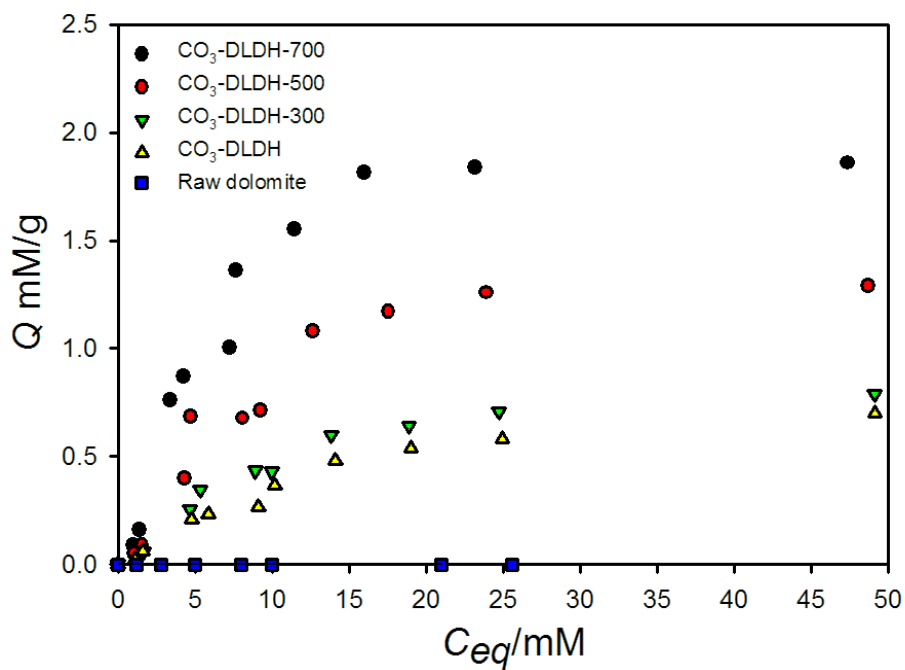


Fig. 2.5 Sorption isotherms of B on raw dolomite,  $\text{CO}_3\text{-DLDH}$ ,  $\text{CO}_3\text{-DLDH-300}$ ,  $\text{CO}_3\text{-DLDH-500}$  and  $\text{CO}_3\text{-DLDH-700}$ .

It can be found that the sorption of borate by calcinated dolomite and dolomite without calcination were much lower than that of CO<sub>3</sub>-DLDH with and without calcination. For dolomite without calcination treatment, its main component is CaMg(CO<sub>3</sub>)<sub>2</sub> and no MgO is contained so that borate could not be adsorbed. After calcination at 900 °C, though dolomite was converted into CaO and MgO, the surface of MgO is passivated under high temperature, which consequently retarded the interaction between MgO and borate and lead to lower adsorption ability [12]. In addition, the sorption isotherms of B was greater with increasing calcination temperature (**Fig. 2.5**) and the results indicate that the maximum sorption capacity of CO<sub>3</sub>-DLDH-700 reached 1.86 mmol/g, which was higher than that of other materials in this research. Meanwhile, the changing with time of Mg<sup>2+</sup> and Al<sup>3+</sup> concentrations and pH differed significantly, depending on calcination temperature (**Fig. 2.4(b-d)**).

The higher equilibrium pH values seen for higher calcination temperatures are caused by hydration of the MgO and CaO present in the products calcined at higher temperatures (**Fig. 2.4(d)**). Higher equilibrium pH favors the generation of hydrotalcite, resulting in more significant decreases in Mg concentrations for products calcined at higher temperatures (**Fig. 2.4(b)**). The largest release of Al was also CO<sub>3</sub>-DLDH-700. This is expected, because in strongly alkaline solutions, Al should exist as an anionic species, Al(OH)<sub>4</sub><sup>-</sup> (**Fig. 2.4(c)**). The results in **Fig. 2.4**, when combined with the results for characterization of the sorbents, suggest that the mechanisms for removal of borate by CO<sub>3</sub>-DLDH-300 and the uncalcined CO<sub>3</sub>-DLDH were different from those of CO<sub>3</sub>-DLDH-700 and CO<sub>3</sub>-DLDH-500.

CaCO<sub>3</sub> and hydrotalcite were identified as the main phases in the uncalcined CO<sub>3</sub>-DLDH (**Fig. 2.1(a)**). CaCO<sub>3</sub> is chemically stable at room temperature at the pH of the borate solutions used, and the amount of borate adsorbed by CaCO<sub>3</sub> is very limited.

Therefore, the sorption density of borate by uncalcined CO<sub>3</sub>-DLDH can be mainly ascribed to hydrotalcite. Previous studies have reported that ion exchange is the predominant mechanism by which LDHs remove anionic species [13, 14]. In this mechanism, the anionic species can be removed by the LDHs only when its binding force with the host layer of LDHs is stronger than that of the original anions within the LDHs interlayer. In addition, anions with greater valences have higher affinity with LDHs layers [15]. Therefore, the strong affinity of carbonate ions (CO<sub>3</sub><sup>2-</sup>) to the host layer in LDHs should prevent sorption of borate by CO<sub>3</sub>-DLDH. Similarly, although CO<sub>3</sub>-DLDH-300 was considered to be dehydrated, it retained its layered structure intact because CO<sub>3</sub><sup>2-</sup> occupied the sorption sites in the guest layers. Thus, CO<sub>3</sub>-DLDH-300 has few sorption sites available for ion exchange with tetrahydroborate, resulting in low boron sorption capacity.

The removal mechanism of borate by CO<sub>3</sub>-DLDH-700 and CO<sub>3</sub>-DLDH-500, which showed greater sorption capacities in the present work, appears to be more complicated. MgO is contained in both CO<sub>3</sub>-DLDH-500 and CO<sub>3</sub>-DLDH-700, and CaO was present in CO<sub>3</sub>-DLDH-700. Because the sorption performance of CO<sub>3</sub>-DLDH-700 was high (**Fig. 2.4**) and the water chemistry during the sorption of borate by CO<sub>3</sub>-DLDH-700 was more favorable for regenerating hydrotalcite, CO<sub>3</sub>-DLDH-700 was chosen for further investigation of its mechanism of sorption of borate.

Solid residues of CO<sub>3</sub>-DLDH-700, obtained using different initial concentrations of borate were examined using XRD, FTIR, and <sup>11</sup>B-NMR analyses. The XRD patterns of the solid residues of CO<sub>3</sub>-DLDH-700 before and after sorption of 1 mM or 20 mM B are shown in **Fig. 2.6**. The peaks assigned to MgO (**Fig. 2.7**) and CaO completely disappeared after sorption. In preliminary experiments the sorption ability of borate on CaO was very low (**Fig. 2.8**).

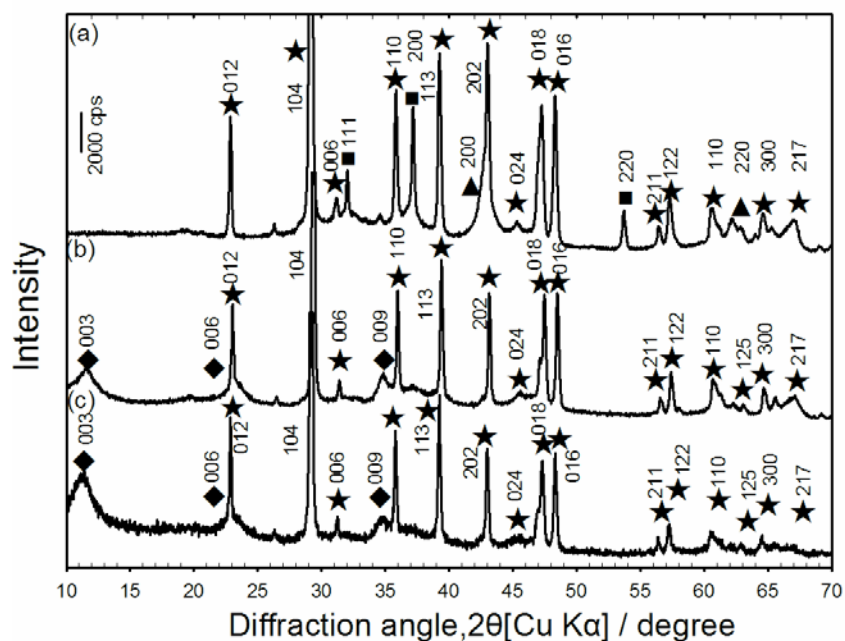


Fig. 2.6 XRD patterns of  $\text{CO}_3\text{-DLDH-700}$  (a) before and (b, c) after sorption of B. The initial B concentrations were (b) 1 mM and (c) 20 mM. Symbols are the same as in Fig. 2.1.

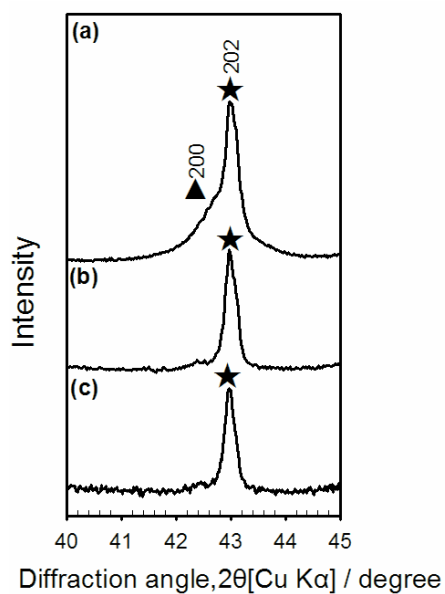


Fig. 2.7 XRD patterns from  $2\theta = 40$  to  $45^\circ$  of  $\text{CO}_3\text{-DLDH-700}$  (a) before sorption and (b, c) after sorption of B. The initial B concentrations were (b) 1 mM and (c) 20 mM. Symbols are the same as in Fig. 2.1.

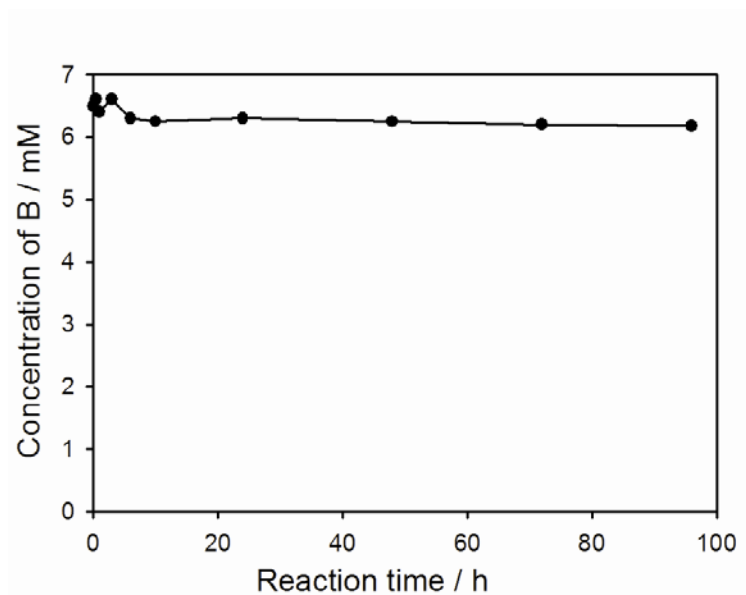


Fig. 2.8 Changes in B concentration with time during sorption of 6.5 mM B on 2.5 g/L CaO.

In addition, the peak assigned to the (003) reflection in the new LDHs was broader than that in the uncalcined starting materials; the  $d$ -spacing evaluated from this peak corresponds to the interlayer space, and increased from 7.78 Å (**Fig. 2.6(b)**) to 7.89 Å (**Fig. 2.6(c)**) with an increase in the amount of boron adsorbed in the LDHs from 0.088 to 1.813 mg/g. This result suggests that the interlayers in the regenerated LDHs have an important role in the sorption of borate, and borate ions, acting as guests, may exist in the interlayer. Generally, guest ions in LDHs should have negative charges. Tetrahydroborate, which is in a dissociated form, has a negative charge, while boric acid is in a molecular form. However, the FTIR spectra (**Fig. 2.9**) of the solid residues after sorption of 1 mM or 20 mM borate show that both tetragonal B ( $^{14}\text{B}$ ) and trigonal B ( $^{13}\text{B}$ ) exist in the solid residues.



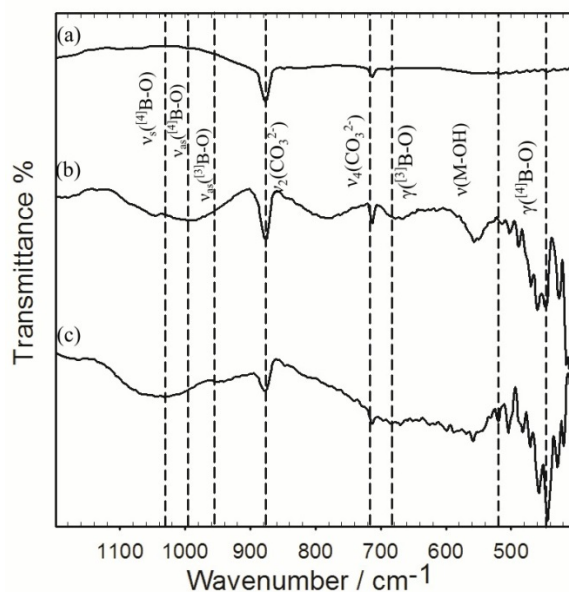


Fig. 2.9 FTIR spectra of CO<sub>3</sub>-DLDH-700 (a) before and (b, c) after sorption of (b) 1 mM B and (c) 20 mM B.

In **Fig. 2.9**, the peaks at 872 and 710 cm<sup>-1</sup> were attributed to the vibration modes of CO<sub>3</sub><sup>2-</sup> (**Fig. 2.6**) [16], and the peaks at 1037, 997, and 448 cm<sup>-1</sup> in the spectra after sorption of B could be assigned to the asymmetric, symmetric, and bending vibration modes of [<sup>4</sup>]B-O, respectively. The peak at 690 cm<sup>-1</sup> may be assigned to the bending vibration mode of [<sup>3</sup>]B-O [17]. Similarly, the <sup>11</sup>B-NMR spectra also indicate that the solid residues contain [<sup>3</sup>]B and [<sup>4</sup>]B (**Fig. 2.10**).

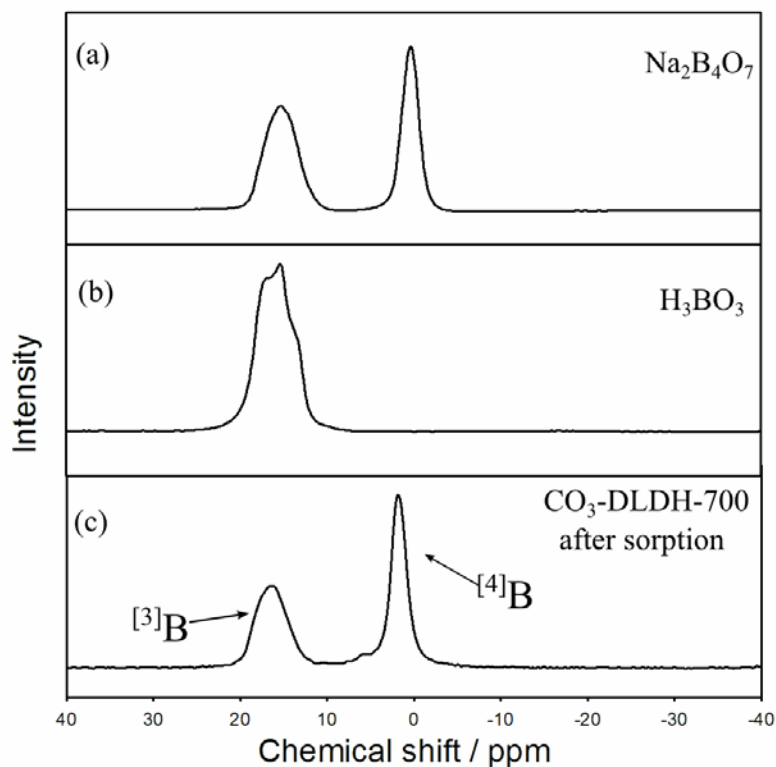


Fig. 2.10  $^{11}\text{B}$ -NMR MAS spectra of (a)  $\text{Na}_2\text{B}_4\text{O}_7$ , (b)  $\text{H}_3\text{BO}_3$  and (c) solid residues of  $\text{CO}_3\text{-DLDH-700}$  after sorption of 20 mM B.

As shown in **Fig. 2.10**, the peaks at approximately 16 and 1.8 ppm were assigned to  $^{[3]}\text{B}$  and  $^{[4]}\text{B}$ , respectively. The relative peak area of  $^{[4]}\text{B}/^{[3]}\text{B}$  borate was 1.25 (which represents the molar ratio of  $^{[4]}\text{B}/^{[3]}\text{B}$ ), and means that  $^{[4]}\text{B}$  was dominant in the solid residues. Therefore, we hypothesize that the removal of borate by  $\text{CO}_3\text{-DLDH-700}$  involves a two-step mechanism.

The main crystalline phase in  $\text{CO}_3\text{-DLDH-700}$  was transformed into bimetallic oxides, in which Al ions are dissolved in the lattice of an  $\text{MgO}$ -like structure to form a solid solution, after calcination [5]. After  $\text{CO}_3\text{-DLDH-700}$  came into contact with water, reconstruction of LDHs occurs via dissolution-precipitation of the oxide residue [18]. In this process, bimetallic oxides are hydrated to form layered double hydroxides [19].

Ligand-promoted dissolution of MgO and co-precipitation of borate with Mg(OH)<sub>2</sub> occur during hydration of MgO in the presence of H<sub>3</sub>BO<sub>3</sub> [12]. <sup>13</sup>B was mainly immobilized by ligand-promoted dissolution and precipitation during the conversion process of MgO to Mg(OH)<sub>2</sub>. This process is the first mechanism of boron removal by CO<sub>3</sub>-DLDH-700. In addition, when MgO reacted with water to generate hydroxide, the Al which was dissolved in the MgO structure also reacted with water to become hydrated, and this type of aluminum hydroxide is mostly incorporated into the Mg(OH)<sub>2</sub>. Since the Al ion has a charge of +3, the generation of Mg-Al hydrotalcite requires a certain number of negatively-charged guest ions to neutralize this additional charge and allow the interlayer structure to form. Some of the <sup>4</sup>B (B(OH)<sub>4</sub><sup>-</sup>) in the solution can act as the anions required for LDH formation. In other words, the <sup>4</sup>B was absorbed during LDHs regeneration, and this removed the B(OH)<sub>4</sub><sup>-</sup> from the solution. This process is the second mechanism of boron removal by CO<sub>3</sub>-DLDH-700. It is also the main process responsible for the existence of <sup>4</sup>B in the <sup>11</sup>B-NMR. We also suggest that uncharged H<sub>3</sub>BO<sub>3</sub> molecules must have been located near the metal layers in the newly generated LDHs because the LDHs was generated from Mg(OH)<sub>2</sub>, and <sup>4</sup>B existed in the interlayer of the new LDH as a guest ion to sustain the structure of the LDHs.

Furthermore, comparing CO<sub>3</sub>-DLDH-700 and CO<sub>3</sub>-DLDH-500, CO<sub>3</sub>-DLDH-700 has a higher adsorption efficiency than CO<sub>3</sub>-DLDH-500, because the magnesium oxide calcined at 700 °C is more basic than the material calcined at 500 °C [20], and the reconstruction of the LDH structure originates from magnesium oxide [21]. Therefore, the reaction rate of MgO with H<sub>2</sub>O is faster for than for CO<sub>3</sub>-DLDH-500. This can be confirmed by the faster release of Mg<sup>2+</sup> during borate sorption by CO<sub>3</sub>-DLDH-700.

Furthermore, as shown in **Fig. 2.11**, the leaching of Ca in CO<sub>3</sub>-DLDH-700 cannot be found during the time processing since the chemical stability of CaCO<sub>3</sub>. But the leaching of Mg and Al were clearly found and varied with the reaction time. When the reaction time reached 1 hour, the concentrations of Mg and Al were up to 0.15 mM and 2.07 mM, respectively. And then, the concentrations of Mg and Al in the solution started to decreased. At 96 hours, the concentrations of Mg and Al both were under the detection limits. During this sorption processing, the concentration of Al exceeded the maximum concentration limit of aluminum (0.2 mg/L) for drinking water quality in China (GB5749-2006). Therefore, in practical application, it is necessary to add appropriate follow-up processing steps to avoid the aluminum desolving in excess.

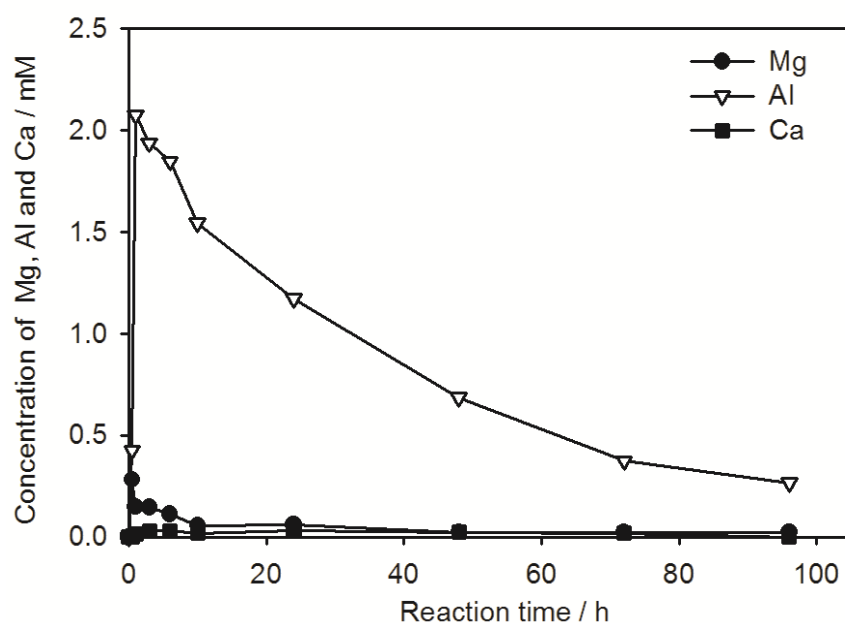


Fig. 2.11 Changes of Mg, Al and Ca concentrations during sorption of 6.5 mM B by CO<sub>3</sub>-DLDH-700.

### 2.3.3 Effect of pH on the sorption of borate

The removal of borate by CO<sub>3</sub>-DLDH-700 was examined over a pH range of 4.0 to 10.0. Boron uptake by CO<sub>3</sub>-DLDH-700 is presented in **Fig. 2.12**. A high and stable uptake capacity (0.42 mmol/g) was obtained at pH 4.0 to 7.0. Furthermore, the

influence of solution pH was not very significant in the low pH range (pH 4 to 6). However, the uptake capacity of borate decreased at pH 8.0 and then sharply declined to 0.26 mmol/g when the equilibrium pH was 10.0. This trend is different from those previously reported for MgO [22], but is the same as that reported for borate removal by LDHs [23].

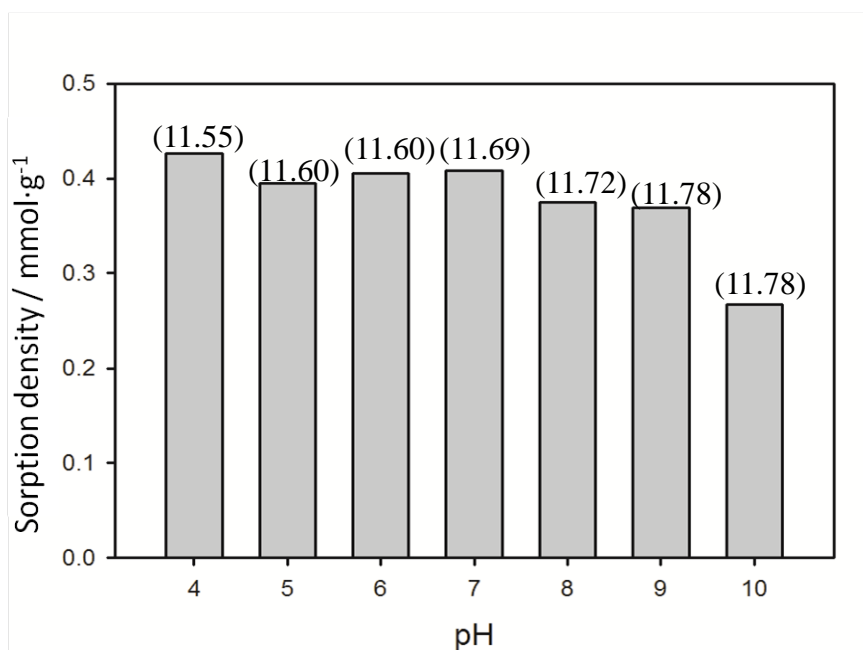


Fig. 2.12 Effect of initial pH on boron removal. The initial B concentration was 5 mM. Numbers in the bracket indicate the equilibrium pH.

Sorption of borate by CO<sub>3</sub>-DLDH-700 has two steps as we mentioned above. First, the rehydration of MgO-like structure resulted in coprecipitation of Mg(OH)<sub>2</sub> (brucite-like) and boric acid. Second, electrostatic sorption of borate after Mg(OH)<sub>2</sub> has been converted to LDHs. Since Mg(OH)<sub>2</sub> plays an important role in these two steps, and the acidic initial pH condition can promote the dissolution of Mg<sup>2+</sup>, thus providing magnesium ion needed for conversion to brucite and then transform into LDHs for following the sorption of borate. Therefore, sorption capacity of CO<sub>3</sub>-DLDH-700 under low pH condition is slightly.

### 2.3.4 Effect of competing anions on sorption of borate

The effects of competing anions on boron removal are shown in **Fig. 2.13**. The sorption capacity of borate by CO<sub>3</sub>-DLDH-700 was decreased in the presence of competing anions. The higher the valences of competing anions were, the more strongly boron sorption by CO<sub>3</sub>-DLDH-700 was inhibited. For example, CO<sub>3</sub>-DLDH-700 could only take up 0.09 mmol/g of the boron in the presence of sulfate, because divalent ions can enter the interlayer of LDHs preferentially (compared to borate) and occupy the guest layers [24]. Therefore, borate is more difficult to intercalate into the interlayer, and the amount removed is decreased. This result is also supported by FTIR analysis (**Fig. 2.14**). Compared with the FTIR spectra of the solid residues from tests with no competing ions, the vibration modes assigned to <sup>[4]</sup>B-O almost disappeared in the infrared spectra of the solid residues with divalent competing ions (**Fig. 2.14(c), (d)**). This is because divalent anions can intercalated into the sorption sites in preference to borate. A small peak attributed to the vibration mode of <sup>[4]</sup>B-O was seen in the FTIR spectrum of the residue taken from the solution with Cl<sup>-</sup>. The Cl<sup>-</sup> affected the sorption of B(OH)<sub>4</sub><sup>-</sup>, but was not able to completely replace borate and occupy all sites in the interlayer; this meant that small amounts of <sup>[4]</sup>B were found in the solid residues.

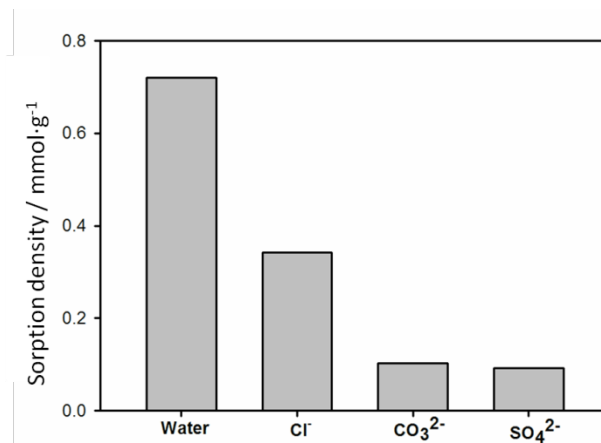


Fig. 2.13 Effect of competing ions on the sorption of boron.

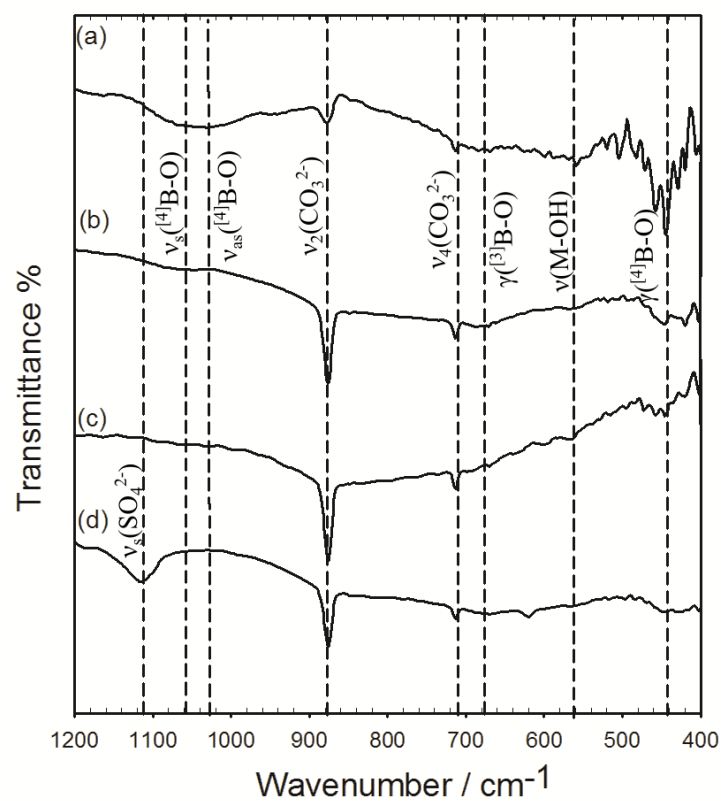


Fig. 2.14 FTIR spectra of CO<sub>3</sub>-DLDH-700 after sorption of 5.5 mM boron in the presence of different competing ions. (a) water, (b) 50 mM Cl<sup>-</sup>, (c) 50 mM CO<sub>3</sub><sup>2-</sup>, (d) 50 mM SO<sub>4</sub><sup>2-</sup>.

## 2.4. Conclusion

LDHs for environmental applications was prepared using calcined dolomite as the raw magnesium source. Sorption results suggest that CO<sub>3</sub>-DLDH can be used to remove borate from aqueous solution at ambient temperature and pressure. The maximum borate sorption capacity was achieved with CO<sub>3</sub>-DLDH-700; this was because CO<sub>3</sub>-DLDH-700 contains more MgO phase, with higher hydration activity. Meanwhile, the efficiency of borate removal decreased with increasing pH and in the presence of competing ions, especially those with higher valences. FTIR, <sup>11</sup>B-NMR results and XRD patterns of the solid residues showed that borate was removed by CO<sub>3</sub>-DLDH-700 in two ways: the co-precipitation of borate with Mg(OH)<sub>2</sub> to form a complex, and the intercalation of borate anions during the formation of LDHs.



## References:

- [1] K. Goh, T. Lim, Z. Dong, Application of layered double hydroxides for removal of oxyanions: A review, *Water Res.*, 42 (2008) 1343-1368.
- [2] Z.P. Xu, G.Q.M. Lu, Hydrothermal Synthesis of Layered Double Hydroxides (LDHs) from Mixed MgO and Al<sub>2</sub>O<sub>3</sub>: LDH Formation Mechanism, *Chem. Mater.*, 17 (2005) 1055-1062.
- [3] S. Fu, P. Li, Q. Feng, X. Li, P. Li, Y. Sun, Y. Chen, Soil quality degradation in a magnesite mining area, *Pedosphere*, 21 (2011) 98-106.
- [4] D. Wacey, D.T. Wright, A.J. Boyce, A stable isotope study of microbial dolomite formation in the Coorong Region: South Australia, *Chem. Geol.*, 244 (2007) 155-174.
- [5] F. Millange, R.I. Walton, D. O'Hare, Time-resolved X-ray diffraction study of the liquid-phase reconstruction of Mg-Al-carbonate hydrotalcite-like compounds, *J. Mater. Chem.*, 10 (2000) 1713-1720.
- [6] E. Kanezaki, Effect of Atomic Ratio Mg/Al in Layers of Mg and Al Layered Double Hydroxide on Thermal Stability of Hydrotalcite-Like Layered Structure BY Means of In Situ High Temperature Powder X-Ray Diffraction, *Mater. Res. Bull.*, 33 (1998) 773-778.
- [7] E. Kanezaki, K. Kinugawa, Y. Ishikawa, Conformation of intercalated aromatic molecular anions between layers of Mg/Al- and Zn/Al-hydrotalcites, *Chem. Phys. Lett.*, 226 (1994) 325-330.
- [8] L. Lutterotti, M. Bortolotti, G. Ischia, I. Lonardelli, H.R. Wenk, Rietveld texture analysis from diffraction images, *Zeitschrift fur Kristallographie Supplements*, 2007 (2007) 125-130.
- [9] M.K. R.Reddy, Z.P. Xu, G.Q.M. Lu, J.C.D.D. Costa, Layered Double Hydroxides for CO<sub>2</sub> Capture: Structure Evolution and Regeneration, *Ind. Eng. Chem. Res.*, 45 (2006) 7504-7509.
- [10] Y. Kim, W. Yang, P.K.T. Liu, M. Sahimi, T.T. Tsotsis, Thermal evolution of the structure of a Mg-Al-CO<sub>3</sub> layered double hydroxide: Sorption reversibility aspects, *Ind. Eng. Chem. Res.*, 43 (2004) 4559-4570.
- [11] T.Y. Jun, L.Y. Ming, S. Jing, P.Z. Dong, Structural characterization and thermal decomposition behavior of micro-sized and nano-sized CaCO<sub>3</sub>, *Acta Phys. Chim. Sin.*, 05 (2007) 717-722.
- [12] K. Sasaki, X.H. Qiu, Y. Hosomomi, S. Moriyama, Tsuyoshi, Hirajima, Effect of natural dolomite calcination temperature on sorption of borate onto calcined products, *Micropor Mesopor Mat*, 171(2013)1-8.

- [13] K.S. Triantafyllidis, E.N. Peleka, V.G. Komvokis, P.P. Mavros, Iron-modified hydrotalcite-like materials as highly efficient phosphate sorbents, *J. Colloid Interf. Sci.*, 342 (2010) 427-436.
- [14] L. Kentjono, J.C. Liu, W.C. Chang, C. Irawan, Removal of boron and iodine from optoelectronic wastewater using Mg-Al (NO<sub>3</sub>) layered double hydroxide, *Desalination*, 262 (2010) 280-283.
- [15] S. Miyata, Anion-exchange properties of hydrotalcite-like compounds, *Clay. Clay Miner.*, 31 (1983) 305-311.
- [16] A.I. Rat'Ko, A.I. Ivanets, A.I. Kulak, E.A. Morozov, I.O. Sakhar, Thermal decomposition of natural dolomite, *Inorg. Mater.*, 47 (2011) 1372-1377.
- [17] W.J. Zhen, Z.H. Liu, X.G. Chen., Differential FTIR and raman spectroscopic analysis of saturated aqueous solution of borax, 23 (2003) 705-707.
- [18] M. Rajamathi, G.D. Nataraja, S. Ananthamurthy, P.V. Kamath, Reversible thermal behavior of the layered double hydroxide of Mg with Al: mechanistic studies, *J. Mater. Chem.*, 10 (2000) 2753-2754.
- [19] T. Sato, H. Fujita, T. Endo, M. Shimada, A. Tsunashima, Synthesis of hydrotalcite-like compounds and their physico-chemical properties, *React. Solids*, 5 (1988) 219-228.
- [20] K. Sasaki, N. Fukumoto, S. Moriyama, T. Hirajima, Sorption characteristics of fluoride on to magnesium oxide-rich phases calcined at different temperatures, *J. Hazard. Mater.*, 191 (2011) 240-248.
- [21] T. Hibino, A. Tsunashima, Characterization of Repeatedly Reconstructed Mg-Al Hydrotalcite-like Compounds: Gradual segregation of aluminum from the structure, *Chem. Mater.*, 10 (1998) 4055-4061.
- [22] M.M. de la Fuente Garca-Soto, E. Muoz Camacho, Boron removal by means of adsorption processes with magnesium oxide-Modelization and mechanism, *Desalination*, 249 (2009) 626-634.
- [23] O.P. Ferreira, S.G. de Moraes, N. Dur n, L. Cornejo, O.L. Alves, Evaluation of boron removal from water by hydrotalcite-like compounds, *Chemosphere*, 62 (2006) 80-88.
- [24] K. Goh, T. Lim, Influences of co-existing species on the sorption of toxic oxyanions from aqueous solution by nanocrystalline Mg/Al layered double hydroxide, *J. Hazard. Mater.*, 180 (2010) 401-408.

## **Chapter 3 One-step synthesis of layered double hydroxide-intercalated gluconate for removal of borate**

### **3.1 Introduction**

Previously, Ferreira et al. and Jiang et al. used LDHs to remove borate from solution [1, 2]. These studies, based on the synthesis of LDHs intercalated with nitrate, achieved boron removal by taking advantage of the stronger adhesion between borate and the host layer compared with the adhesion between the nitrate and metal layer, resulting in ion exchange of borate with nitrate in the LDHs interlayer. Although this method effectively removes borate, different anions in aqueous environments, especially divalent anions, significantly influence borate sorption by LDHs [3]. The attractive force within the interlayer is far greater than that between the monovalent anions[4]. Therefore, LDHs is ineffective in immobilizing borate in complicated practical water systems, such as the results in **Fig. 2.13** in **Chapter 2**.

The main improvement needed to develop technology for boron removal by LDHs is to increase the selectivity of sorption and the sorption rate of boron by LDHs. Considering the simple synthesis, low cost and environmental friendliness of LDHs, the insertion of a polyhydroxylic organic group into the LDHs ion layer could make the LDHs for boron sorption less susceptible to interference from other anions, and increase its sorption rate. So, in the present work, an easy and efficient method to intercalate the gluconate into the LDHs (G-LDH) was developed. The resultant new material was characterized using several techniques and applied to removal of borate, to evaluate its efficiency. The sorption mechanism was carefully examined based on

XRD and  $^{11}\text{B}$ -NMR characterization of solid residues after sorption of borate. Related to **Chapter 2**, dolomite also can be used as raw materials for this method.

## **3.2 Experimental method**

### **3.2.1 Chemicals**

Magnesium nitrate ( $\text{Mg}(\text{NO}_3)_2 \cdot 6\text{H}_2\text{O}$ ), aluminum nitrate nonahydrate ( $\text{Al}(\text{NO}_3)_3 \cdot 9\text{H}_2\text{O}$ ), sodium gluconate ( $\text{C}_6\text{H}_{11}\text{NaO}_7$ ), boric acid ( $\text{H}_3\text{BO}_3$ ), sodium sulfate ( $\text{Na}_2\text{SO}_4$ ) and sodium chloride ( $\text{NaCl}$ ) were special grade, and used as-received from WAKO (Osaka, Japan). A boron-specific chelating resin (Diaion® CRB 05) was purchased from Mitsubishi Chemical Co. (Tokyo, Japan).

### **3.2.2 Preparation of hydrotalcite with gluconate radical intercalation**

1.87 g  $\text{Al}(\text{NO}_3)_3$  and 2.56 g  $\text{Mg}(\text{NO}_3)_2$  were added to 50 mL of water containing 1.09, 2.18, 4.36 or 6.5 g sodium gluconate to form molar ratios of  $[\text{gluconate}]/[\text{Mg}^{2+}] = 0.5, 1, 1.5$  or  $2$ . Once the solution became transparent with stirring, its pH was adjusted to  $10 \pm 0.2$  with 1 mol/L NaOH. The solution was stirred continuously for 30 min, transferred to a Teflon vessel, placed in a microwave digestion system (ETHOS A, Milestone, Italy) and its temperature increased to  $120^\circ\text{C}$  in  $10^\circ\text{C}/\text{min}$  increments. The temperature was maintained for 180 min and the solution then allowed to cool to room temperature. The cooled reaction mixture was processed through solid-liquid separation on a supercentrifuge at 10000 rpm for 10 min and cleaned several times with ultrapure water. The solid residues were dried for 12 h in a vacuum freeze drier and designated as G-LDH-0.5, G-LDH-1, G-LDH-1.5 or G-LDH-2, where the numbers represent the molar ratios of  $[\text{gluconate}]/[\text{Mg}^{2+}]$  used in preparation.

Hydrotalcite intercalated with nitrate (NO<sub>3</sub>-LDH) was prepared by a similar method, but without sodium gluconate, to compare the borate sorption efficiency with that of the G-LDH series.

### 3.2.3 Characterization

The crystalline phases of various G-LDHs were determined using an X-ray diffractometer (XRD, Ultima IV, Rigaku, Japan) with Cu K $\alpha$  radiation. A D/teX Ultra detector and no reflection sample holder were applied. The accelerating voltage and current were 40 kV and 40 mA, with a scanning speed of 2°/min and scanning step of 0.02°. Simultaneous thermogravimetric and differential thermal analyses (TG-DTA 2000SA, Bruker, Japan) were performed atmospherically from room temperature to 800°C at a heating rate of 10°C/min. Fourier transform infrared (FTIR) spectra were recorded on a JASCO FTIR spectrometer (FT/IR-670 Plus, Japan). Transmission electron microscopy (TEM) images were obtained using a TECNAI-20 (Philips, Netherlands) transmission electron microscope.

Solid-state <sup>11</sup>B-NMR spectra for sorption residues were collected using an ECA 800 (JEOL, Japan). Two dimensional <sup>11</sup>B-NMR spectra were acquired. Multi-quantum magic angle spinning (MQ-MAS) was employed to acquire the <sup>11</sup>B-NMR spectra at a field strength of 18.79 T, acquisition time of 5.12 ms and F2 and F1 resolutions of 195.31 and 2.00 kHz, respectively.

The solid-state <sup>13</sup>C MAS NMR spectra of sodium gluconate and G-LDH, before and after borate sorption, were also recorded using an ECA 400 (JEOL, Japan); the cross-polarization (CP) contact time was 5 ms and 10000 scans were taken. Chemical shifts were referenced externally to tetramethylsilane (TMS;  $\delta$  = 0 ppm) using the methyl signal of hexamethylbenzene ( $\delta$  = 17.36 ppm) as a secondary standard.

To investigate the metallic, organic carbon and nitrate contents of the G-LDH series and NO<sub>3</sub>-LDH, LDHs samples prepared under different conditions were dissolved in 0.01 mol/L HCl. Solutions were diluted to determine the Mg and Al concentrations using an inductively coupled plasma emission spectrometer (ICP-AES, VISTA-MPX, Seiko Instruments, Japan). A total organic carbon analyzer (TOC-V CHS, Shimadzu, Japan) was used to determine the organic carbon and total nitrogen contents in solution.

### **3.2.4 Sorption experiments**

A total of 40 mL of simulated solution containing a known concentration of boric acid was prepared at pH 7.0. Because borate at neutral pH is predominantly in a molecular form, it is not removed by many water treatments, such as reverse osmosis, at pH <9.2. To test the sorption of boron on new materials, the initial pH of the solution should be <9.2. However, LDHs always dissolve to some extent under acidic conditions, thus influencing their properties. Therefore, the solution pH for testing the sorption behavior of these new LDHs should be neutral or weakly alkaline. Thirdly, several researchers have reported that boron-specific resins containing n-methyl glucamine showed good performance for boron removal at neutral pH [5, 6]. The gluconate in our LDHs has a similar structure to that of glucamine, and acts in a similar way to remove boron. So, we chose an initial pH of 7.0 for the boron solutions in this study. Then, 0.100 g of G-LDH, NO<sub>3</sub>-LDH or CRB 05 were added into these simulated solutions. The temperature was kept at  $25 \pm 2^\circ\text{C}$  and the solutions were stirred at 200 rpm in an oscillator. After each time interval, aqueous solution was taken out and filtered through a 0.20- $\mu\text{m}$  membrane filter. The total reaction time for experiments to measure the rate of sorption was 30 min, while the time for the sorption isotherm experiments was 24 h. The filtered solutions were diluted and then

subjected to ICP-AES to determine boron concentrations. The solid residues after sorption of borate were freeze-dried and supplied for X-ray diffraction, FTIR,  $^{11}\text{B}$ -NMR and  $^{13}\text{C}$ -NMR. The influence of pH on sorption of borate was also determined through a similar process to that described above, but the initial pH was adjusted to be either 4.0, 7.0, 9.0 or 11.0 using 1 M NaOH and 1 M HCl.

To explore the effects of competitive anions on the sorption of boron by G-LDH-1.5, 0.100 g sorbent was added to 40 mL of 2.5 mmol/L boron solution containing 50 mmol/L competing anions ( $\text{SO}_4^{2-}$  or  $\text{Cl}^-$ ) and the mixtures were shaken for 24 h. After this time, the supernatant was taken out and filtered through a 0.2  $\mu\text{m}$  membrane before determination of B content by ICP-AES.

The effect of temperature on the sorption was examined as follows. Firstly, 40 mL of 2.5 mmol/L borate solution, initial pH 7.0, was placed in a constant temperature oscillator for 1 hour, with the temperature increased to the required value. After that, 0.100 g G-LDH-1.5 was added to the solution. At each time interval, the supernatant was removed out and filtered through a 0.20  $\mu\text{m}$  membrane filter before ICP measurement.

### **3.3. Results and discussion**

#### **3.3.1 Characterization**

The XRD patterns of the  $\text{NO}_3$ -LDH and G-LDH series samples are shown in **Fig. 3.1**. The XRD pattern for  $\text{NO}_3$ -LDH clearly shows three characteristic reflections, assigned to 003, 006 and 009 planes at 11.04, 22.64 and 34.65°  $2\theta$ , respectively, which indicate that  $\text{NO}_3$ -LDH has a regularly layered structure. The interlayer spacing

of the 003 reflection ( $d_{003}$ ) for NO<sub>3</sub>-LDH is 8.01 Å, very close to the previously reported value [7]. Elemental compositions are summarized in **Table 3.1**.

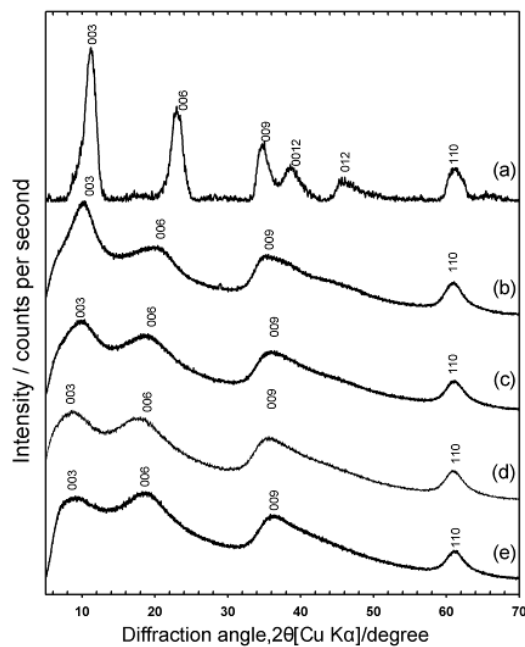


Fig. 3.1 XRD patterns for (a) NO<sub>3</sub>-LDH, (b) G-LDH-0.5, (c) G-LDH-1, (d) G-LDH-1.5 and (e) G-LDH-2.



Table 3.1 Elemental compositions and molar ratios of Mg/Al and Al/gluconate in different LDHs

Sample	Al	Mg	NO <sub>3</sub> <sup>-</sup>	Gluconate	Total anions	Molar ratio	Molar ratio	Molar ratio NO <sub>3</sub> <sup>-</sup> /Al
	(mmol/g)	(mmol/g)	(mmol/g)	(mmol/g)	(mmol/g)	Mg/Al	gluconate/Al	
NO <sub>3</sub> -LDH	5.82	12.81	5.83	-----	5.83	2.20	-----	1.00
G-LDH-0.5	3.39	7.04	1.62	1.95	3.57	2.08	0.58	0.48
G-LDH-1	3.24	6.46	1.07	2.35	3.42	1.99	0.73	0.31
G-LDH-1.5	3.19	6.27	0.31	2.64	2.95	1.96	0.83	0.10
G-LDH-2	3.01	5.60	0.12	3.39	3.41	1.86	1.12	0.04

Without gluconate, the molar ratio of Mg/Al was 2.20 and the excess positive charge in the Mg-Al host layers was entirely compensated by  $\text{NO}_3^-$  in the guest layers of  $\text{NO}_3$ -LDH. With an increase in intercalated gluconate, the 003 and 006 reflections shifted toward lower angles, and became broader (**Fig. 3.1(b-e)**). This broadening is caused by the presence of a mixture of different  $d$  spacings within the LDHs, since some  $\text{NO}_3^-$  still remains, even after intercalation with gluconate (**Table 3.1**).

The interlayer spaces,  $d_{003}$ , were calculated as 8.74, 9.08, 10.28 and 10.43 Å for G-LDH-0.5, 1.0, 1.5 and 2.0, respectively. This indicates that the LDH basal spacing was expanded because of the intercalation of gluconate into the LDHs galleries; this is expected, because gluconate is a larger ion than nitrate [8, 9]. The ionic length of free gluconate was calculated as 6.4 Å (**Fig. 3.2**) using Gaussian 09 (Revision C.01) [10].

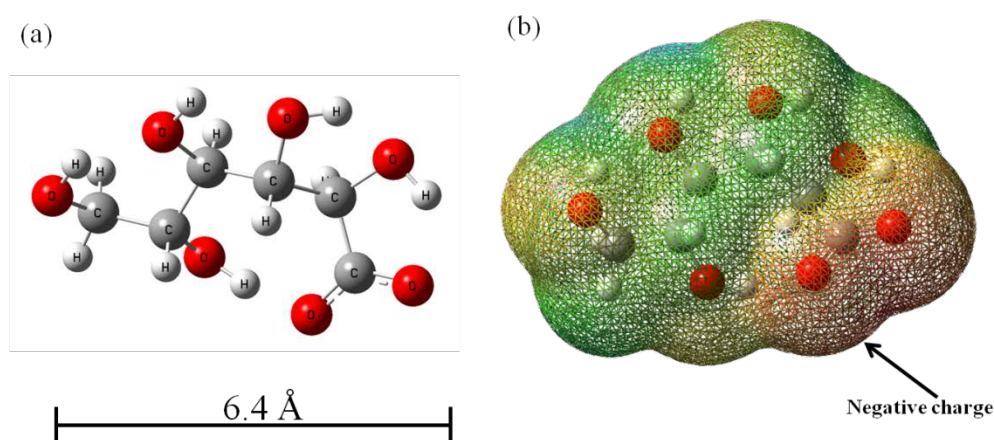


Fig. 3.2 Three-dimensional molecular model of gluconate calculated and (b) Electrostatic potential mapped with total density in Gaussian 09, b3lyp/6-31G(d).

Therefore, the space occupied by gluconate in G-LDH-1.5 is approximately 5.5 Å; this implies that the arrangement of gluconate in the LDHs interlayer may be a monolayer, with the molecules arranged at an angle to the host layers.

The molar ratio of Mg/Al decreased around 15% with an increase in intercalated gluconate, as shown in **Table 3.1**. This suggests that gluconate reacted with the  $\text{Mg}^{2+}$  during preparation, resulting in variation in the LDHs composition [11]. Furthermore, if gluconate were completely replaced with  $\text{NO}_3^-$  in the G-LDH, the molar ratio of gluconate/Al should be equal to 1.00. However, the observed value was less than 1.0 in the G-LDH-0.5 to -1.5 samples, as shown in **Table 3.1**, indicating that the doped gluconate is not completely replaced with  $\text{NO}_3^-$  in G-LDH-0.5 to -1.5. This means that the G-LDH series have some  $\text{NO}_3^-$  remaining, even after intercalation with gluconate.

In addition, with increase in gluconate concentration from 1.95 to 3.39 mmol/g, the molar ratio of Mg/Al decreased slightly, and the nitrate content in G-LDH decreased from 1.62 to 0.12 mmol/g. Such differences in composition may affect the TEM images for the G-LDH series compared with those for  $\text{NO}_3$ -LDH. **Fig. 3.3** shows the TEM images of  $\text{NO}_3$ -LDH (**Fig. 3.2(a)**) and the G-LDH series samples (**Fig. 3.3(b-e)**). As shown in **Fig. 3.3(a)**, the  $\text{NO}_3$ -LDH is in nanosheets, 50–70 nm wide and 5 nm thick. The individual particle size of G-LDH-0.5 is similar to that of  $\text{NO}_3$ -LDH; however, the granules in G-LDH-0.5 were extensively agglomerated. With G-LDH-1.0, the nanosheet structure was maintained (**Fig. 3.3(c)**), but the granule size increased significantly to ~150 nm. Meanwhile, for G-LDH-1.5 (**Fig. 3.3(d)**), the morphology was similar to that of G-LDH-1.0, but the granule size increased to ~250 nm. For G-LDH-2.0, agglomeration progressed further, with the granule size soaring to ~400 nm (**Fig. 3.3(e)**). The possible interaction of gluconate with metallic ions might influence LDH crystal growth, leading to enhancement of disordered stacking with increased gluconate/Mg.

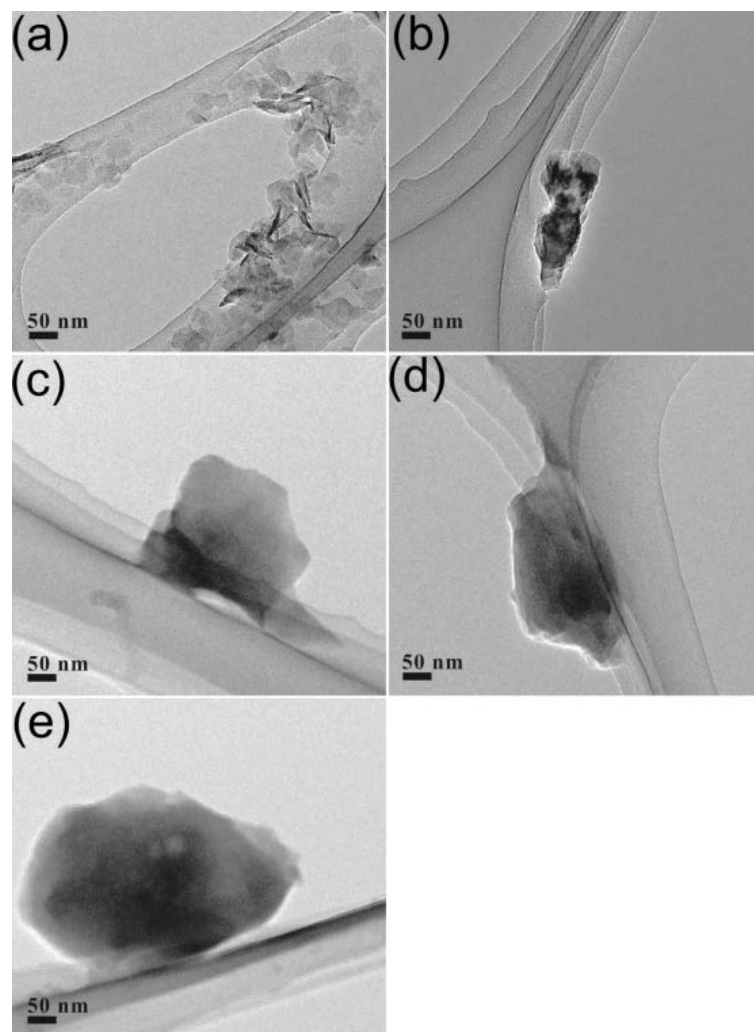


Fig. 3.3 TEM images of (a)  $\text{NO}_3$ -LDH, (b) G-LDH-0.5, (c) G-LDH-1, (d) G-LDH-1.5 and (e) G-LDH-2. Horizontal bars indicate 50 nm.

**Fig. 3.4** displays the FTIR spectra for  $\text{NO}_3$ -LDH and G-LDH-1.5, in which the broad peak at  $3400\text{ cm}^{-1}$  corresponds to  $\nu(\text{OH})$  [12]. This indicates that both LDHs have -OH groups, as further verified by the out-of-plane bending vibration mode,  $\gamma(\text{OH})$ , at  $660\text{ cm}^{-1}$ . For the  $\text{NO}_3$ -LDH, the strong peak at  $1384\text{ cm}^{-1}$  corresponds to the  $\nu_s(\text{NO}_3)$  vibration, while a small peak at  $832\text{ cm}^{-1}$  was assigned to the out-of-plane bending vibration mode,  $\gamma(\text{NO}_3)$  [9]. The FTIR spectra of G-LDH series are different from that of  $\text{NO}_3$ -LDH. Stretching vibration modes of  $\nu(\text{CH})$  were observed at  $2924$  and  $2854\text{ cm}^{-1}$ , indicating that the compound has saturated carbons [13].

However, the spectrum shows the presence of a peak at  $1427\text{ cm}^{-1}$  and the absence of an observable peak at  $1380\text{ cm}^{-1}$ , suggesting that the compound only contains  $-\text{CH}_2$ . The stretching vibration mode of C-O was observed at  $1090$ ,  $1234$  and  $1132\text{ cm}^{-1}$  and the asymmetric stretching vibration mode of C=O at  $1634\text{ cm}^{-1}$  was strengthened, both of which indicate the presence of carboxylic groups in the compound [9, 14]. The vibration mode near  $440\text{ cm}^{-1}$  was assigned to the vibration mode of metal-oxygen in hydrotalcite [15]. These results also indicate that gluconate is intercalated in LDHs. Meanwhile, characteristic  $-\text{NO}_3$  absorption peaks appear at  $1384\text{ cm}^{-1}$  indicating that nitrate has entered the LDHs interlayer.

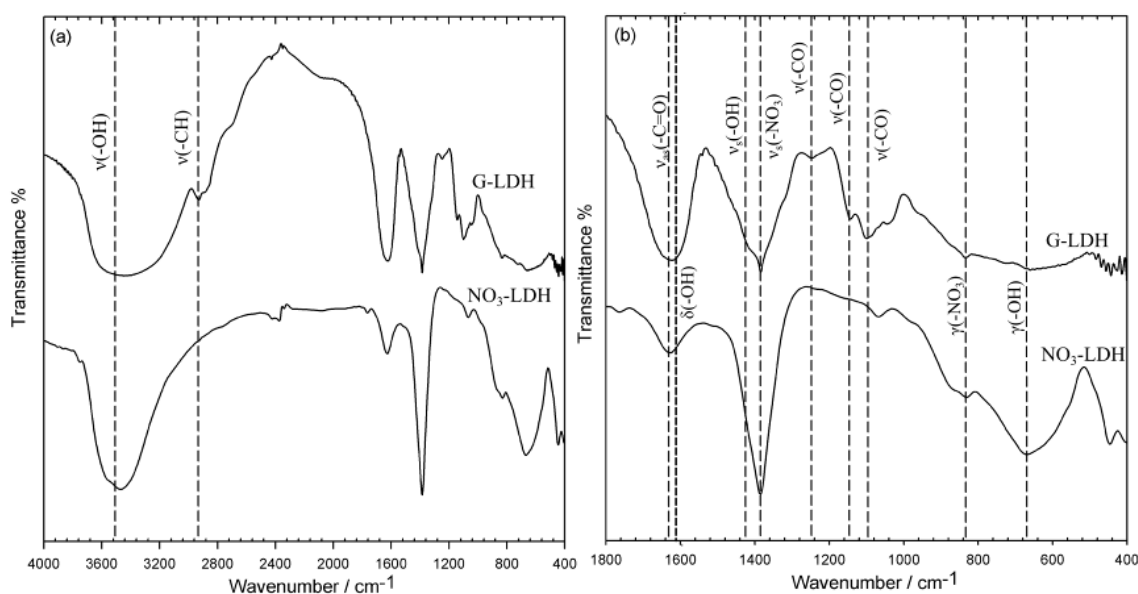


Fig. 3.4 FTIR spectra in (a) full range from  $4000$  to  $400\text{ cm}^{-1}$  and (b) blown-up range from  $1800$  to  $400\text{ cm}^{-1}$  for G-LDH-1.5 and  $\text{NO}_3$ -LDH.

**Fig. 3.5(a) and (b)** show the solid-state  $^{13}\text{C}$ -NMR spectra for sodium gluconate (as a reference), and G-LDH-1.5 before borate sorption. The  $^{13}\text{C}$ -NMR spectrum of sodium gluconate has six peaks, of which the highest chemical shift at  $178.99\text{ ppm}$  is assigned to a carboxylic carbon ( $\text{C}_1$ ) [16]. Another five peaks were observed from  $60$

to 90 ppm, which all correspond to -C- that were bound to -OH groups. The peak at 61.75 ppm is assigned to -CH<sub>2</sub>-OH (C<sub>6</sub>), while the chemical shifts for the remaining four peaks were at 80.85, 74.26, 71.42 and 70.65 ppm. These four C atoms were at slightly different positions because of their different electron densities. Compared with the <sup>13</sup>C-NMR spectrum for sodium gluconate, the spectrum of G-LDH-1.5 showed essentially the same chemical shifts, but with broader peaks; this is as expected because of the strong interactions with different atoms and functional groups such as metal and nitrate in G-LDH [17].

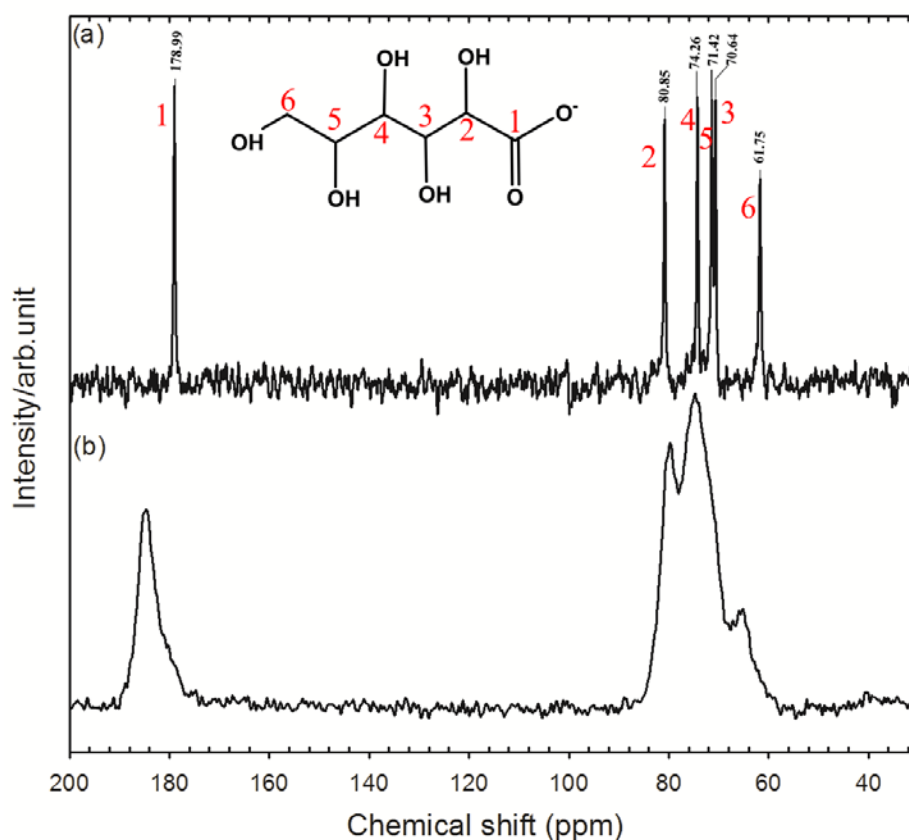


Fig. 3.5 <sup>13</sup>C-NMR MAS spectra for (a) sodium gluconate and (b) G-LDH-1.5.

TG/DTA results of NO<sub>3</sub>-LDH and G-LDH-1.5 in air are shown in **Fig. 3.6**. Both TG curves decreased with increasing temperature. This occurred because of

desorption of surface water and interlayer-adsorbed water in NO<sub>3</sub>-LDH and G-LDH-1.5 from room temperature to around 160°C. Endothermic peaks were observed from water evaporation at 68.4 and 80.2°C, associated with mass losses of 12.45 and 13.79 %, in NO<sub>3</sub>-LDH and G-LDH-1.5, respectively. With continuing increase in temperature, the mass loss of these two LDHs occurs for different reasons, although both masses decreased gradually. From 162 to 322 °C, NO<sub>3</sub>-LDH showed a slow decrease in mass, corresponding to lattice water desorption, and a 3.61 % mass loss [18]. However, during this period, G-LDH showed 10.33 % mass loss through lattice water evaporation, as well as stepwise decomposition of the gluconate in G-LDH; this mass loss which was significantly larger than that of NO<sub>3</sub>-LDH in this temperature range. When the temperature exceeded 350°C, both NO<sub>3</sub>-LDH and G-LDH exhibited clear weight loss, until their masses stabilized near 600°C. During this period, the mass loss of NO<sub>3</sub>-LDH was caused mainly by the desorption of laminated -OH and interlayer NO<sub>3</sub><sup>-</sup> [19]. However, no obvious thermal effect was produced during decomposition, because these are non-instantaneous reactions. The DTA curve revealed two weak endothermic peaks at 354.1 and 425.3°C, corresponding to a mass loss of 33.76 % for NO<sub>3</sub>-LDH (**Fig. 3.6(a)**). Although the mass loss of G-LDH during this period is also caused by hydroxyl desorption in the host layer and interlayer anions, the DTA of G-LDH showed more obvious thermal variation than seen for NO<sub>3</sub>-LDH. Combustion of interlayer gluconate at 447.6°C produced an obvious exothermic peak in the DTA curve, with a mass loss of approximately 36.84 % during this period (**Fig. 3.6(b)**). TGA results also confirm the presence of gluconate in the LDHs.

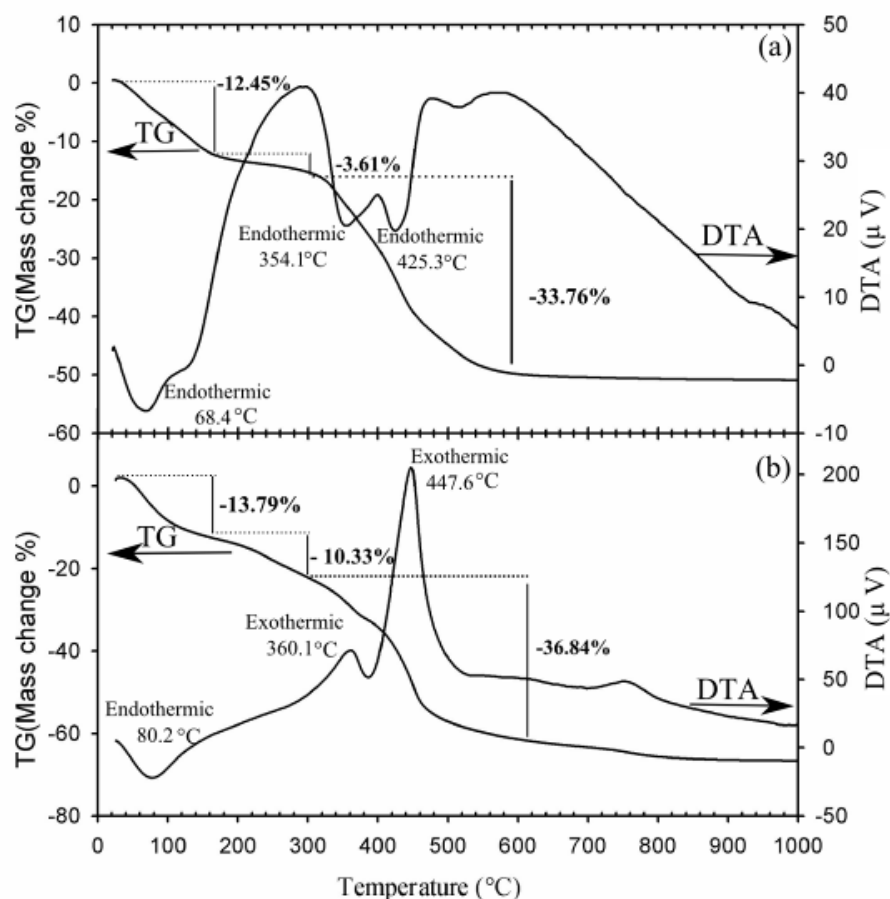


Fig. 3.6 TG-DTA of (a) NO<sub>3</sub>-LDH and (b) G-LDH-1.5. The numbers in % indicate mass changes.

### 3.3.2 Removal of borate using different LDHs

The sorption results of G-LDH and NO<sub>3</sub>-LDH in 2.3 mM borate solutions are shown in **Fig. 3.7**. The sorption densities of borate by G-LDH-0.5, G-LDH-1, G-LDH-1.5 and NO<sub>3</sub>-LDH were 0.43, 0.44, 0.48 and 0.18 mmol/g, respectively. The G-LDH series achieved greater sorption densities than the NO<sub>3</sub>-LDH sample, because of the stable and rapid complexation of polyhydroxyl groups in gluconate with borate. The borate removal capacity of G-LDH increased with increasing G-LDH dosage (**Fig. 3.8**).



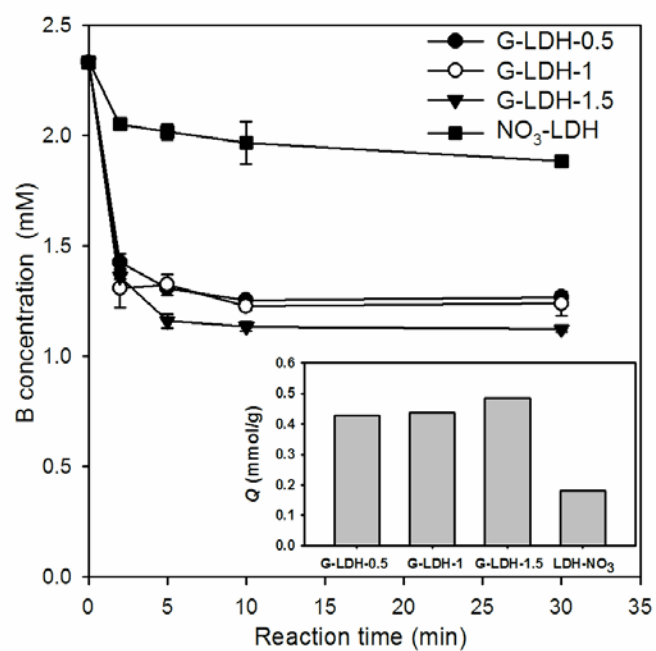


Fig. 3.7 Changes in B concentrations with elapsed time on NO<sub>3</sub>-LDH, G-LDH-0.5, G-LDH-1 and G-LDH-1.5. Inset shows sorption capacities of different sorbents (sorbents: 2.5 g/L, initial B concentration: 2.5mM, initial pH was adjusted to 7).

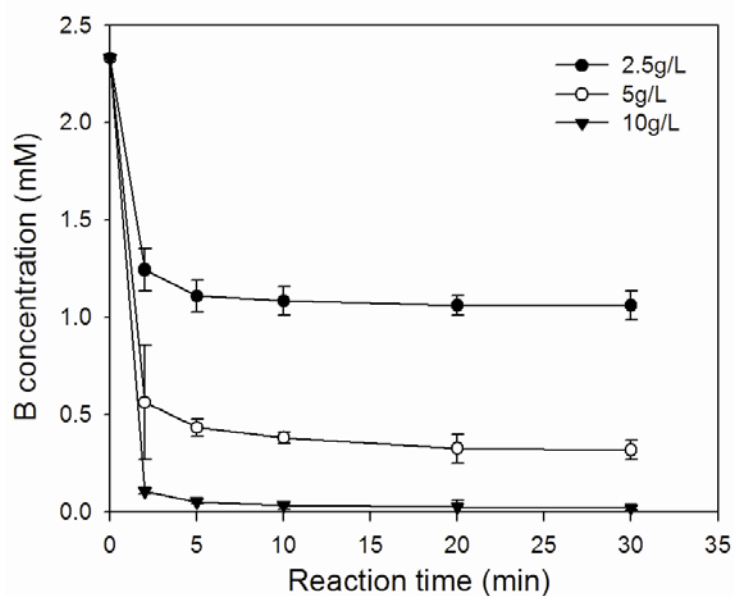


Fig. 3.8 Changes in B concentrations with the elapsed time using different amounts of G-LDH-1.5 at the initial pH 7.

When the dosage of G-LDH-1.5 is 2.5 g/L, the boron concentration in the water after treatment was 0.09 mM/L, which does not meet the standard for drinking water in Japan (1 mg/L). As the LDHs concentration increased to 5 g/L and 10 g/L, the boron concentration decreased to 0.03 mM/L and  $2 \times 10^{-3}$  mg/L. Both comply with the drinking water standards of Japan.

However, the removal rate and sorption density did not increase significantly with increase in LDHs gluconate content (**Fig. 3.7** and **Table 3.1**). This may be caused by an LDHs layer structure that enables the borate species to infiltrate from the guest layer edge. Considering that borate rapidly complexes with -OH groups in LDHs when it enters the guest layer, it easily complexes with the gluconate at the edge of the guest layer. Steric hindrance by these complexes may prevent borate penetration into the guest layers, thereby reducing the adsorbability of borate by G-LDH. Considering that the gluconate anions inside the guest layer were not used fully, increasing the gluconate concentration in the LDHs under the same initial borate concentration did not lead to a significant increase in sorption density.

### 3.3.3 Sorption mechanism

It is suggested that borate removal by NO<sub>3</sub>-LDH and G-LDH-1.5 is based on different mechanisms. **Fig. 3.9(a)** shows the FTIR spectra of G-LDH-1.5 before and after sorption. In the infrared spectrum of G-LDH-1.5 after sorption of borate, the stretching vibration modes of -CH at 2924 and 2854 cm<sup>-1</sup>, C-O at 1090, 1234 and 1132 cm<sup>-1</sup>, as well as asymmetric stretching vibration modes of C=O at 1634 cm<sup>-1</sup> are characteristic of gluconate, and indicate that gluconate groups are present in the LDHs even after sorption of borate [9, 13]. In contrast to this, the characteristic -NO<sub>3</sub> peaks at 1384 and 855 cm<sup>-1</sup> in the FTIR spectra of NO<sub>3</sub>-LDH weaken significantly after

exposure to borate solution, because NO<sub>3</sub>-LDH immobilizes borate through ion exchange between nitrate and borate, rather than by complexation (as occurs between gluconate and borate in G-LDH-1.5) (**Fig. 3.9(b)**). Therefore, the nitrate in the LDHs guest layer is exchanged with B(OH)<sub>4</sub><sup>-</sup> after reaction, leading to decreases in nitrate peak intensities for NO<sub>3</sub>-LDH after borate sorption.

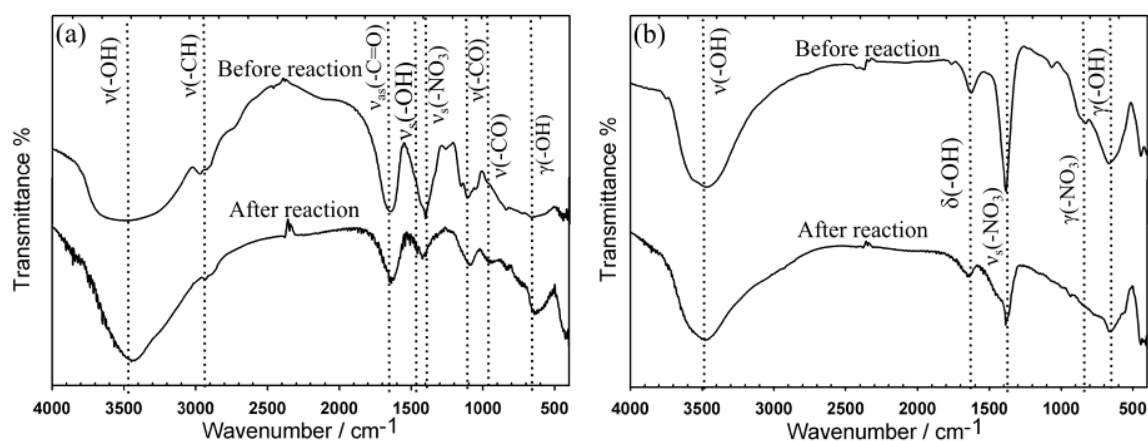


Fig. 3.9 FTIR spectra for (a) G-LDH-1.5 and (b) NO<sub>3</sub>-LDH before and after sorption.

In addition, <sup>11</sup>B MQ-MAS NMR spectra were collected for NO<sub>3</sub>-LDH and G-LDH-1.5 after borate sorption to understand the mechanism further, and the contour plots are shown in **Fig. 3.10**.

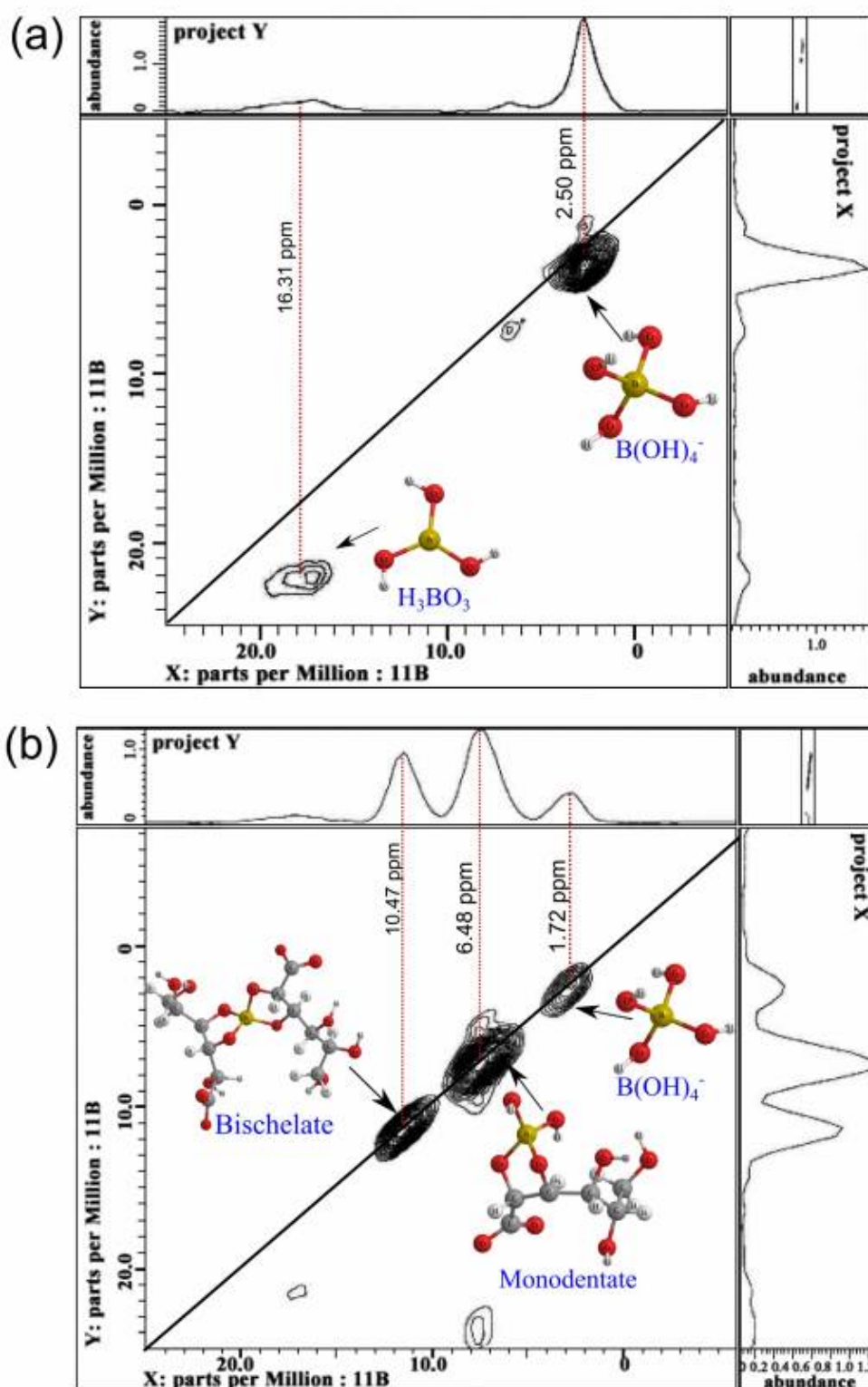


Fig. 3.10 Two-dimensional  $^{11}\text{B}$  -NMR for (a)  $\text{NO}_3$ -LDH and (b) G-LDH-1.5 after sorption of borate.

The contour maps of boron in the two-dimensional  $^{11}\text{B}$  MAS NMR of  $\text{NO}_3\text{-LDH}$  and  $\text{G-LDH-1.5}$  were close to the diagonal line, indicating that the quadrupole interaction was small [20]. According to previous reports, the chemical shifts of tetrahedral borate ( $^{11}\text{B}$ ) ranged mainly from 3 to -3 ppm [21]. Correspondingly, the chemical shift of the trigonal boron ( $^{11}\text{B}$ ) contour map was approximately 15-20 ppm. Furthermore, according to Bishop et al. [22] and Takahashi et al. [20], the contour plots with 10 to 14 ppm and 5 to 8 ppm chemical shifts represent mainly bischelate and monodentate complexes, respectively. Based on the aforementioned results, boron clearly has different complexation patterns in  $\text{NO}_3\text{-LDH}$  and  $\text{G-LDH-1.5}$ . In  $\text{NO}_3\text{-LDH}$ , the contour plots indicate that boron occurs mainly as  $\text{B}(\text{OH})_4^-$  in  $\text{NO}_3\text{-LDH}$ . This further demonstrates that  $\text{NO}_3\text{-LDH}$  adsorbed boron by ion exchange of  $\text{NO}_3^-$  with  $\text{B}(\text{OH})_4^-$  to immobilize borate in LDHs. However, the behavior of  $\text{G-LDH-1.5}$  was different. Its boron contour plots were concentrated in three different areas: one is around 1.72 ppm, assigned to  $\text{B}(\text{OH})_4^-$ ; the second is located at 6.48 ppm, and assigned to monodentate complexes, and the third is located at 10.47 ppm, and assigned to bischelate complexes. According to Yoshimura et al. [23], the reaction between boron and the *N*-methyl-D-glucamine group can yield three different complexes: monodentate (combination of one *N*-methylglucamine group and one borate), bischelate (complexes of one borate and two *N*-methylglucamine groups) and tetradentate (complexes of one borate and multi-hydroxy in one *N*-methylglucamine group) complexes. Based on the  $^{11}\text{B}$  MAS NMR spectrogram of  $\text{G-LDH-1.5}$ , the monodentate complexes are predominant followed by bischelate in  $\text{G-LDH-1.5}$ , along with trace amounts of  $\text{B}(\text{OH})_4^-$ . In addition, considering that the relative intensities of monodentate: bischelate:  $\text{B}(\text{OH})_4^-$  were 100: 55: 21, the dominant form of boron in  $\text{G-LDH-1.5}$

LDH is as a monocomplex. This finding indicates that G-LDH has similar performance and selectivity to *N*-methylglucamine-type resins.

The structures of these two LDHs were not damaged after reaction, and their XRD patterns were not affected by borate sorption (**Fig. 3.11**). Therefore, based on the aforementioned discussion, a schematic illustration of the boron sorption mechanisms of G-LDH-1.5 and NO<sub>3</sub>-LDH is shown in **Fig. 3.12**. In the NO<sub>3</sub>-LDH system, borate was eliminated through ion exchange with the nitrate in the LDH interlayer (**Fig. 3.12(a)**). In contrast, borate was removed by G-LDH mainly through complexation, producing two different monodentate and bischelate complexes (**Fig. 3.12(b)**).

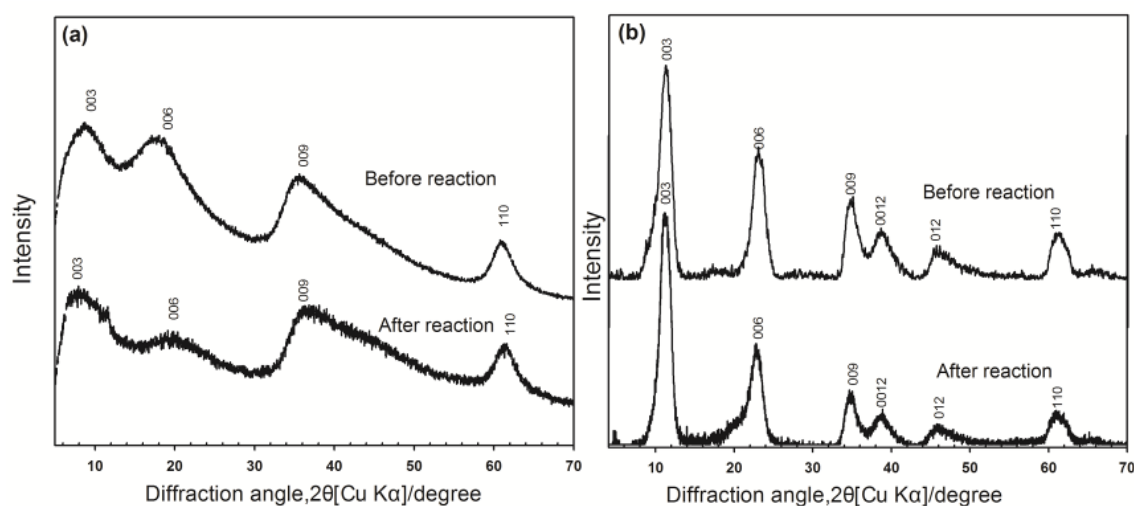


Fig. 3.11 XRD patterns of (a) G-LDH-1.5 and (b) NO<sub>3</sub>-LDH before and after sorption of borate.

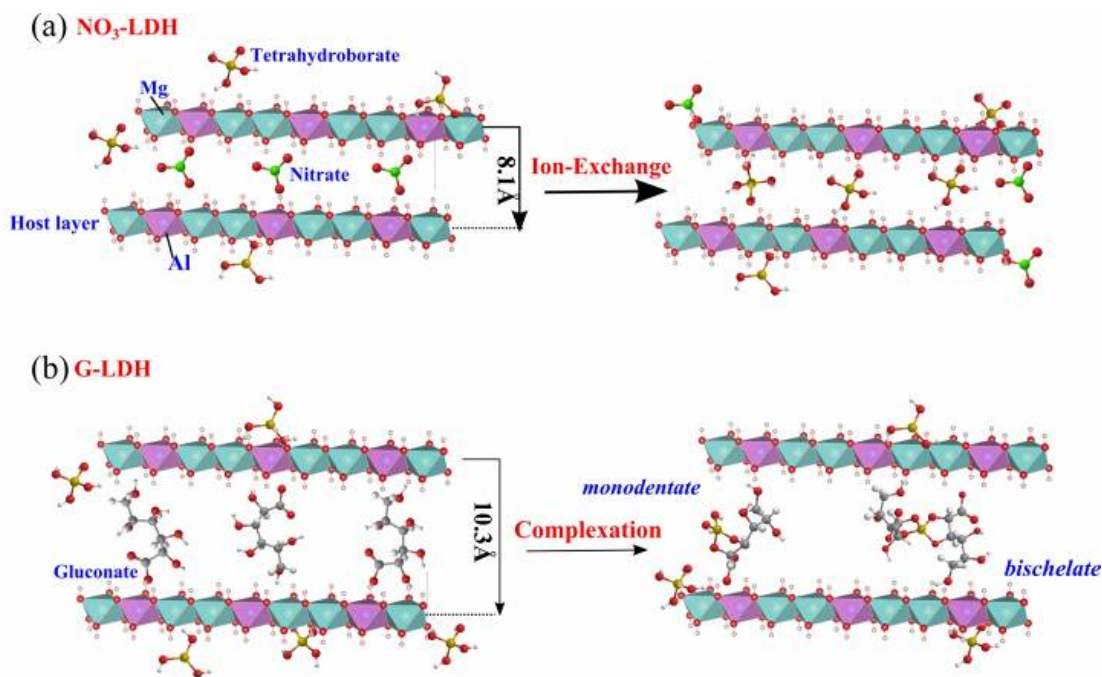


Fig. 3.12 Schematic illustration to show sorption mechanism of borate onto (a) NO<sub>3</sub>-LDH and (b) G-LDH-1.5.

Based on the aforementioned sorption mechanism, the total sorption capacity of NO<sub>3</sub>-LDH may be larger than that of G-LDH using the same adsorbent mass. Through ion exchange, the highest sorption density for NO<sub>3</sub>-LDH occurs when 1 mol of NO<sub>3</sub><sup>-</sup> ion is exchanged with 1 mol of borate. In contrast, borate sorption by G-LDH occurs by the formation of a partial bischelate (complex of two gluonate and a borate) so that 1 mol of gluonate cannot react with 1 mol of borate. Hence, the total sorption capacity of G-LDH is theoretically lower than that of NO<sub>3</sub>-LDH, as shown in the sorption isotherms of NO<sub>3</sub>-LDH and G-LDH (**Fig. 3.13**). Although the sorption density of NO<sub>3</sub>-LDH is slightly larger than that of G-LDH, G-LDH clearly shows stable sorption and a high sorption rate.

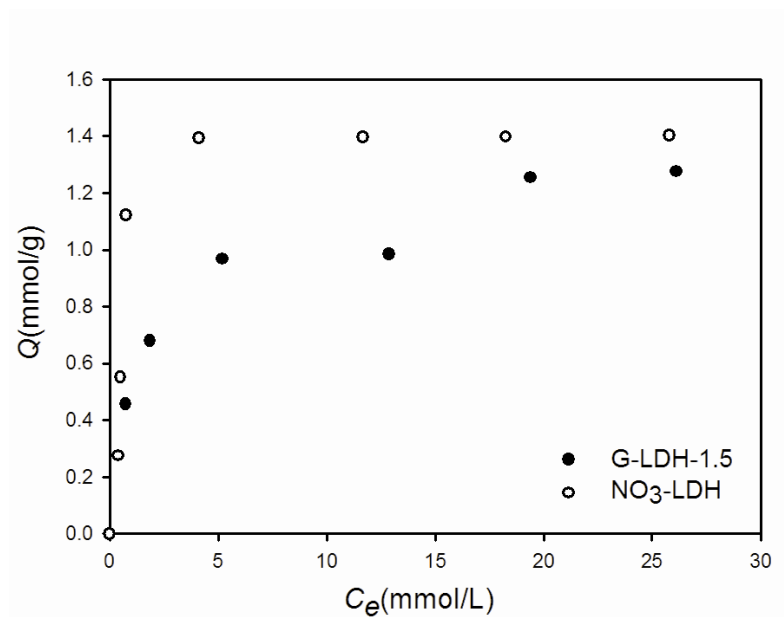


Fig. 3.13 Sorption isotherms of borate onto NO<sub>3</sub>-LDH and G-LDH-1.5 (sorbents: 2.5 g/L, initial pH 7, reaction time: 24 h, temperature : 25°C).

### 3.3.4 Effect of co-existing anions on sorption of borate

The borate removal efficiency of G-LDH-1.5 and NO<sub>3</sub>-LDH under these conditions is shown in **Fig. 3.14**, revealing that the borate sorption density of NO<sub>3</sub>-LDH decreased significantly in the presence of other anions. For example, the borate sorption density of NO<sub>3</sub>-LDH in the presence of 50 mM Cl<sup>-</sup> decreased from 0.66 to 0.32 mmol/g. Furthermore, in the borate solution with 50 mM SO<sub>4</sub><sup>2-</sup>, no borate sorption was observed with NO<sub>3</sub>-LDH, because SO<sub>4</sub><sup>2-</sup> adheres more strongly than B(OH)<sub>4</sub><sup>-</sup> to the host layers in LDH. However, the borate removal capacity of G-LDH-1.5 was not affected by other co-existing anions, and was maintained consistently around 0.57 mmol/g regardless of the co-existing Cl<sup>-</sup> and SO<sub>4</sub><sup>2-</sup>. This result implies that G-LDH should be more applicable in real waters than NO<sub>3</sub>-LDH, because of its selectivity and stability.



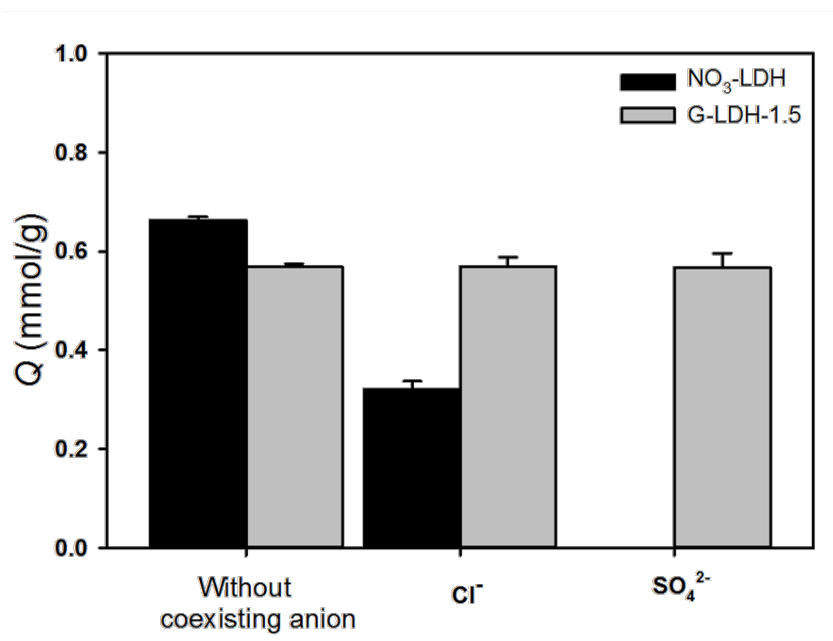


Fig. 3.14 Effect of coexisting anions on sorption of borate onto NO<sub>3</sub>-LDH and G-LDH-1.5 (sorbents: 2.5 g/L, coexisting anionic concentration: 50 mM; initial B concentration: 2.5 mM, initial pH was adjusted to 7.00, reaction time :24 h, temperature :25°C).

Undoubtedly, during borate sorption with competing ions, gluconate in the LDH interlayer could be exchanged with co-existing anions and released into solution, especially in the solution containing divalent ions, since the binding force between the divalent anions and metallic hydroxide layers is greater than that of the monovalent anions with host layers. This is shown by the gluconate contents, as determined by TOC measurements. In the borate solution without coexisting ions, the TOC value in solution, which comes from the gluconate released into solution, was 0.27 mg/L. In the Cl<sup>-</sup> solution, the TOC value was 0.38 mg/L and increased to 0.58 mg/L in the SO<sub>4</sub><sup>2-</sup> solution after 24 h. However, the amount of gluconate released into solution was too low to affect borate sorption by G-LDH. Because borate complexes with gluconate were divalent (monodentate) and trivalent (bischelate) anions and anions with higher valences more easily occupy sorption sites in the guest layer of LDH,

because of their stronger electrostatic interactions with the host layer [4], ion exchange between the complexes and coexisting anions becomes difficult and the complexes remain immobilized in G-LDH.

### 3.3.5 Comparison of G-LDHs with boron-specific resin

The sorption isotherms of G-LDH-1.5 and CRB 05, as well as their sorption capacity variation curve with time, are shown in **Fig. 3.15(a)**. Both borate sorption isotherms were evaluated by fitting to the Langmuir isotherm:

$$Q_e = \frac{Q_{max} K C_e}{1 + K C_e}, \quad (1)$$

where  $Q_e$  is the amount sorbed at equilibrium (mmol/g),  $C_e$  is the borate concentration at equilibrium (mmol/L),  $K$  is the sorption equilibrium constant (L/mmol) and  $Q_{max}$  is the sorption capacity (mmol/g). The data fitted well to the Langmuir isotherm. The Langmuir constants,  $K$  and  $Q_{max}$ , determined using non-linear least squares analyses, are shown in **Table 3.2**.

Table 3.2 Langmuir fitting parameters for sorption isotherm of borate onto G-LDH-1.5 and CRB05

Sample	$Q_{max}$ (mmol/mmol)	$K$ (L/mmol)	$R^2$
G-LDH-1.5	0.43	0.28	0.97
CRB05	0.37	0.28	0.99

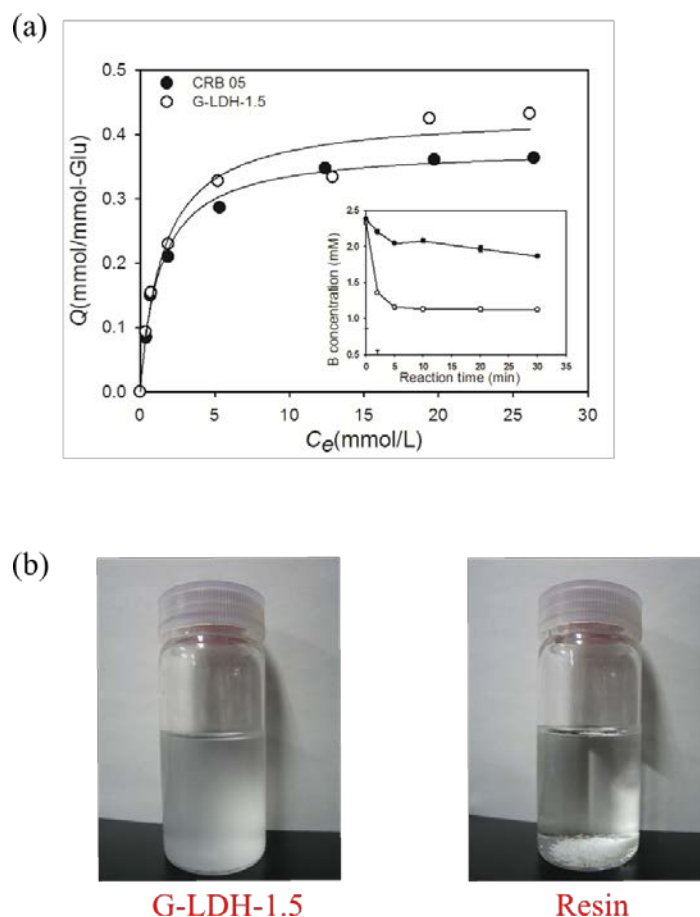


Fig. 3.15 Sorption isotherms (a) and photographs of suspensions in 2.5 mM borate ; (b) for boron specific-resin (CRB 05) and G-LDH-1.5 (sorbents: 2.5 g/L, initial pH 7, reaction time: 24 h, temperature :25°C). Inset in Fig. 11(a) shows changes in borate concentration by CRB 05 and G-LDH-1.5 with elapsed time (sorbent: 2.5 g/L, initial B concentration: 2.5 mM, initial pH 7, reaction time: 30 min, temperature :25°C).

The maximum sorption capacity of G-LDH reached 0.43 mmol/mmo based on the weight of gluconate, which is slightly higher than that of CRB 05 based on the N-methylglucamine [24]. In addition, comparison of their sorption capacity variation curves indicated that within 30 min, G-LDH-1.5 exhibited a higher sorption rate than CRB05 because the resin does not disperse as well as G-LDH-1.5 in solution. As shown in **Fig. 3.15(b)**, the solution turned white after G-LDH was dispersed in the solution, while the resin rapidly sank to the bottom. The smaller particles of G-LDH

are easier than CRB 05 to disperse within a shorter time in borate solution, resulting in sorption rates for G-LDH faster than that of CRB 05.

### 3.3.6 Temperature effect on the sorption of borate by G-LDH-1.5

The effect of temperature on boron removal was studied over a range of temperatures from 25 to 55°C. According to **Fig. 3.16**, the sorption rates of borate by G-LDH-1.5 at different temperatures were similar, and increasing the temperature only slightly enhanced the boron sorption density after 24 h (from 0.53 mmol/g to 0.61 mmol/g). What is more, the TOC results showed that the amount of dissolution of gluconate after 24 h was only slightly increased with increasing temperature (from 2.95 mg/L at 25°C to 3.30 mg/L at 55°C), and this rise in amount of gluconate released into solution was too small to affect borate sorption by G-LDH-1.5. In other words, the sorption density of borate by G-LDH-1.5 was stable between 25 and 55 °C.

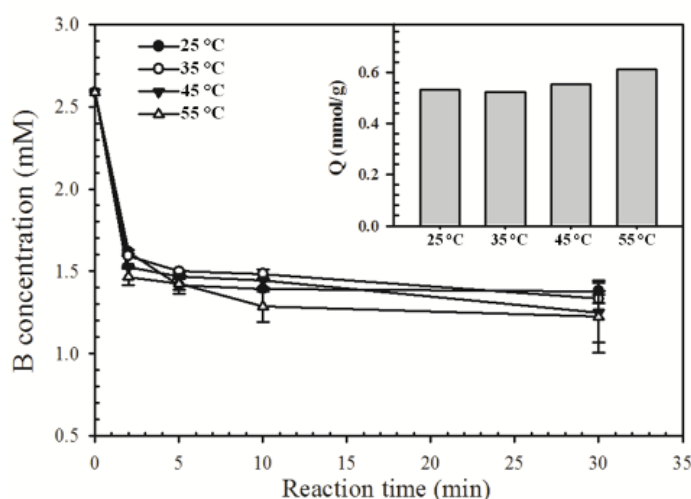
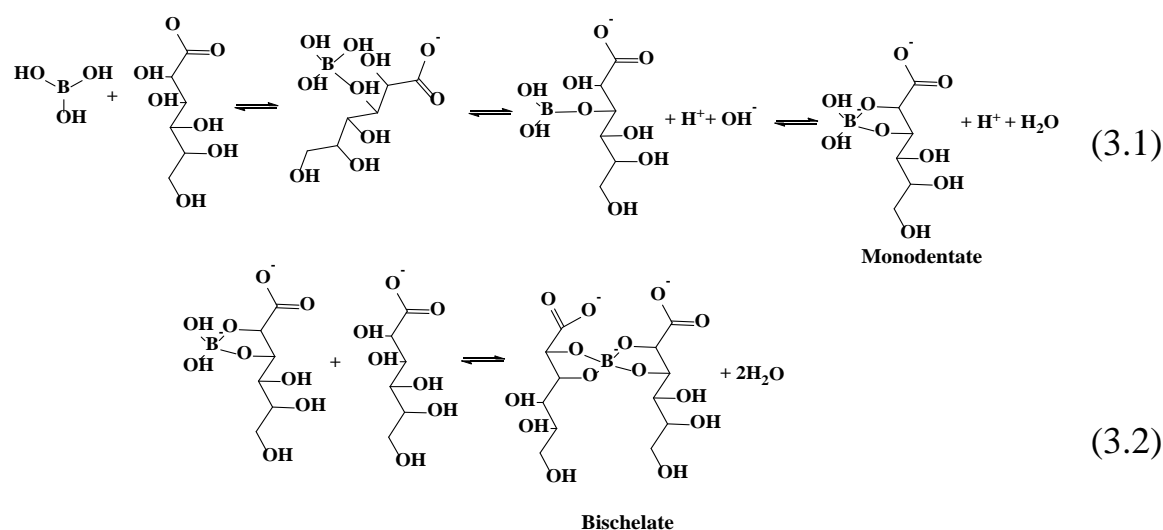


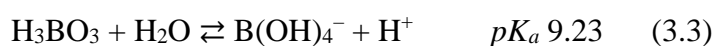
Fig.3.16 Effect of temperatures on the sorption of borate by G-LDH-1.5 with elapsed time (sorbent: 2.5 g/L, initial B concentration: 2.5 mM, initial pH 7, reaction time: 30 min). Inset in Fig.12 shows sorption densities of borate by G-LDH-1.5 under different temperatures. (sorbent: 2.5 g/L, initial B concentration: 2.5 mM, initial pH 7, reaction time: 24 h).

### 3.3.7 Effect of pH on the sorption of borate by G-LDH-1.5

The effect of the initial pH on the sorption of borate by G-LDH-1.5 is presented in **Fig. 3.17**. Better sorption rates of borate by G-LDH-1.5 were obtained at pH 7 and pH 9. This is because the sorption rate of borate on G-LDH-1.5 was mainly through complexation between the borate and gluconate (eqs.(3.1) and (3.2)).



When the pH was higher than 9.23,  $\text{H}_3\text{BO}_3$  could be changed into  $\text{B}(\text{OH})_4^-$  (eq.(3.3)):



So, when the initial pH was increased to 11, the main borate species in solution was  $\text{B}(\text{OH})_4^-$ , which cannot react with gluconate, resulting in a lower sorption rate. For pH 4, although the boron mainly existed as  $\text{H}_3\text{BO}_3$ , the structure of G-LDH-1.5 was partially dissolved and damaged by the acidic conditions, and thus the sorption density of borate decreased.

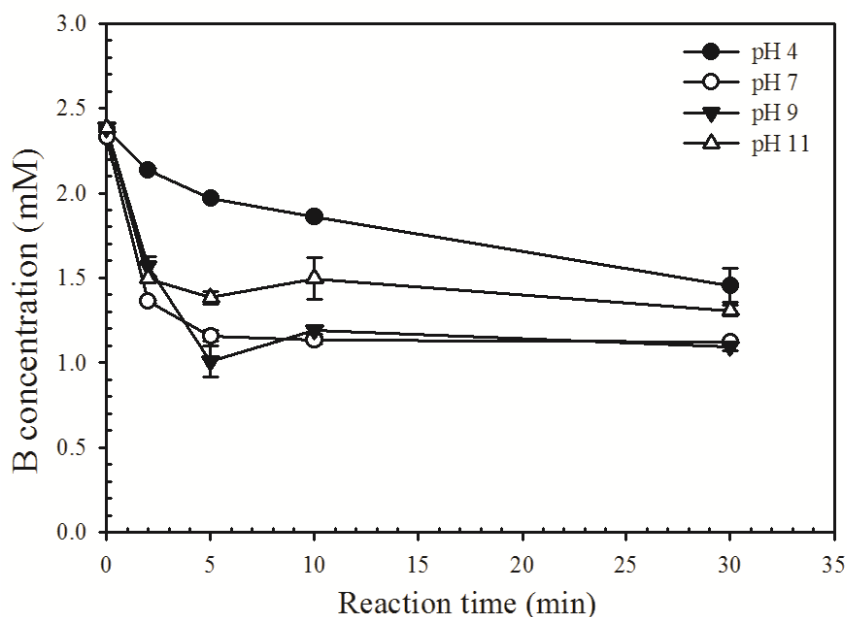


Fig. 3.17 Effect of pH on the sorption of borate by G-LDH-1.5 with elapsed time (sorbent: 2.5 g/L, initial B concentration: 2.5 mM, reaction time: 30 min, temperature : 25°C).

### 3.4. Conclusion

In this work, we successfully synthesized, in one step, a hydrotalcite-like material intercalated with gluconate (G-LDH) and showed through a series of batch experiments that G-LDH removes borate from solutions effectively. The sorption ability of G-LDH was much higher than that of  $\text{NO}_3$ -LDH, and G-LDH performed well for borate removal, showing little interference from other anions. The sorption rate and sorption stability were higher for G-LDH than for the conventional  $\text{NO}_3$ -LDH. In addition, G-LDH showed a comparable boron sorption capacity to that of CRB05 because of its improved dispersibility in solution. Furthermore, FTIR, XRD and  $^{11}\text{B}$  MAS NMR results of solid residues of G-LDH and  $\text{NO}_3$ -LDH after sorption of borate indicated that the sorption mechanism of G-LDH is complexation of borate

with the gluconate intercalated in the LDHs. This is different from the mechanism of the conventional  $\text{NO}_3$ -LDH, where ion-exchange is the main borate sorption mechanism. Considering the application of G-LDH on an industrial scale, G-LDHs in powdery form would need to be immobilized within mechanically stable materials, and then used in a filter column or fixed bed, as a filler for a continuous reactor.

## References:

- [1] O.P. Ferreira, S.G. de Moraes, N. Durán, L. Cornejo, O.L. Alves, Evaluation of boron removal from water by hydrotalcite-like compounds, *Chemosphere*, 62 (2006) 80-88.
- [2] J. Jiang, Y. Xu, K. Quill, J. Simon, K. Shettle, Laboratory study of boron removal by Mg/Al double-layered hydroxides, *Ind. Eng. Chem. Res.*, 46 (2007) 4577-4583.
- [3] K. Goh, T. Lim, Influences of co-existing species on the sorption of toxic oxyanions from aqueous solution by nanocrystalline Mg/Al layered double hydroxide, *J. Hazard. Mater.*, 180 (2010) 401-408.
- [4] S. Miyata, Anion-exchange properties of hydrotalcite-like compounds, *Clay. Clay Miner.*, 31 (1983) 305-311.
- [5] S. Nishihama, Y. Sumiyoshi, T. Ookubo, K. Yoshizuka, Adsorption of boron using glucamine-based chelate adsorbents, *Desalination*, (2012).
- [6] T. Qi, A. Sonoda, Y. Makita, H. Kanoh, K. Ooi, T. Hirotsu, Synthesis and borate uptake of two novel chelating resins, *Ind. Eng. Chem. Res.*, 41 (2002) 133-138.
- [7] J. Liu, G. Chen, J. Yang, Preparation and characterization of poly(vinyl chloride)/layered double hydroxide nanocomposites with enhanced thermal stability, *Polymer*, 49 (2008) 3923-3927.
- [8] F. Bruna, R. Celis, M. Real, J. Cornejo, Organo/LDH nanocomposite as an adsorbent of polycyclic aromatic hydrocarbons in water and soil-water systems, *J. Hazard. Mater.*, (2012).

- [9] M.Y. Ghotbi, M.Z.B. Hussein, A.H. Yahaya, M.Z.A. Rahman, LDH-intercalated d-gluconate: Generation of a new food additive-inorganic nanohybrid compound, *J. Phys. Chem. Solids*, 70 (2009) 948-954.
- [10] M. J. Frisch, G.W.T. H, M. A. Robb, J.R.C. G, G. A. Petersson, H.N.M. Caricato, A. F. Izmaylov, J.B.G. Zheng, M. Ehara, K.T.R. Fukuda, Jr. Y. Honda, O.K.H. Nakai, J. E. Peralta, F.O.M. Bearpark, K. N. Kudin, V.N.S. T, K. Raghavachari, A.R.J. C, N.R.J.M. M. Cossi, V. Bakken, C.A.J. Jaramillo, O. Yazyev, A.J.A. R, R. L. Martin, K.M.V. G, P. Salvador, J.J.D. S, O. Farkas, J.B.F. J, D.J. Fox, Gaussian, Inc., Wallingford CT, 2010.
- [11] D.T. Sawyer, Metal-gluconate complexes, *Chem. Rev.*, 64 (1964) 633-643.
- [12] F.B.D. Saiah, B. Su, N. Bettahar, Nickel-iron layered double hydroxide (LDH): Textural properties upon hydrothermal treatments and application on dye sorption, *J. Hazard. Mater.*, 165 (2009) 206-217.
- [13] D. Wang, F.R. Costa, A. Vyalikh, A. Leuteritz, U. Scheler, D. Jehnichen, U. Wagenknecht, L. Häussler, G. Heinrich, One-Step Synthesis of Organic LDH and Its Comparison with Regeneration and Anion Exchange Method, *Chem. Mater.*, 21 (2009) 4490-4497.
- [14] B. Stuart, *Infrared Spectroscopy: Fundamentals and Applications*, 2004.
- [15] M.Z.B. Hussein, C.W. Long, Synthesis of organo-mineral nanohybrid material: indole-2-carboxylate in the lamella of Zn-Al-layered double hydroxide, *Mater. Chem. Phys.*, 85 (2004) 427-431.
- [16] M.X. Reinholdt, R.J. Kirkpatrick, Experimental Investigations of Amino Acid-Layered Double Hydroxide Complexes: Glutamate-Hydrotalcite, *Chem. Mater.*, 18 (2006) 2567-2576.
- [17] Y. QuRong-lin, Advances in the analysis of macromolecular materials using solid-state NMR, *Polym. Bull.*, 06 (2006) 69-74.
- [18] S. Guo, D. Li, W. Zhang, M. Pu, D.G. Evans, X. Duan, Preparation of an anionic azo pigment-pillared layered double hydroxide and the thermo- and photostability of the resulting intercalated material, *J. Solid State Chem.*, 177 (2004) 4597-4604.
- [19] F.P. Jiao, X.Q. Chen, Z.D. Fu, Y.H. Hu, Y.H. Wang, Intercalation of Mg-Al layered double hydroxides by (+)-dibenzoyl-d-tartaric acid: Preparation and characterization, *J. Mol. Struct.*, 921 (2009) 328-332.



- [20] T. Takahashi, S. Kashiwakura, K. Kanehashi, S. Hayashi, T. Nagasaka, Analysis of Atomic Scale Chemical Environments of Boron in Coal by  $^{11}\text{B}$  Solid State NMR, *Environ. Sci. Technol.*, 45 (2010) 890-895.
- [21] G.L. Turner, K.A., Smith, R.J. Kirkpatrick, E. Oldfield, Boron-11 nuclear magnetic resonance spectroscopic study of borate and borosilicate minerals and a borosilicate glass, *J. Magn. Reson.*, 67 (1986) 544-550.
- [22] M. Bishop, N. Shahid, J. Yang, A.R. Barron, Determination of the mode and efficacy of the cross-linking of guar by borate using MAS  $^{11}\text{B}$  NMR of borate cross-linked guar in combination with solution  $^{11}\text{B}$  NMR of model systems, *Dalton Trans.*, (2004) 2621-2634.
- [23] K. Yoshimura, Y. Miyazaki, F. Ota, S. Matsuoka, H. Sakashita, Complexation of boric acid with the N-methyl-D-glucamine group in solution and in crosslinked polymer, *J. Chem. Soc., Faraday Trans.*, 94 (1998) 683-689.
- [24] A. Harada, T. Takagi, S. Kataoka, T. Yamamoto, A. Endo, Boron adsorption mechanism on polyvinyl alcohol, *Adsorption*, 17 (2011) 171-178.

## **Chapter 4 Sorption of borate onto layered double hydroxides assembled on filter paper through in situ hydrothermal crystallization**

### **4.1. Introduction**

In practice, solutions may contain a variety of anions that may affect borate sorption efficiency and interfere with boron adsorption. This is one of the key problems that limit the application of LDHs in water treatment. In **chapter 3**, this problem has been solved by using LDHs with gluconate. However, another drawback of LDHs is that they are more difficult (compared with adsorbents of larger particle size) to separate from water after treatment. The small size of LDHs particles means that precipitation and separation may take longer; in turn, more steps may be required for the treatment process, which limit its industrial application. To overcome these limitations and ensure that LDHs can be used for borate removal, separated from solution and also be used as fillers in fixed bed reactors for continuous treatment, it is critical to prevent interference from other anions and immobilize LDHs on an inexpensive porous carrier.

In this chapter, LDHs were fabricated on the surface of common filter papers using an in situ homogeneous precipitation accomplished by urea hydrolysis [1]. Gluconate and chloride were then intercalated into the LDHs interlayer to enhance sorption of borate. The resulting composite filters were characterized physicochemically and their

sorption efficiency, adsorption mechanism and factors affecting boron removal were investigated.

## **4.2 Experimental method**

### **4.2.1 Chemicals**

Magnesium nitrate ( $\text{Mg}(\text{NO}_3)_2 \cdot 6\text{H}_2\text{O}$ ), aluminum nitrate nonahydrate ( $\text{Al}(\text{NO}_3)_3 \cdot 9\text{H}_2\text{O}$ ), sodium gluconate ( $\text{C}_6\text{H}_{11}\text{NaO}_7$ ), boric acid ( $\text{H}_3\text{BO}_3$ ), urea ( $\text{CH}_4\text{N}_2\text{O}$ ), sodium sulfate ( $\text{Na}_2\text{SO}_4$ ) and sodium chloride ( $\text{NaCl}$ ) were used as received without purification (all special grade from WAKO Industrial Chemicals, Osaka, Japan). The main component of the filter paper (M-085, Toyo Advantec, Japan) used was cotton cellulose. The diameter and thickness of the filter paper were 47 and 0.8 mm, respectively.

### **4.2.2 Synthesis of materials**

#### **4.2.2.1 Preparation of filter paper modified by LDHs with carbonate interlayer**

1.71 g  $\text{Mg}(\text{NO}_3)_2 \cdot 6\text{H}_2\text{O}$  (6.65 mmol), 1.25 g  $\text{Al}(\text{NO}_3)_3 \cdot 9\text{H}_2\text{O}$  (3.35 mmol) and 5.60 g urea (93.2 mmol) were completely dissolved in water to form a clear solution with a total volume of 50 mL. Filter paper was placed into the solution before being transferred into a Teflon vessel in a conventional oven at 95°C for 48 h. The paper was removed from the vessel, rinsed thoroughly with deionized water and dried at 60°C overnight. The filter paper prepared in this step was termed  $\text{CO}_3\text{-LDH@F}$ .

#### **4.2.2.2 Preparation of filter paper modified by LDHs intercalated with chloride**

A piece of  $\text{CO}_3\text{-LDH@F}$  was placed in a plastic bottle, to which 50 mL of an aqueous solution containing 2.5 mmol/L HCl and 25 wt.% NaCl was added. The plastic bottle was sealed and placed in a thermostatted chamber at 25°C. The vessel

was agitated at a constant rate for 24 h. The filter paper was washed several times with deionized water and freeze-dried overnight. The resulting product was termed Cl-LDH@F.

#### 4.2.2.3 Preparation of filter paper modified by LDHs intercalated with gluconate

Chloride was ion-exchanged with gluconate in the Cl-LDH@F interlayer. First, sodium gluconate solutions of different concentrations were prepared by adding 0.13, 0.53, 1.06, 2.12 or 2.65 g to water in 50-mL plastic bottles (molar ratio of gluconate/LDH: 5, 20, 40, 80 or 100, respectively). Cl-LDH@F was placed into a bottle and shaken for different reaction times (12, 24 and 48 h) before being removed, washed and freeze-dried overnight. Samples synthesized in this step were termed G-LDH@F-5-24h, G-LDH@F-20-24h, G-LDH@F-40-24h, G-LDH@F-80-24h, G-LDH@F-100-24h, G-LDH@F-40-12h, and G-LDH@F-40-48h; the first and second numbers represent the molar ratio of gluconate/LDH during the preparation process and the reaction time, respectively. The overall G-LDH@F synthesis process is shown in Fig. 4.1.

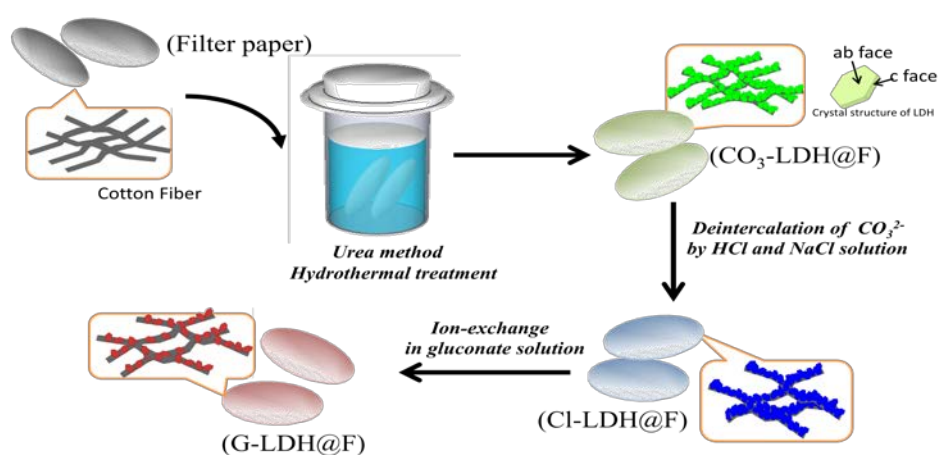


Fig. 4.1 Schematic illustration of syntheses of  $\text{CO}_3\text{-LDH@F}$ ,  $\text{Cl-LDH@F}$  and  $\text{G-LDH@F}$ .

### 4.2.3 Characterization

The crystalline sorbent phases were confirmed by X-ray diffraction (XRD, Ultima IV, Rigaku, Tokyo, Japan) with Cu K $\alpha$  radiation. The accelerating voltage and applied current were 40 kV and 40 mA, respectively, with a scanning speed of 2°/min and scanning step of 0.02°. Fourier transform infrared (FTIR) spectra were collected on a JASCO FTIR spectrometer (FT/IR-670 Plus, Hachioji, Japan) using Attenuation Total Reflection methods. Filter paper morphology was observed using scanning electron microscopy (SEM) VE-9800 (KEYENCE, Osaka, Japan) at an accelerating voltage of 20 kV.

<sup>13</sup>C-NMR spectra were collected on a JEOL-ECA 400 (Akishima, Japan). The resonance frequencies and field strength were 150.91 MHz and 14.09 T, respectively. Chemical shifts were referenced externally to tetramethylsilane at  $\delta$  0 ppm using the methyl signal of hexamethylbenzene at  $\delta$  17.36 ppm as a secondary standard. Solid-state <sup>11</sup>B-NMR spectra for sorption residues were collected on a JOEL ECA 800 (Akishima, Japan) with 4-mm high-speed spinning probes in a single pulse method. At a field strength of 18.8 T, the resonance frequency was 256.6 MHz for <sup>11</sup>B. Typical acquisition parameters were spinning speed 15 kHz, pulse length 2.5 s and recycle delay 10 s (<sup>11</sup>B).

To determine the metal content, 0.05 g of filter paper, CO<sub>3</sub>-LDH@F, Cl-LDH@F or G-LDH@F-40-24h were added to a solution containing 7 mL of 60% HNO<sub>3</sub> and 0.5 mL of 30% H<sub>2</sub>O<sub>2</sub>. This solution was transferred into a Teflon vessel, placed in a microwave digestion system (ETHOS A, Milestone, Italy) and its temperature increased to 230°C in 30 min. This temperature was maintained for 20 min before

allowing the samples to cool to room temperature. All filter paper was then dissolved and the resultant solutions diluted for determination of Mg and Al by inductively coupled plasma atomic emission spectrometry (ICP-AES, VISTA-MPX, Seiko Instruments, Tokyo, Japan).

#### **4.2.4 Sorption experiments**

##### **4.2.4.1 Time effect on sorption of boron by different materials**

Filter paper, CO<sub>3</sub>-LDH@F, Cl-LDH@F or G-LDH@F-40-24h (0.5 g) were added to 40 mL of a 2.5 mmol/L H<sub>3</sub>BO<sub>3</sub> solution in 50-mL bottles. The initial pH of this solution was adjusted to 7.0. Then, the bottles were shaken on a shaker for 20 min before 1 mL of liquor was removed with a syringe and filtered through a membrane filter (pore size 0.2 µm) for ICP-AES analysis.

##### **4.2.4.2 Sorption densities of different materials**

The sorption densities of the filter paper, CO<sub>3</sub>-LDH@F, Cl-LDH@F and G-LDH@F-40-24h were determined. Solutions of H<sub>3</sub>BO<sub>3</sub> (0-60 mmol/L) were prepared and their initial pH was adjusted to 7.0. A filter paper was added to 40 mL of borate solution, followed by shaking at 100 rpm at 25°C. After 24 h, supernatants were filtered (0.2 µm) for determination of total B concentration by ICP-AES.

##### **4.2.4.3 Effect of competing anions**

To explore the effects of competitive anions on the sorption of boron by G-LDH@F-40-24h, 0.5 g sorbent was added to 40 mL of 2.5 mM boron solutions containing 50 mM competing anions (SO<sub>4</sub><sup>2-</sup> or Cl<sup>-</sup>) and the mixtures were shaken for 24 h. After this time, the supernatant was removed and filtered through a 0.2 µm membrane before determination of B concentration by ICP-AES.

## 4.3 Results and discussion

### 4.3.1 Characterizations

The XRD patterns of the filter paper and modified filter papers are shown in **Fig. 4.2**. In **Fig. 4.2a**, the peaks located at  $2\theta = 14.8, 16.4, 22.6$  and  $33.9^\circ$  are typical of the cellulose crystalline form and are consistent with a previous report [2]. Compared with the original filter paper, the XRD patterns of the  $\text{CO}_3\text{-LDH@F}$  exhibited characteristic diffractions of hydrotalcite-like compounds (**Fig. 4.2b**), such as the peak at around  $2\theta = 11.9^\circ$  (003), which indicates an interlayer spacing ( $d$  value) of  $7.43 \text{ \AA}$ . After deintercalation of carbonate by the  $\text{HCl/NaCl}$  solution, the XRD patterns of LDHs in the filter paper were similar to that of the  $\text{CO}_3\text{-LDH@F}$ . However, the reflection for the 003 plane was shifted to a slightly lower angle, showing that the  $d$  value of the interlayer increased to  $7.54 \text{ \AA}$ ; this is because the attraction between  $\text{Cl}^-$  and the host layers is weaker than that for  $\text{CO}_3^{2-}$  (**Fig. 4.2c**) [3]. However, in the previous report [3], the  $d$  values found for LDHs containing  $\text{CO}_3^{2-}$  and  $\text{Cl}^-$  were  $7.7 \text{ \AA}$  and  $7.9 \text{ \AA}$ , respectively, compared with the  $7.43 \text{ \AA}$  and  $7.54 \text{ \AA}$  in the present work. We suggest two possible reasons for this. The interlayer distance for LDHs with the same type of anion increases with increasing  $\text{Mg/Al}$  molar ratio. This is because the electrostatic attraction between the excess positively charged layers is decreased when divalent  $\text{Mg}$  ions are substituted for trivalent  $\text{Al}$  in the LDH structures [4,5]. In addition, the interlayer distance of LDHs may also be influenced by synthetic methods. Adachi-Pagano et al. [6] showed that the interlayer distance of LDHs synthesized by coprecipitation at constant pH was larger ( $7.78 \text{ \AA}$ ) than that of LDHs prepared by the urea method ( $7.36 \text{ \AA}$ ). This may result from the higher

temperature and higher pressure in the urea method compared with the conditions used in the precipitation method. In Miyata's work, the molar ratio of Mg/Al was 3.0 and the precipitation method was used, whereas we have used the urea method with a molar ratio of Mg/Al of 1.8. Therefore the  $d$  values obtained in the two studies were different.

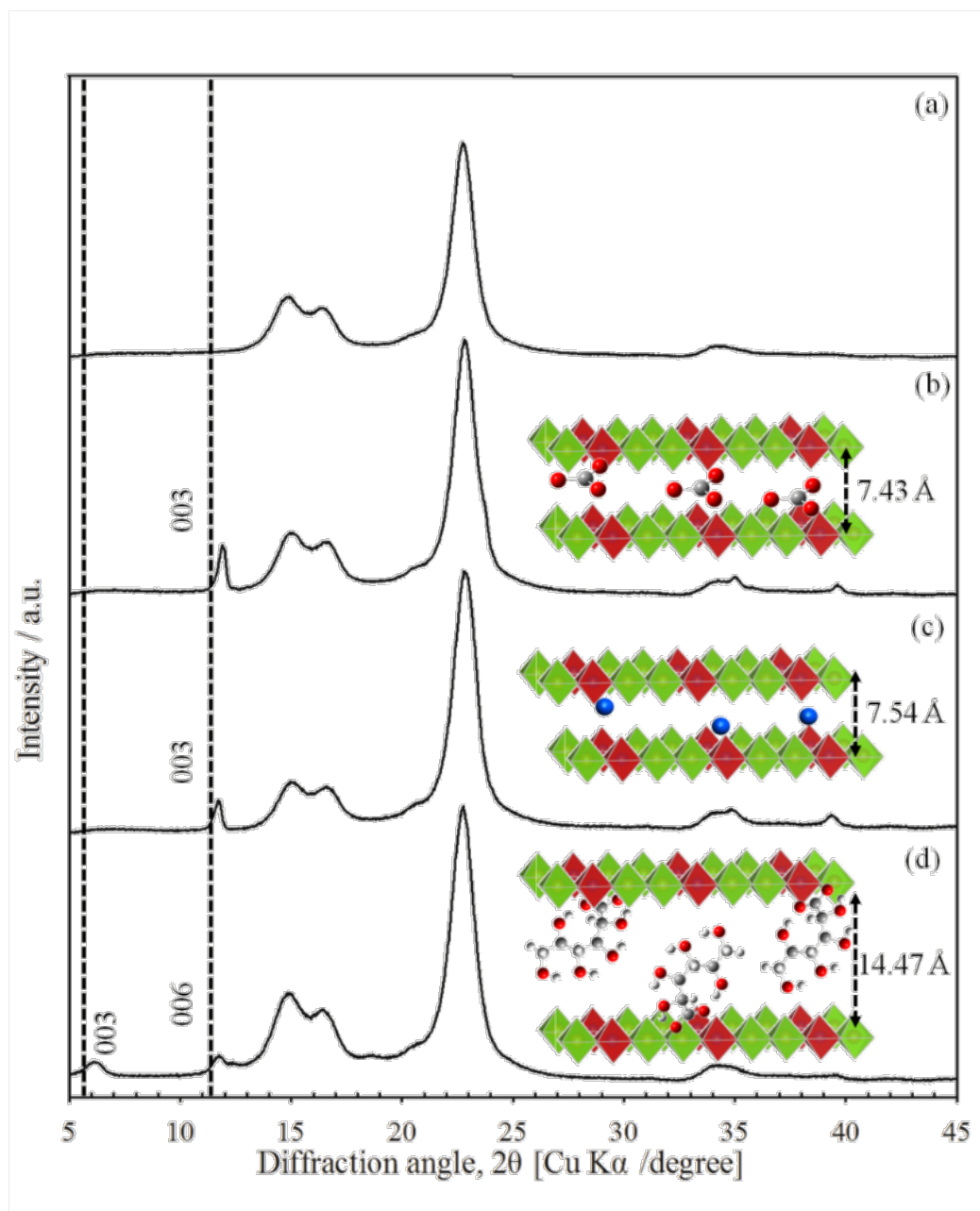


Fig. 4.2 XRD patterns of (a) filter paper, (b) CO<sub>3</sub>-LDH@F, (c) Cl-LDH@F and (d) G-LDH@F-40-24h.



To intercalate gluconate into the Cl-LDH@F interlayers, ion-exchange was conducted under different conditions (**Fig. 4.3(a)**). When the molar ratio of gluconate/LDH was 5.0 (G-LDH@F-5-24h), a weak reflection appeared at  $2\theta = 6.2^\circ$ , suggesting that small amounts of  $\text{Cl}^-$  in the LDHs interlayer were replaced by gluconate. This is because the length of a gluconate molecule (calculated as 6.4 Å) is larger than the diameter of  $\text{Cl}^-$ , so that the interlayer space in the LDH expanded to accommodate gluconate, resulting in a shift in the 003 reflection (which corresponds to the interlayer spacing) to a smaller angle ( $2\theta = 6.2^\circ$ ). With increasing molar ratio of gluconate/LDH during ion-exchange, the relative intensity of the 003 plane reflection increased as more  $\text{Cl}^-$  was replaced with gluconate. For G-LDH@F-40-24h, the  $d$  value increased to 14.47 Å. The space occupied by gluconate in the G-LDH@F was estimated to be approximately 9.68 Å, because the layer thickness of the brucite-like LDH sheet was reported to be 4.8 Å [7, 8]. The gluconate in the G-LDH@F-40-24h is expected to be arranged in a bilayer with a certain angle facing the metal hydroxide layers [9]. Carboxylic groups in the gluconate may be orientated to the Al atoms in the host layers because of electrostatic interactions. However, excess gluconate concentrations negatively impact the G-LDH@F synthesis. In **Fig. 4.3a**, the 003 reflection intensity was decreased in G-LDH@F-80-24h, and the reflections characteristic of hydrotalcite-like compounds mostly disappeared in G-LDH@F-100-24h, when the molar ratio of gluconate/LDH was increased from 40 to 100. This may be explained as follows: when the sodium gluconate is present in the system, the pH of the solution increases with increasing sodium gluconate concentration, because equation (4.2) shifts to the left-hand side.

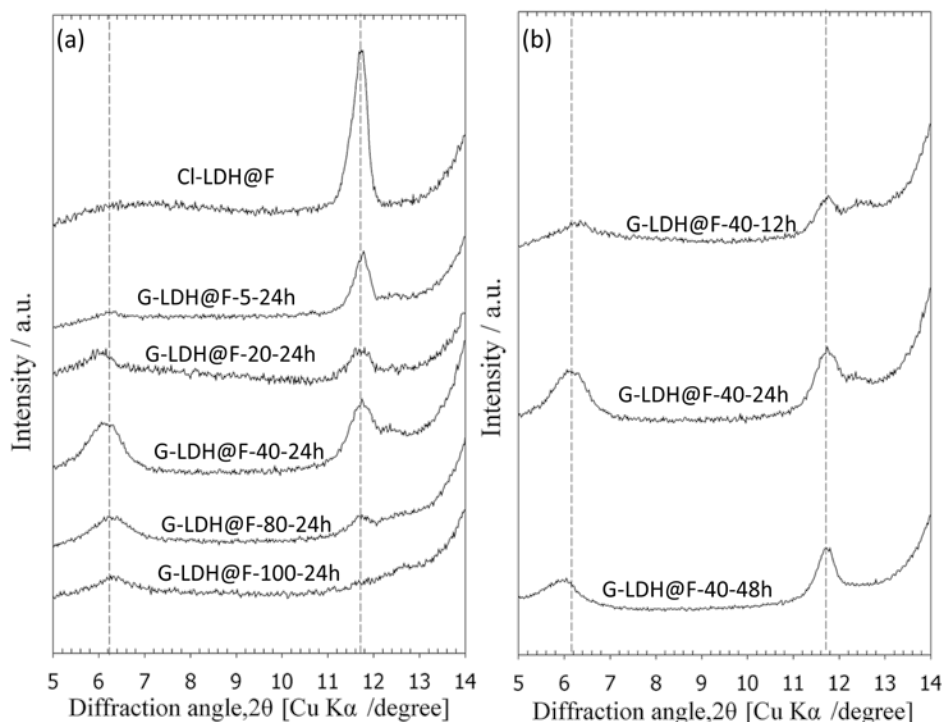
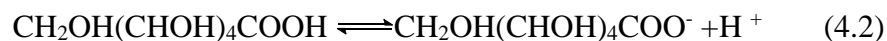
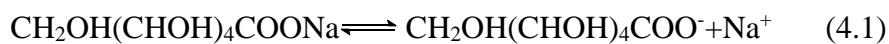
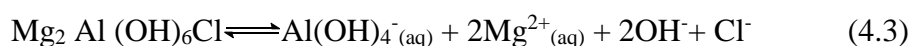


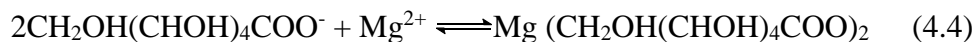
Fig. 4.3 XRD patterns of G-LDH@F prepared with different (a) molar ratios of gluconate/LDH and (b) reaction times.

Meanwhile, LDHs would be partially dissolved [10] and the increase in pH with increasing gluconate concentration could cause the formation of soluble  $\text{Al}$ ,  $\text{Al}(\text{OH})_4^-$  (eq. (4.3)).



During the gluconate intercalation of gluconate into the  $\text{Cl}^-$ -containing interlayers, gluconate ( $\text{CH}_2\text{OH}(\text{CHOH})_4\text{COO}^-$ ) could be complexed with  $\text{Mg}^{2+}$  ions (eq. (4.4)) since the stability constant for Mg gluconate complex was reported to be  $\log K = 0.7$

at 25°C [11]; this reaction could then consume  $\text{Mg}^{2+}$  and enhance the dissolution of the LDHs.



Therefore, there was less LDH than expected in F-LDH-G samples prepared using higher sodium gluconate concentrations.

The reaction time is also an important factor for gluconate intercalation. **Fig. 4.3b** shows XRD patterns for the solid residues of G-LDH@F collected at different time intervals. Within 12 h, broadened peaks assigned to LDHs intercalated with gluconate appeared, suggesting incomplete formation of G-LDH@F. After 24 h these reflections became clearer, and an additional 24 h may be slightly beneficial to intercalation, since the interlayer spacing increased further; however, excess time lowers the efficiency of the synthesis. Therefore, G-LDH@F-40-24h was chosen as the optimal sorbent for subsequent experiments.

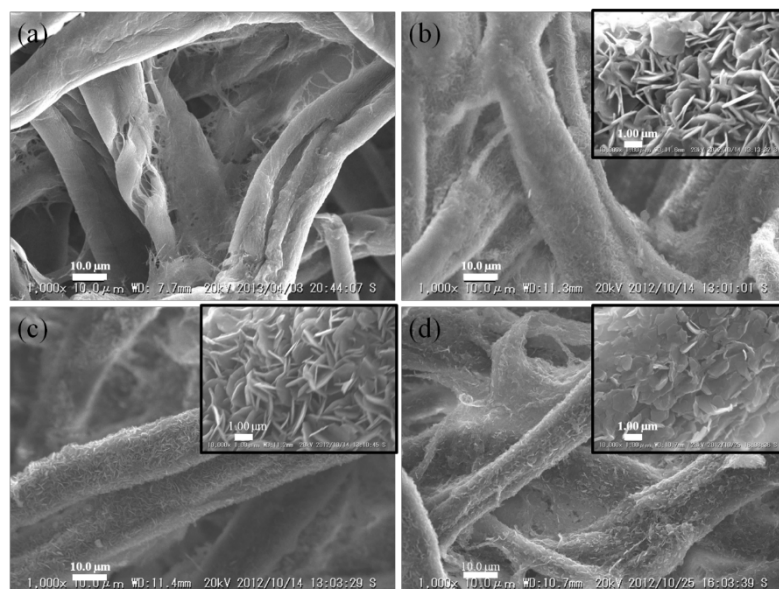


Fig. 4.4 SEM images of (a) filter paper, (b)  $\text{CO}_3\text{-LDH@F}$ , (c)  $\text{Cl-LDH@F}$  and (d)  $\text{G-LDH@F-40-24h}$ ; horizontal bars indicate 10.00  $\mu\text{m}$ . Insets show expanded SEM images of fiber surface; horizontal bars indicate 1.00  $\mu\text{m}$ .

From SEM observations, the CO<sub>3</sub>-LDH@F, Cl-LDH@F and G-LDH@F-40-24h morphologies were altered as shown in **Fig. 4.4** and the alterations were especially clear at higher magnification (**Fig. 4.4(b)-(d)**, insets). Fig. 4.4(a) shows the smooth surface of the filter paper before hydrothermal treatment. After treatment, hexagonal CO<sub>3</sub>-LDH, 2  $\mu$ m in size and approximately 10 nm thick, grew on the surface of the cotton fibers (**Fig. 4.4(b)** inset), since filter paper contains an abundance of hydroxyl groups. These hydroxyl groups may anchor the Mg<sup>2+</sup> and Al<sup>3+</sup> precursors to the cellulose fibers, thus facilitating the growth of the LDH coating (**Fig. 4.4(b)**) [12]. After deintercalation of CO<sub>3</sub>-LDH using HCl/NaCl solution, no significant change in shape and size of the LDH-Cl was observed (**Fig. 4.4(c)**). However, the shape and size of the LDHs in the filter paper became more uniform after ion-exchange with gluconate in the guest layers. In addition, the morphology was influenced by the molar ratios of gluconate/LDH during ion-exchange (**Fig. 4.5**).

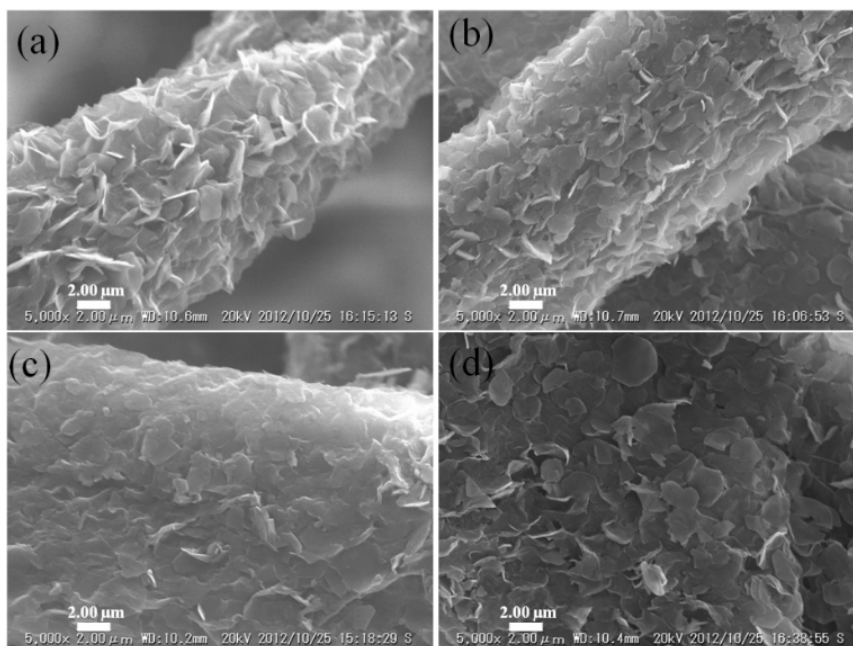


Fig. 4.5 SEM images of G-LDH@F prepared from different molar ratios of gluconate/LDH, (a) 20, (b) 40, (c) 80 and (d) 100. Horizontal bars indicate 2  $\mu$ m.

This may be attributed to complexation of gluconate with  $\text{Mg}^{2+}$  ions and the release of  $\text{Al}(\text{OH})_4^-$ , which was partially dissolved from the host layers in LDHs during the ion-exchange of  $\text{Cl}^-$  with gluconate, as shown in **Table 4.1**. From **Table 4.1**, the ion-exchange process did not change the Mg/Al molar ratio significantly (it remained  $\sim 1.8$ ), although the metal contents per gram of filter decreased from 1.294 to 0.482 mmol/g for Mg and 0.706 to 0.266 mmol/g for Al (**Table 4.1**).

Table 4.1 Mg and Al contents and the molar ratio of Mg/Al in different sorbents

Sample	Mg (mmol/g)	Al (mmol/g)	Contents of LDHs in one filter paper (g/g)	Molar ratio of Mg/Al
$\text{CO}_3\text{-LDH@F}$	1.294	0.706	0.167	1.83
$\text{Cl-LDH@F}$	1.166	0.623	0.132	1.87
$\text{G-LDH@F-40-24}$	0.482	0.266	0.098	1.81

This loss in metal content in the filter paper also caused morphological changes in the LDH (**Fig. 4.4(d)**). **Fig. 4.4(a and b)** show that the growth orientation of the ab face (**Fig. 4.1**) of the  $\text{CO}_3\text{-LDH}$  and  $\text{Cl-LDH}$  particles is perpendicular to the fiber and follows the evolution selection growth mechanism first used by [12, 13] to explain the orientation of a Zn-Al-LDH film fabricated on pure aluminum. For the  $\text{G-LDH@F-40-24h}$ , however, LDHs were orientated with their c-axes perpendicular to the substrate. This could be the result of LDHs dissolution during synthesis and damage to the stacking structure. The FTIR spectrum of the raw filter paper (**Fig. 4.6(b)**) shows adsorption bands at 990 and 1030  $\text{cm}^{-1}$  characteristic of the skeletal vibration of  $\nu(\text{C-O})$  and a peak at 1110  $\text{cm}^{-1}$ , which is assigned to the stretching vibration mode

of  $\nu(\text{C-O})$  in  $\text{C-OH}$  [14]. Based on the previous report [15], the weak adsorption band at  $1430\text{ cm}^{-1}$  is assigned to the  $\text{CH}_2$  in cellulose.

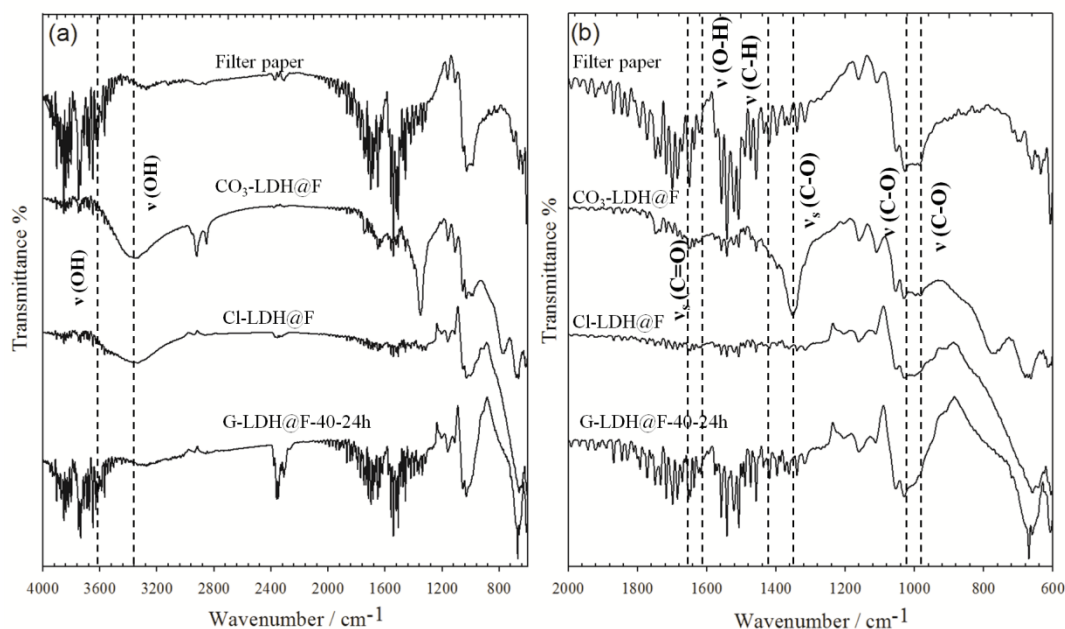


Fig. 4.6 FTIR spectra from  $400$  to  $1800\text{ cm}^{-1}$  for (a) filter paper, (b)  $\text{CO}_3\text{-LDH@F}$ , (c)  $\text{Cl-LDH@F}$  and (d)  $\text{G-LDH@F-40-24h}$ . Inset shows FTIR spectra from  $400$  to  $4000\text{ cm}^{-1}$  for (a) filter paper, (b)  $\text{CO}_3\text{-LDH@F}$ , (c)  $\text{Cl-LDH@F}$  and (d)  $\text{G-LDH@F-40-24h}$ .

Additionally there is one broad band at  $3300\text{-}3400\text{ cm}^{-1}$  and noisy signals at  $3600\text{-}3650\text{ cm}^{-1}$ , which are attributed to  $\nu(\text{OH})$  in all spectra (**Fig. 4.6(a)**). The former is assigned to hydrogen-bonded O-H stretching and the latter to free O-H stretching in adsorbed water molecules included in the LDHs [16]. A peak around  $1616\text{ cm}^{-1}$  is also assigned to the H-O-H bending vibration mode of water molecules (**Fig. 4.6(b)**) [17]. The hydroxyl groups on the surface of the fibers supply preferable conditions for growth of LDHs. Compared with the raw filter paper,  $\text{CO}_3\text{-LDH@F}$  has a strong peak at  $1354\text{ cm}^{-1}$  (**Fig. 4.6(b)**) attributed to the asymmetric stretching vibration mode of  $\nu_{\text{as}}(\text{C-O})$  in  $\text{CO}_3^{2-}$  [6]; a similar peak was reported previously when  $\text{CO}_3\text{-LDH}$  was prepared using the urea method [18]. After treatment with  $\text{HCl/NaCl}$  solution,

elimination of  $\text{CO}_3^{2-}$  can be confirmed from the FTIR spectrum of Cl-LDH@F, where the asymmetric stretching vibration mode of  $\nu_{\text{as}}$  (C-O) at  $1354\text{ cm}^{-1}$  almost disappeared (**Fig. 4.6(b)**). Subsequently,  $\text{Cl}^-$  in LDH@F was replaced with gluconate, resulting in an increase in the intensity of a band at  $1634\text{ cm}^{-1}$ , assigned to the asymmetric stretching vibration mode of  $\nu_{\text{as}}$  (C=O) compared with that found in Cl-LDH@F (**Fig. 4.6(b)**); this increase in intensity was probably due to the carboxylate in gluconate. Since the characteristic peaks derived from gluconate are not clear in the FTIR spectra,  $^{13}\text{C}$ -NMR was used for further confirmation.

**Fig. 4.7** represents the liquid  $^{13}\text{C}$ -NMR spectra of sodium gluconate and the acid-extracted solution of G-LDH@F. In  $^{13}\text{C}$ -NMR spectrum for sodium gluconate, a peak assigned to the carboxylic carbon was located at the highest chemical shift, around  $178.66\text{ ppm}$  [19]. Another five peaks located at  $74.28$ ,  $72.81$ ,  $71.44$ ,  $71.18$  and  $62.89\text{ ppm}$  are assigned to carbons bound to -OH groups (**Fig. 4.7(a)**). The peak at  $62.89\text{ ppm}$  is assigned to  $-\text{CH}_2\text{-OH}$ . Compared with the  $^{13}\text{C}$ -NMR spectrum of F-LDH-G-40-24h, similar chemical shifts were observed, although some small peaks may originate from the acid-extraction process (**Fig. 4.7(b)**). Combining the results of XRD, FTIR and  $^{13}\text{C}$ -NMR shows that gluconate was successfully intercalated into the LDH@F.

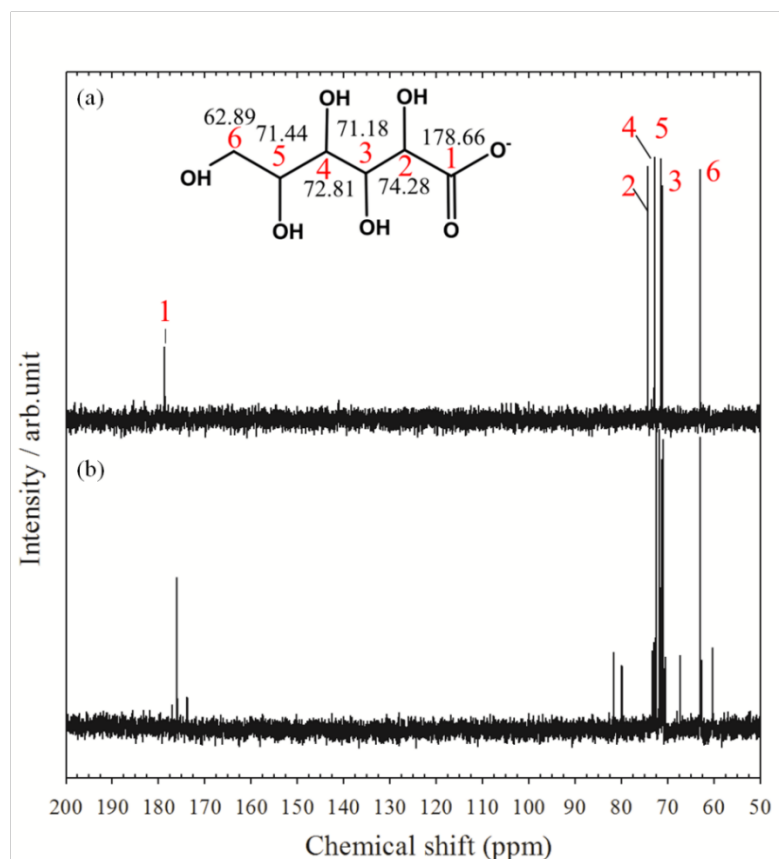


Fig. 4.7 Liquid  $^{13}\text{C}$ -NMR spectra for (a) sodium gluconate and (b) acidic solution of G-LDH@F-40-24h.

#### 4.3.2 Boron removal by F-LDH

The sorption densities of borate (**Fig. 4.8**) after 20 min by filter paper,  $\text{CO}_3$ -LDH@F, Cl-LDH@F and G-LDH@F-40-24h were 0, 0, 0.01 and 0.18 mmol/g, respectively. However, the sorption densities of borate by different materials changed when the reaction time was increased to 24 h and also depended upon the initial borate concentration.



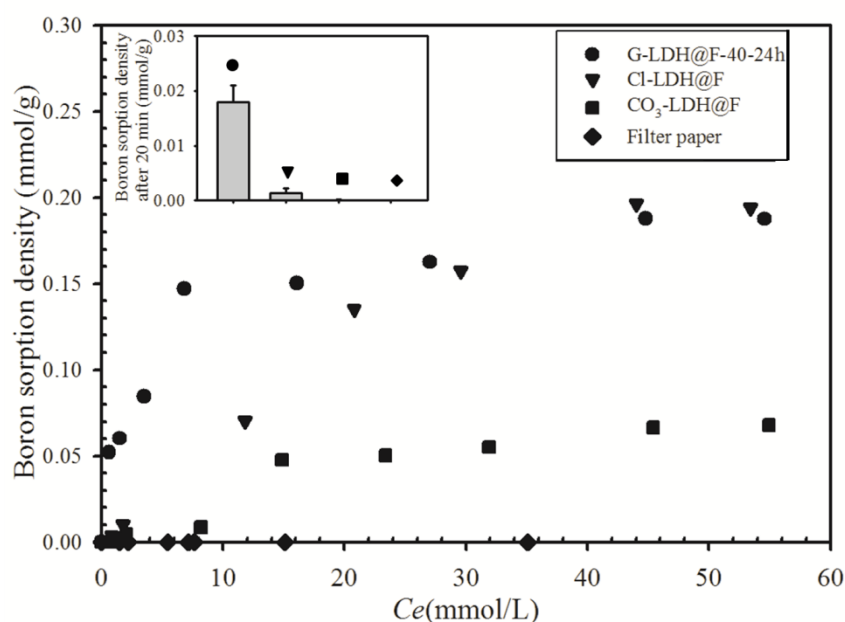


Fig. 4.8 Sorption densities of borate after 24 h on (a) filter paper, (b) CO<sub>3</sub>-LDH@F, (c) Cl-LDH@F and (d) G-LDH@F-40-24h. Inset shows sorption density of different sorbents after 20 min. Amount of sorbent: one piece of filter paper (0.5 g) in 40 mL; initial boron concentration: 2.5 mM; initial pH: 7.0.

After 24 h, the sorption densities of G-LDH@F-40-24h and Cl-LDH@F were 0.18 mmol/g and 0.19 mmol/g. To compare the sorption densities of borate by LDHs in the filter with other reports, the sorption densities of LDHs in G-LDH@F-40-24h and Cl-LDH@F were calculated based on the weight of LDH in one filter (mmol/g-LDH). The sorption densities of borate by different LDHs in G-LDH@F-40-24h and Cl-LDH@F were calculated in this way as 1.83 mmol/g-LDH and 1.44 mmol/g-LDH, respectively. These values are greater than the 1.29 mmol/g-LDH and 1.20 mmol/g-LDH reported by [20] and [21]. This may be because the LDHs powders were dispersed onto the surface of filter paper to avoid agglomeration.

Furthermore, the greatest boron-sorption density value was achieved by G-LDH@F-40-24h at low initial borate concentration while Cl-LDH@F had the greatest sorption density at higher initial borate concentration. Differences in sorption density

may arise because of different sorption mechanisms in G-LDH@F-40-24h and Cl-LDH@F, CO<sub>3</sub>-LDH@F and filter paper. CO<sub>3</sub>-LDH and Cl-LDH appear to have a similar ion-exchange mechanism; that is, intercalation to immobilize pollutants. The attraction between the carbonate and LDH metal layer, which is stronger than that of the chloride ion, results in a smaller sorption density of borate. Owing to their better performance, the sorption mechanisms of G-LDH@F-40-24h and Cl-LDH@F were studied further.

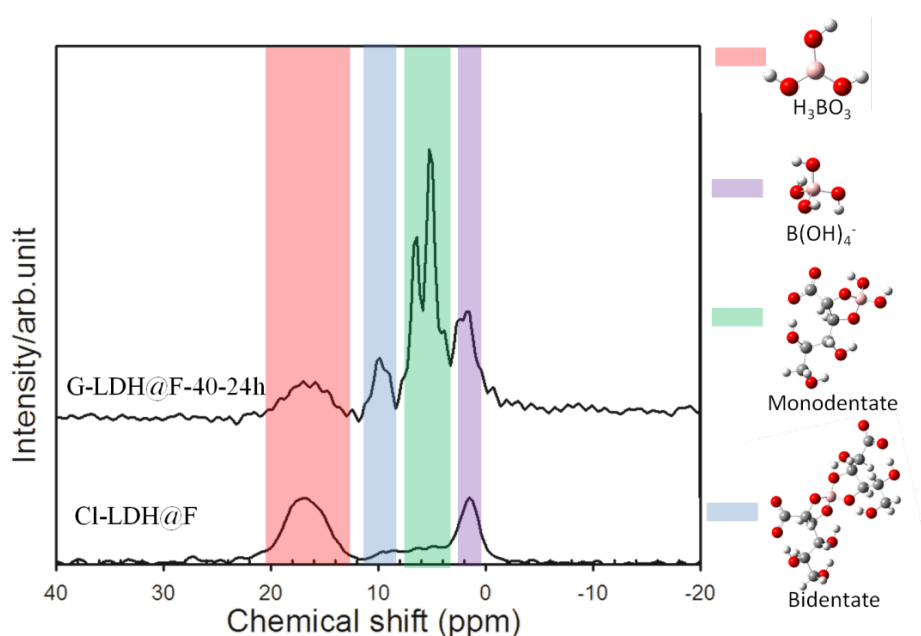


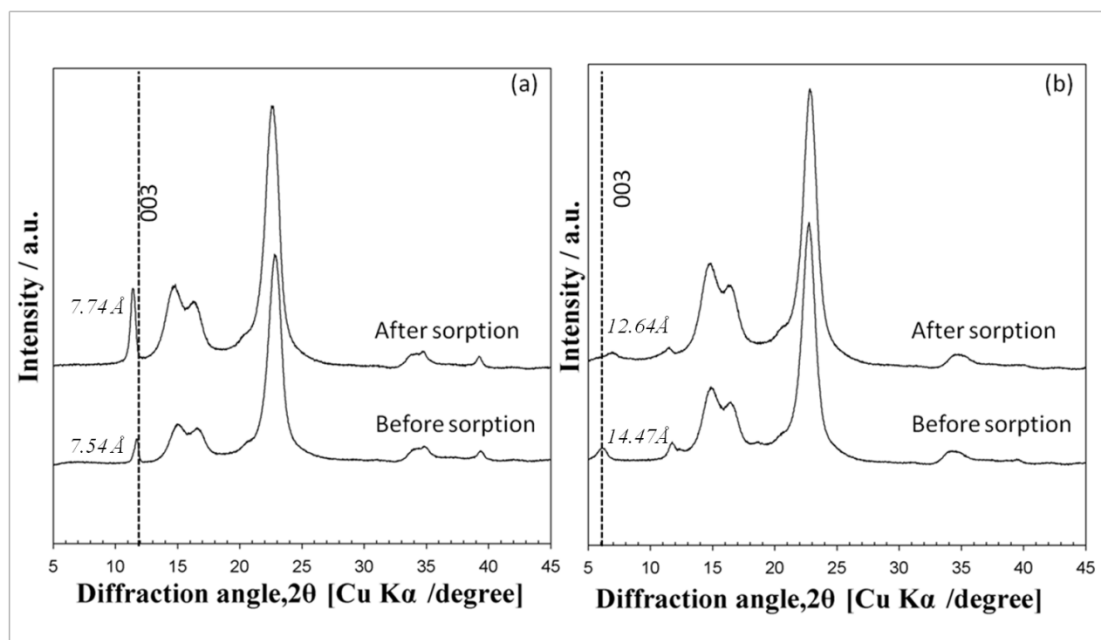
Fig. 4.9 Solid <sup>11</sup>B MAS NMR of Cl-LDH@F and G-LDH@F-40-24h after sorption of borate.

<sup>11</sup>B MAS NMR spectra for the solid residues after borate sorption are shown in **Fig. 4.9**. Comparison of Cl-LDH@F and G-LDH@F-40-24h after borate sorption shows that the coordination of borate was different. In Cl-LDH@F, the chemical shifts of the main boron peaks are at 1.6 and 16.8 ppm, indicating that B(OH)<sub>4</sub><sup>-</sup> and H<sub>3</sub>BO<sub>3</sub> are present in the solid residues [22,23]. The existence of B(OH)<sub>4</sub><sup>-</sup> demonstrates that the

sorption of borate onto Cl-LDH@F is explained by ion-exchange of  $\text{Cl}^-$  with  $\text{B}(\text{OH})_4^-$ . Some  $\text{H}_3\text{BO}_3$  molecules may enter into the interlayers of the LDHs structure together with the aqueous solution or be present and become fixed in the filter paper interspace. In the F-G-LDH@F-40-24h, however, boron is mainly immobilized in four forms. The first gives a peak at 5-6 ppm, and was assigned to mono-complexes. The second is located at 10.1 ppm and exists in bis-complexes, similar to the complexes formed by boron-specific resins [24]. The other two peaks are located at 1.7 and 16.7 ppm and are assigned to  $\text{B}(\text{OH})_4^-$  and  $\text{H}_3\text{BO}_3$ , as they were for Cl-LDH@F. These B species could enter into the LDH's structure and/or exist in filter paper through ion-exchange or by entry with the aqueous solution, analogous to Cl-LDH@F. In addition, from the **Fig. 4.9**, it could be noticed that different type of monodentate and bidentate compounds may be existed in the products since there are several peaks with different chemical shift in the similar range. Base on previously reports, reaction between multi-hydroxyl molecule and borate can form different compounds [25]. But there are difficult to distinguish from the  $^{11}\text{B}$ -NMR.

Meanwhile, in the reaction process, the structure is undamaged, because the XRD patterns are similar to those before sorption (**Fig. 4.10**). However, it is worth noting that the interlayer distance changed with sorption of borate. The layer distance of Cl-LDH@F increased from 7.54 Å to 7.74 Å when the chloride ions were replaced with borate after sorption, resulting in an expanded layer distance because of the larger molecular size of borate. In contrast, the interlayer distance of G-LDH@F-40-24h decreased from 14.47 Å to 12.64 Å after borate sorption. This occurred because a part of the gluconates is released for each borate molecule adsorbed during the sorption process. The second reason is that the gluconates between the layers are arranged in a bilayer structure, and the carboxylic groups with negative charge may face mainly

towards the  $\text{Al}^{3+}$  ions in the metallic layers before sorption. When borate is complexed with gluconate, the negatively charged sites should change. Therefore, complexation leads to different arrangements in the LDHs, which may decrease the



interlayer distances.

Fig. 4.10 XRD patterns for (a) Cl-LDH@F and (b) G-LDH@F -40-24h before and after borate sorption.

Based on the above discussion, a boron-sorption mechanism is proposed in **Fig. 4.11**.  $\text{H}_3\text{BO}_3$  and  $\text{B}(\text{OH})_4^-$  that may enter into the LDHs of the filter paper react differently with different materials. In the Cl-LDH system,  $\text{B}(\text{OH})_4^-$  is removed from solution through ion-exchange with the  $\text{Cl}^-$  ion in the LDHs guest layers. However, the removal of borate by G-LDH@F-40-24h occurs mainly through complexation as mono- and bidentate complexes.

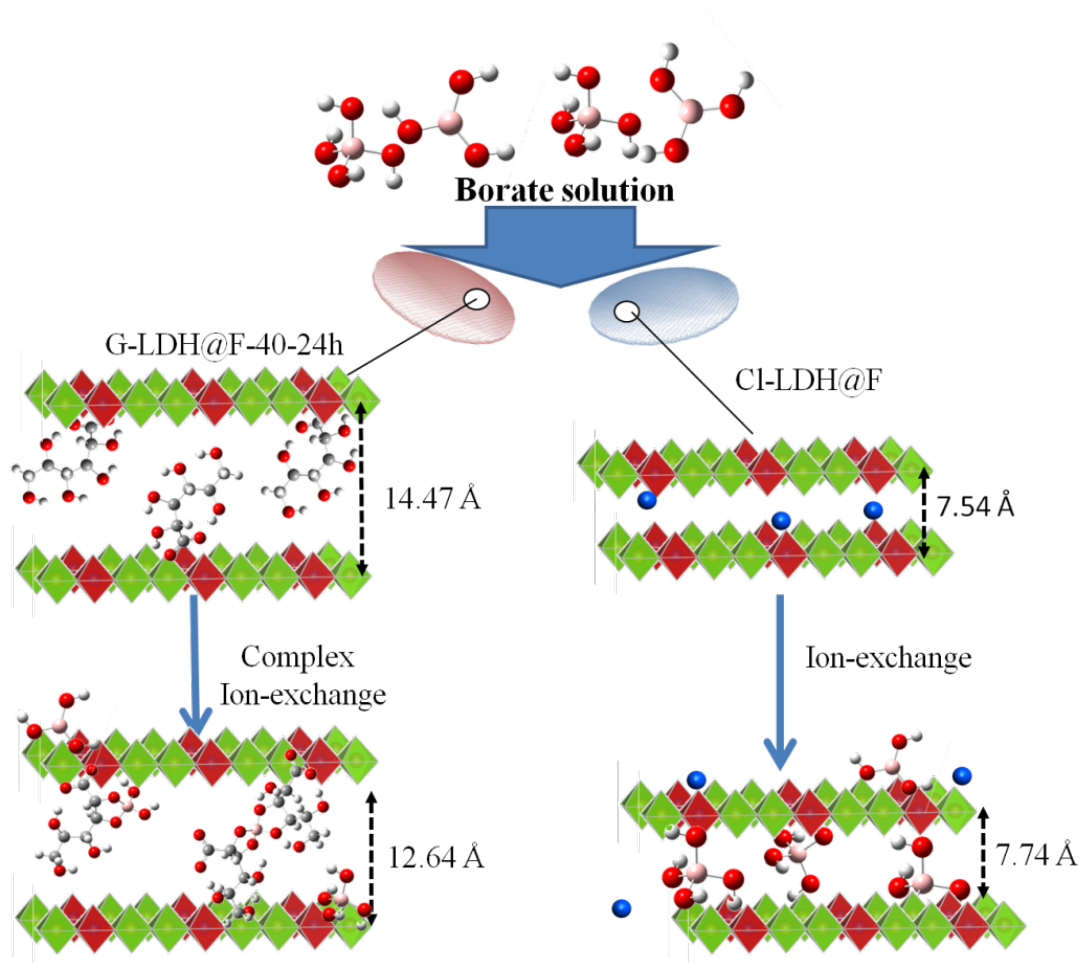


Fig. 4.11 Schematic illustrations of sorption mechanism of borate onto Cl-LDH@F and G-LDH@F-40-24h.

#### 4.3.2 Sorption of borate in the presence of coexisting anions

Coexisting anions such as hydrogen carbonate, sulfate and chloride occur in aqueous environments and may interfere with the absorption of borate onto LDHs. Polyvalent anions and ions that can be ionized into polyvalent anions may be especially problematic in practical cases. This is because polyvalent anions have a strong electrostatic interaction with the metallic layers in LDHs and can be easily exchanged into the guest layers in LDHs, occupying absorption sites and impacting pollutant removal. The sorption density of borate onto G-LDH@F-40-24h was investigated at an initial pH of 7.00 in the presence of coexisting anions (sulfate and

chloride), which are common in natural and industrial environments (**Fig. 4.12**). The sorption density of borate onto Cl-LDH@F decreased from 0.03 mmol/g to almost 0 mmol/g in the presence of coexisting anions. This occurs because the binding force of the LDH host layers with sulfate is greater than that with  $\text{B(OH)}_4^-$ . However, for G-LDH@F-40-24h, the sorption density of borate was not seriously influenced by coexisting anions. The amount of borate removed by G-LDH@F-40-24h is approximately 0.05 mmol/g, which is almost equal to that in borate solution without coexisting anions. This may occur because the mono-complex of borate with gluconate has a charge of -2, while the bi-complex of one borate with two gluconate groups has a charge of -3. Anions with larger valence states are more easily immobilized into the LDH layers. As a consequence, G-LDH@F-40-24h showed stronger sorption densities and selectivity for borate removal.

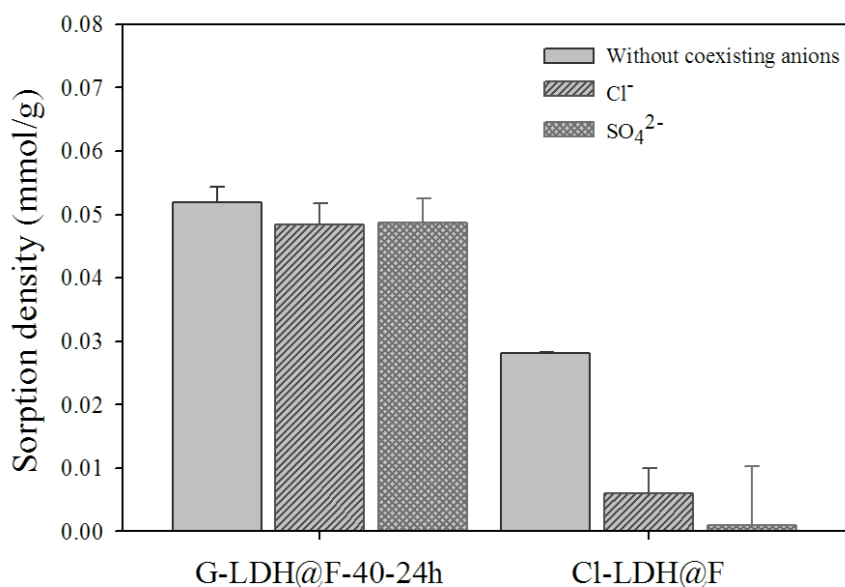


Fig. 4.12 Effects of coexisting anions on boron-sorption density onto Cl-LDH@F and G-LDH@F-40-24h. Amount of sorbent: one piece of filter paper (0.5 g) in 40 mL; coexisting anion concentration: 50 mM; initial boron concentration: 2.5 mM; initial pH: 7.0; reaction time: 24 h.

## 4.4 Conclusion

In this work, we synthesized a novel composite for borate sorption by in situ microwave-assisted crystal growth, in which gluconate-intercalated LDHs was assembled on the surface of filter paper. Inexpensive and environmentally friendly gluconate was intercalated as the interlayer LDHs anion in this composite filter paper to enhance the sorption density of the modified filter paper. The sorption results demonstrated that G-LDH@F-40-24h removes borate efficiently from solution in the presence of coexisting anions, and does so more rapidly and steadily than Cl-LDH@F or CO<sub>3</sub>-LDH@F. Based on FTIR, XRD and <sup>11</sup>B-NMR characterization of solid residues of G-LDH@F-40-24h and Cl-LDH@F after sorption, a possible adsorption mechanism was proposed. It is suggested that the borate is removed by G-LDH@F-40-24h mainly because gluconate intercalation results in rapid borate complexation.

## References:

- [1] U. Costantino, F. Marmottini, M. Nocchetti, R. Vivani, New Synthetic Routes to Hydrotalcite-Like Compounds-characterisation and properties of the obtained materials, *Eur. J. Inorg. Chem.*, 1998 (1998) 1439-1446.
- [2] C. Yin, J. Li, Q. Xu, Q. Peng, Y. Liu, X. Shen, Chemical modification of cotton cellulose in supercritical carbon dioxide: Synthesis and characterization of cellulose carbamate, *Carbohydr. Polym.*, 67 (2007) 147-154.
- [3] S. Miyata, Anion-exchange properties of hydrotalcite-like compounds, *Clay. Clay Miner.*, 31 (1983) 305-311.
- [4] Y. You, G.F. Vance, H. Zhao, Selenium adsorption on Mg-Al and Zn-Al layered double hydroxides, *Appl. Clay Sci.*, 20 (2001) 13-25.
- [5] U. Sharma, B. Tyagi, R.V. Jasra, Synthesis and characterization of Mg-Al-CO<sub>3</sub> layered double hydroxide for CO<sub>2</sub> adsorption, *Ind. Eng. Chem. Res.*, 47 (2008) 9588-9595.

- [6] M. Adachi-Pagano, C. Forano, J. Besse, Synthesis of Al-rich hydrotalcite-like compounds by using the urea hydrolysis reaction-control of size and morphology, *J. Mater. Chem.*, 13 (2003) 1988-1993.
- [7] S. Miyata, The Syntheses of hydrotalcite-like compounds and their structures and physico-chemical properties I: The systems  $\text{Mg}^{2+}\text{-Al}^{3+}\text{-NO}_3^-$ ,  $\text{Mg}^{2+}\text{-Al}^{3+}\text{-Cl}$ ,  $\text{Mg}^{2+}\text{-Al}^{3+}\text{-ClO}_4^-$ ,  $\text{Ni}^{2+}\text{-Al}^{3+}\text{-Cl}$  and  $\text{Zn}^{2+}\text{-Al}^{3+}\text{-Cl}$ , *Clay. Clay Miner.*, 23 (1975) 369-375.
- [8] S. Miyata, T. Kumura, Synthesis of new hydrotalcite-like compounds and their physico-chemical properties, *Chem. Lett.*, 2-3(1973) 843-848.
- [9] S. Carlinio, The intercalation of carboxylic acids into layered double hydroxides: a critical evaluation and review of the different methods, *Solid State Ion.*, 98 (1997) 73-84.
- [10] J.W. Boclair, P.S. Braterman, Layered double hydroxide stability. 1. Relative stabilities of Layered Double Hydroxides and Their Simple Counterparts, *Chem. Mater.*, 11 (1999) 298-302.
- [11] D.T. Sawyer, Metal-gluconate complexes, *Chem. Rev.*, 64 (1964) 633-643.
- [12] X. Guo, S. Xu, L. Zhao, W. Lu, F. Zhang, D.G. Evans, X. Duan, One-step hydrothermal crystallization of a layered double hydroxide/alumina bilayer film on aluminum and its corrosion resistance properties, *Langmuir*, 25 (2009) 9894-9897.
- [13] X. Guo, F. Zhang, S. Xu, D.G. Evans, X. Duan, Preparation of layered double hydroxide films with different orientations on the opposite sides of a glass substrate by in situ hydrothermal crystallization, *Chem. Commun.*, 44 (2009) 6836-6838.
- [14] I. Pastorova, R.E. Botto, P.W. Arisz, J.J. Boon, Cellulose char structure: a combined analytical Py-GC-MS, FTIR, and NMR study, *Carbohydr. Res.*, 262 (1994) 27-47.
- [15] S.H. Ha, N.L. Mai, G. An, Y. Koo, Microwave-assisted pretreatment of cellulose in ionic liquid for accelerated enzymatic hydrolysis, *Bioresource Technol.*, 102 (2011) 1214-1219.
- [16] M. Del Arco, S. Gutierrez, C. Martin, V. Rives, FTIR study of isopropanol reactivity on calcined layered double hydroxides, *Phys. Chem. Chem. Phys.*, 3 (2001) 119-126.
- [17] J.T. Klopogge, D. Wharton, L. Hickey, R.L. Frost, Infrared and Raman study of interlayer anions  $\text{CO}_3^{2-}$ ,  $\text{NO}_3^-$ ,  $\text{SO}_4^{2-}$  and  $\text{ClO}_4^-$  in Mg/Al-hydrotalcite, *Am. Mineral.*, 87 (2002) 623-629.



- [18] L. Lv, J. He, M. Wei, D.G. Evans, X. Duan, Factors influencing the removal of fluoride from aqueous solution by calcined Mg-Al-CO<sub>3</sub> layered double hydroxides, *J. Hazard. Mater.*, 133 (2006) 119-128.
- [19] M.X. Reinholdt, R.J. Kirkpatrick, Experimental investigations of amino acid-layered double hydroxide complexes: glutamate-hydrotalcite, *Chem. Mater.*, 18 (2006) 2567-2576.
- [20] O.P. Ferreira, S.G. de Moraes, N. Durán, L. Cornejo, O.L. Alves, Evaluation of boron removal from water by hydrotalcite-like compounds, *Chemosphere*, 62 (2006) 80-88.
- [21] J. Jiang, Y. Xu, K. Quill, J. Simon, K. Shettle, Laboratory study of boron removal by Mg/Al double-layered hydroxides, *Ind. Eng. Chem. Res.*, 46 (2007) 4577-4583.
- [22] M. Bishop, N. Shahid, J. Yang, A.R. Barron, Determination of the mode and efficacy of the cross-linking of guar by borate using MAS <sup>11</sup>B NMR of borate cross-linked guar in combination with solution <sup>11</sup>B NMR of model systems, *Dalton Trans*, 17(2004) 2621-2634.
- [23] T. Takahashi, S. Kashiwakura, K. Kanehashi, S. Hayashi, T. Nagasaka, Analysis of atomic scale chemical environments of boron in coal by <sup>11</sup>B solid state NMR, *Environ. Sci. Technol.*, 45 (2010) 890-895.
- [24] J. Wolska, M. Bryjak, N. Kabay, Polymeric microspheres with N-methyl-d-glucamine ligands for boron removal from water solution by adsorption-membrane filtration process, 32 (2010) 349-352.
- [25] K. Kustin, R. Pizer, Temperature-jump study of the rate and mechanism of the boric acid-tartaric acid complexation, *J. Am. Chem. Soc.*, 91 (1969) 317-322.

## Chapter 5 Conclusions

Boron and its compounds have a wide variety of applications, such as in the chemical industry, electronics and medicine. However, excess boron is harmful to organisms. Methods for borate removal are developed and LDHs, which is similar in structure to the naturally occurring hydrotalcite mineral, has been proved that it can remove borate from the water solution efficiently. However, some shortcomings of LDHs that limited the application in engineering were also suggested by many researchers. Therefore, this thesis focuses on weak points of LDHs and solved them by using different modified methods. All the products are characterized and their application and mechanism in boron removal were investigated from the perspective of environmental and engineering.

In **Chapter 1**, a brief background of previous works regarding the environmental distribution and harmful of boron compounds was overviewed and then the conventional methods on boron compounds removal were also introduced. Finally, the structure and application of LDHs were summarized and the reasons and purposes of this thesis were explained.

A hydrotalcite-like compound prepared through chemical deposition using calcined dolomite as the magnesium source (DLDH) was synthesized and applied to remove borate in **Chapter 2**. DLDH calcined at different temperatures was characterized by specific surface area measurements, scanning electron microscope images, X-ray diffraction (XRD) patterns, and Fourier transform infrared (FTIR) spectra to optimize the calcination temperature and maximize the sorption capacity of borate. Greater

sorption density of borate was observed at higher calcination temperature, and the sample calcined at 700 °C showed the maximum sorption density. In addition, the sorption density of borate by DLDH calcined at 700 °C decreased with increasing initial pH. Solid residues after the sorption of borate were characterized by FTIR,  $^{11}\text{B}$  NMR ( $^{11}\text{B}$  Boron nuclear magnetic resonance), and XRD to explore the sorption mechanism of the calcined product at 700 °C.

In **Chapter 2** and other previous reports, coexisting anions in the solution influenced the sorption of borate by traditional LDHs. In **Chapter 3**, LDHs intercalated with gluconate (G-LDH) was synthesized through a one-step microwave-assisted treatment and characterized by XRD, TEM, FTIR, TG/DTA and two-dimensional  $^{11}\text{B}$  NMR. Several factors that influence sorption of borate were investigated: gluconate content in the LDH, G-LDH dosage, coexisting anions, initial pH of borate solution and sorption temperature. The synthesized adsorbent exhibited a greater borate sorption rate than the traditional hydrotalcite ( $\text{NO}_3\text{-LDH}$ ) or a boron-specific resin. The maximum sorption capacity was 1.27 mmol/g (obtained by fitting to the Langmuir model). The G-LDH sorption density increased with increasing initial borate concentration and adsorbent dosage. In the presence of 50 mM sulfate, sorption of borate by  $\text{NO}_3\text{-LDH}$  significantly decreased and no obvious sorption could be observed, whereas the sorption of borate by G-LDH was maintained at 0.57 mmol/g.  $^{11}\text{B}$  NMR indicated that the sorption mechanism of borate by G-LDH is mainly through bischelate and monodentate types of complexation with borate. This mechanism is similar to that of CRB05, and fundamentally different from that of  $\text{NO}_3\text{-LDH}$ . Moreover, this prepared also can use dolomite as raw materials to instead of  $\text{Mg}(\text{NO}_3)_2$ .

LDHs intercalated gluconate has shown good performance in the borate removal in **Chapter 3**. However, this kind of product with small particles is difficult to separate from water solution and apply to industrial application. In **Chapter 4**, novel composites of Mg-Al type of LDH, synthesized onto filter papers and then intercalated with gluconate (G-LDH@F) were prepared. LDHs with interlayer of carbonate form was first immobilized onto the surface of filter paper (CO<sub>3</sub>-LDH@F) by in situ hydrothermal crystallization, and then ion-exchanged sequentially with chloride (Cl-LDH@F) followed by gluconate. The influence of the molar ratio of gluconate/LDH and reaction time on G-LDH@F synthesis was explored. Products were characterized by XRD, SEM, FTIR and NMR as well as measurements of borate sorption. The optimal molar ratio of gluconate/LDHs and reaction time for preparing G-LDH@F from Cl-LDH@F were 40 and 24 h (G-LDH@F-40-24 h), respectively. G-LDH@F-40-24 h had higher sorption density and greater stability than both the original filter paper and the filter papers containing other LDHs, even in the presence of other anions. <sup>11</sup>B NMR and XRD results indicate that the principal mechanism for borate immobilization on G-LDH@F-40-24 h is complexation of gluconate with borate in both bischelate and monodentate forms. The novel composite is boron-specific and facilitates solid/liquid separation.

In **Chapter 5**, the main experiments and important conclusions of this research were summarized. From these chapters, the results of the removal of borate from the solution by the products we synthesized are satisfactory. However, at the present stage, new sorption materials such as LDHs cannot compete against the resin in market competition for the reason that the stability, recycling capability, toxicity and environmental impact of them still need to be further studied. But due to the special sorption capability of LDHs or other new materials, they can still be used to deal with

the environmental emergency. Hence, I also believe that new materials will be playing an increasingly significant role in the field of environment after further development.

## Acknowledgement

My deepest gratitude goes first and foremost to my supervisor, Prof. Keiko Sasaki, for her constant encouragement and guidance. It is my honor to be her student. During these years, she always supports me a very conducive environment and gives me good advices for my research. From her, I know how to carry a good experiment and how to explain the experimental results precisely which I did not learn before. And the most important I am impressed is how enthusiastic she is in her life and work. I am grateful for what I have learnt from her and hope one day I can be like her.

Sincere gratitude shall be also paid to Prof. Tsuyoshi Hirajima for his support and valuable discussions, as well as for accepting to be member of my doctoral thesis examination committee. He is a precise and a very nice person, he always inspires me from other research fields. Meanwhile, I would also like to express my thanks to Prof. Hiroshige Matsumoto at International Institute for Carbon-Neutral Energy Research, Kyushu University, as the co-examiners of my dissertation and gave me advices in my research.

I sincerely express my deepest condolences and special thanks to late Prof. Yasutake Teraoka at Department of Energy and Materials Sciences, Kyushu University. I appreciate all the helps and the comments for improving my thesis from him, and he will not be forgotten by everyone who admired and respected him.

I want to thank the help from Associate Professor Jin Miyawaki and Ms. Keiko Ideta at Institute for Materials Chemistry and Engineering, Kyushu University. Without their work and help in NMR measurement and analysis, I do not have such important data to support my results.

The members of mineral processing, recycling and environmental remediation laboratory, who always help, encourage and support me in profession and personal, are my important friendship and source of passion. Much thanks should be dedicated to Graduate Doctoral student: Dr. Sayo Moriyama, Dr. Dewi Agustina Iryani, Dr. Limsuwan Pilasinee, Dr. Qianqian Yu; and Graduate Master course students: Naoyuki Fukumoto, Shoichi Tsuruyama, Emiko Morioka, Masaharu Koga, Mikoto Koga, Masayuki Kuwata, and Yoshinobu Nagashima. I also appreciate Associate Prof. Naoko Okibe, Ms. Makiko Semba, Dr. Tomoyo Goto, Mr. Moriyasu Nonaka and Assistant Prof. Hajime Miki, since they are so kind and help me a lot. Of course it is also necessary to appreciate the help from Widi Astuti, Mutia Dewi Yuniati and Luo Wuhui, Yusei Masaki, Taichi Momoki, Mari Yoshida, Yu Takaki, Kenta Toshiyuki and others students in our lab.

Most important, I would wish to thank my parents. They gave me life and are always standing behind me and supporting me.

Last but not least, I am grateful to the scholarship provided by the Ministry of Education, Culture, Sports, Science and Technology, Japan (MEXT), and financial support to Prof. Keiko Sasaki by Funding Program for Next Generation of World-Leading Researchers (“NEXT program” GR078) in Japan Society for Promotion of Science (JSPS).

Xinhong Qiu